Predesign of an experimental (5-10 MWt) disk MHD facility and prospects of commercial (1000 MWt) MHD/steam systems

Research Report
ISSN 0167-9708
Coden: TEUEDE

Eindhoven
University of Technology
Netherlands

Faculty of Electrical Engineering

Predesign of an Experimental (5-10 MWt) Disk MHD Facility and Prospects of Commercial (1000 MWt) MHD/Steam Systems

by
P. Massee
H.A.L.M. de Graaf
W.J.M. Balemans
H.G. Knoopers
H.H.J. ten Kate

EUT Report 90-E-243
ISBN 90-6144-243-5
October 1990

Eindhoven University of Technology Research Reports

EINDHOVEN UNIVERSITY OF TECHNOLOGY

Faculty of Electrical Engineering
Eindhoven The Netherlands

ISSN 0167- 9708 Coden: TEUEDE

PREDESIGN OF AN EXPERIMENTAL (5 - 10 MW_t) DISK MHD FACILITY AND PROSPECTS OF COMMERCIAL (1000 MW_t) MHD/STEAM SYSTEMS

by

P. Massee, H.A.L.M. de Graaf and W.J.M. Balemans
Eindhoven University of Technology
Division Electrical Energy Systems
Eindhoven, The Netherlands

H.G. Knoopers and H.H.J. ten Kate
University of Twente
Low Temperature Division
Applied Superconductivity Centre
Enschede, The Netherlands

EUT Report 90-E-243
ISBN 90-6144-243-5

Eindhoven
October 1990

These investigations in the programme of the Foundation for Fundamental Research on Matter FOM have been supported in part by the Netherlands Technology Foundation STW, Utrecht, The Netherlands.

CIP-GEGEVENS KONINKLIJKE BIBLIOTHEEK, DEN HAAG

Predesign

Predesign of an experimental (5-10 MWt) disk MHD facility and prospects of commercial (1000 MWt) MHD/steam systems / by P. Massee, H.A.L.M. de Graaf, W.J.M. Balemans, H.G. Knoopers and H.H.J. ten Kate. - Eindhoven: Eindhoven University of Technology, Faculty of Electrical Engineering. - Fig., tab. - (EUT report, ISSN 0167-9708; 90-E-243)
Met lit. opg., reg.
ISBN 90-6144-243-5
SISO 661.5 UDC 621.313.522 NUGI 832
Trefw.: magnetohydrodynamica.

ABSTRACT

In this report an experimental disk MHD facility has been designed. After designing the superconducting magnet for the open cycle disk MHD generator, the warm bore of the magnet has been used as a constraint in designing the closed cycle disk MHD generator.

In the experimental MHD facility an enthalpy extraction of 8.7 % could be obtained with a 10 MWt open cycle MHD generator and 37.0 % by means of a 5 MWt closed cycle MHD generator.

System studies of four commercial scale (≈ 1000 MWt) MHD/steam systems have also been performed.

The 1000 MWt open cycle disk generator leads to the smallest coal to busbar efficiency of 42.8 %.

The highest coal to busbar efficiency of 50.0 % is obtained in a commercial system with a closed cycle disk gererator.

The open cycle linear MHD/steam system leads to a coal to busbar efficiency of 49.4 %. When the details of the heat source and the required heat exchangers are considered, it can be anticipated that the system with an open cycle linear MHD generator will have the lowest cost of electricity (fl/kWh) of the four systems.

The design of the superconducting magnet system for the experimental disk facility has used principles that are valid also for large commercial systems. However, verification of these principles in an actual 1000 MWt superconducting magnet design needs further investigation.

CONTENTS

PREFACE

This study was started in order to open the possibility of continuation of the dutch efforts in MHD research, which have received large international recognition. Further it may provide an improved research position in this field because of the cooperation of two well-known groups i.e. the division Electrical Energy Systems at the Eindhoven University of Technology and the Applied Superconductivity Centre at the University of Twente. This cooperation can lead to the construction of an advanced facility to test MHD generators which is equipped with a compact superconducting magnet using Nb_3Sn technology.

At the beginning of this project the following information was available on the best, established performance of the four MHD systems studied here: open cycle linear generator, 22 MW_e during 30 minutes (10 MW_e during 80 hours); closed cycle linear generator, 740 kW_e during 10 seconds; closed cycle disk generator, 470 kW_e during 10 seconds; and open cycle disk generator, 0.7 kW_e during about 30 seconds. This survey illustrates the big difference in development of the various systems. This was the reason to focus especially on the open cycle disk MHD generator and work out a predesign of a 10 MW_t test facility for this apparatus. At the same time system studies were performed of all four MHD cycles at a commercial (1000 MW_t) scale in order to get a more solid basis for our choice. From the system studies it was concluded that the closed cycle disk MHD generator leads to the most attractive system as far as efficiency is concerned. Therefore the predesign of an experimental facility in which a closed cycle disk generator can be tested was also worked out (using the warm bore of the superconducting magnet as a constraint).

Apart from the continuation of the dutch MHD research the proposed experimental facility will serve the following purposes:

- obtaining high enthalpy extractions in an MHD disk generator during at least 10 seconds,
- thereby gaining the much needed extension of the knowledge on the behaviour of the disk generator,

- verifying the theoretical models with experimental results, and
- acquiring experience with the construction of forced flow cooled superconducting Nb_3Sn magnets.

The size of the experimental facility mentioned above (10 MW_t) should be considered as a meticulous choice. When a smaller size would have been chosen then the boundary layers in the MHD generator would dominate the conversion process and the results could not be scaled up to commercial-size generators. When a larger size would have been chosen then little would have been gained in physical insight resulting from the experiments but the investment costs would be greatly enhanced. Therefore the chosen size is seen as the optimum for a test facility that could be financed inside the Netherlands.

NOMENCLATURE

A : Channel cross section [m^2]

A : Cross section of wire [m^2]

A : Cross sectional area of coolant channel [m^2]

$\bar{B}$: Magnetic field vector [T]

B : Magnetic field [T]

B_{c1} : Lower critical field [T]

B_{c2} : Upper critical field [T]

C_p : Specific heat at constant pressure [J/kg K]

C_v : Specific heat at constant volume [J/kg K]

c : speed of sound [m/s]

c_f : Friction coefficient [-]

D : Hydraulic diameter [m]

d_{fil} : Filament diameter [m]

$\bar{E}$: Electrical field vector [V/m]

E : Young's modulus [Pa]

E_i : Ionization energy [eV]

e : Electron charge [$1.6022 \cdot 10^{-19}$ C]

F_{pc} : Pinning force [N/m^3]

F_v : Lorentz force [N/m^3]

f : Fanning friction factor [-]

G : Specific mass flow rate [kg/m^2s]

H : Stagnation enthalpy [J/kg]

h : Enthalpy [J/kg]

h : Channel height [m]

h : Planck's constant [J s]

h : Cable thickness [m]

h_c : Heat transfer coefficient [W/m^2K]

I : Current [A]

I_c : Critical current [A]

i_1 : Distance between throat and generator entrance [m]

$\bar{J}$: Current density vector [A/m^2]

J : Current density [A/m^2]

J_c : Critical current density [A/m^2]

k : thermal conductivity [W/m K]

k : Boltzmann's constant [$1.38066 \cdot 10^{-23}$ J/K]

k_f : Load factor linear generator [-]

k_i : Ionization rate coefficient [-]

k_r : Recombination rate coefficient [-]

l : Channel length [m]

M : Mach number [-]

$\dot{m}$: Mass flow rate [kg/s]

m_e : Electron mass [$9.1095 \cdot 10^{-31}$ kg]

m_s : Mass of particle of species s [kg]

N : Number of supporting rods [-]

Nu : Nusselt number [-]

n : Total density [m^{-3}]

n_a : Atom density [m^{-3}]

n_e : Electron density [m^{-3}]

n_i : Ion density [m^{-3}]

$\bar{\bar{P}}$: Pressure tensor [N/m^3]

P_{comp} : Compressor power [W]

P_{el} : Generated electrical power [W]

P_{hl} : Heat loss [W]

P_{in} : Thermal input power [W]

P_{MHD} : Electrical power output of the MHD generator [W]

P_{wall} : Power loss through the wall [W]

Pr : Prandtl number [-]

p : Wetted perimeter [m]

p : Pressure [Pa]

p_{cb} : Combustor pressure [Pa]

$\dot{Q}$: Heat loss through walls [W/m^2]

$\dot{q}$: Average heat loss through walls [W/m^3]

$\bar{q}$: Heat flux vector [W/m^2]

q : Heat flux [W/m^2]

$\bar{q}_e$: Electron heat flux vector [W/m]

R : Radius [m]

R : Universal gas constant [8314.3 J/((kg-mole)·K)]

$\dot{R}$: Radiated energy [W/m^3]

Re : Reynolds number [-]

R_{gas} : Gas constant [J/kg K]

R_i : Internal resistance [Ω]

R_{in} : Inner radius of the coil [m]

R_l : Load resistance [Ω]

R_m : Magnetic Reynolds number [-]

r : Radius of disk channel [m]

r_a : Anode radius [m]

S : Swirl (Va/Vr) [-]

s : Entropy [J/kg K]

s : Distance between electrodes (linear generator) [m]

s_r : Seed ratio [-]

T : Temperature [K]

T_c : Critical temperature [K]

T_{cs} : Current sharing temperature [K]

T_e : Electron temperature [K]

T_0 : Coolant temperature [K]

t : Time [s]

u : Helium flow velocity [m/s]

$\bar{v}$: Gas velocity vector [m/s]

v : Gas velocity [m/s]

$\bar{v}_e$: Electron drift velocity vector [m/s]

W : Wall friction [N/m^2]

W_{jh} : Joule heat [W/m^3]

w : Channel width [m]

z : Channel height [m]

α : Stekly stability parameter [-]

α_l : Load factor disk generator [-]

β : Expansivity [1/K]

β : Hall parameter [-]

γ : Ratio of specific heats (C_p/C_v) [-]

δ : Energy loss factor [-]

ε : Wall roughness [m]

ε : Permittivity [F/m]

ε_b : Bending strain [-]

ε_0 : Permittivity of vacuum [$8.8542 \cdot 10^{-12}$ F/m]

η : Dynamic viscosity [Ns/m^2]

η : Fraction of superconductor in the composite [-]

η_{cb} : Coal to busbar efficiency [-]

η_{el} : Electrical efficiency [-]

η_{ent} : Enthalpy extraction [-]

η_{is} : Isentropic efficiency [-]

η_L : Local electrical efficiency [-]

κ : Compressibility [Pa^{-1}]

λ : Thermal conductivity [W/m K]

μ_0 : Permeability of vacuum [$1.2566 \cdot 10^{-6}$ H/m]

ν_{ei} : Collision frequency of electrons and ions [s^{-1}]

ν_{ea} : Collision frequency of electrons and atoms [s^{-1}]

ν_s : Collision frequency of electrons and species s [s^{-1}]

ρ : Density [kg/m^3]

ρ_e : Charge density ($=n_i-n_e$) [kg/m^3]

ρ_r : Electrical resistivity [Ωm]

σ : Electrical conductivity [$\Omega^{-1}m^{-1}$]

ϕ : Flux quantum [Wb]

ψ : Joule-Thomson coefficient [K/Pa]

Subscripts

app : Apparent

Ar : Argon

aw : Adiabatic wall

cb : Coal to busbar

cb : Combustor

comp : Compressor

crit : Critical

Cs : Cesium

dif : At outlet of subsonic diffuser

eff : Effective

el : Electric

in : Inlet

is : Isentropic

net : net (to the grid)

o : At generator entrance

opt : Optimum

out : Outlet r : Radial direction

ref : Reference

st : Stagnation

steam : From steam cycle

tot : Total

w : Wall

x : Axial direction

y : Vertical direction

θ : Azimuthal direction

1 INTRODUCTION

In this report the predesign of an experimental disk MHD facility is presented. In order to provide a thorough basis for the proposal that construction of such a facility should be considered, also system studies of 1000 MWt MHD/steam cycles has been performed. Systems of 1000 MWt can be applied in base load power stations which is the final application that is kept in mind. In the mentioned system studies both open and closed cycle systems are considered and generator configurations of both the linear and the disk type have been studied.

In the following the various special terms which may be new to the reader, will be shortly explained. The three characters MHD stand for Magneto Hydro Dynamic; in the case of a generator this denotes the principle that electric power is generated when a medium (fluid) is moving through a magnetic field. This can be illustrated most easily by means of figure 1.1 which shows the principle of a linear MHD generator.

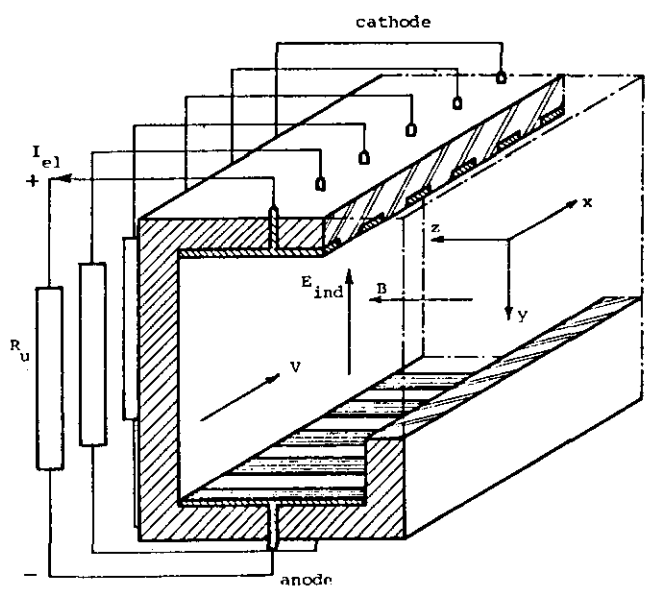

Figure 1.1 Principle of a segmented Faraday generator; $\bar{v}$ denotes the velocity of the plasma, $\bar{B}$ the magnetic induction, I_{el} the current through a generator segment and R_u the load of that segment.

When an electrically conducting medium is moving through a magnetic field perpendicular to the flow direction, an electric field $\bar{E}_{ind}$ is

induced in the direction shown in figure 1.1. Thus electrodes can be situated in the top and bottom wall and when these electrodes are connected by means of a load resistor, electric power is generated. Due to the fact that the current in the generator is carried almost completely by the electrons a so called Hall electric field is created in the axial direction. In order to avoid a shorting of the Hall field the upper and lower wall electrodes are segmented. Each electrode segment is insulated from its neighbours and is connected to a separate resistor. The configuration shown in figure 1.1 is of the so called segmented Faraday type. When the electric field in the axial direction is larger than the field in the vertical direction (the ratio of the two fields equals the so called Hall parameter), it may be advantageous to use the former field for power generation which then leads to a so called Hall generator. This type of generator can also be used in the linear configuration (with segmented electrodes) but usually the disk configuration is then preferred (see figure 1.2).

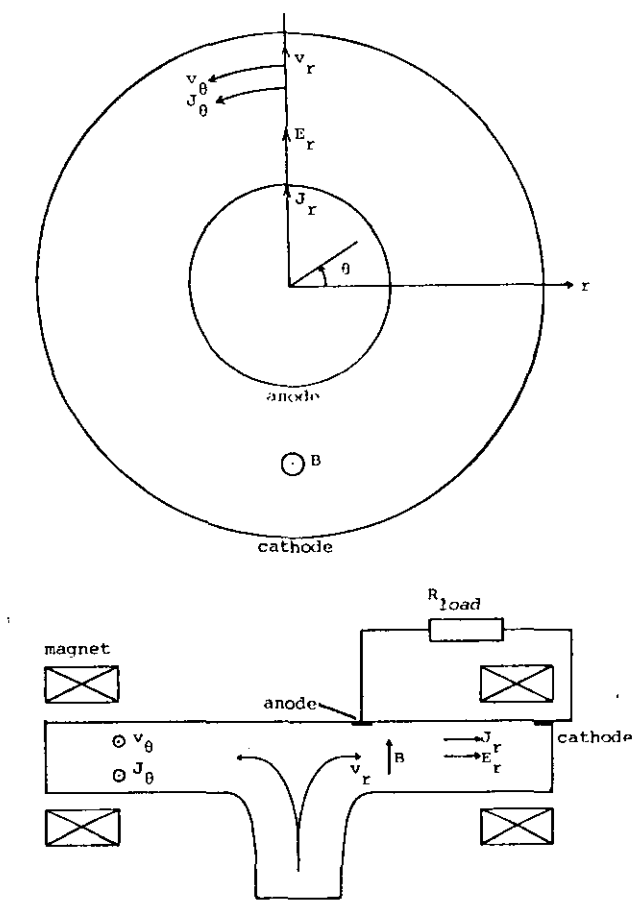

Figure 1.2 Electrical current densities J_r and J_θ, gas velocities v_r and v_θ and electrical field E_r in the disk MHD generator.

In the disk generator the medium expands radially outwards, the electrodes are circular rings placed in the wall and the electric field and electrical current in the Hall direction are used for power generation. It will be clear from the above that the disk generator is suitable only when the Hall parameter is substantially larger than 1.

Considering now the medium that can be used in the MHD generator, three different types can be considered. Systems that can be suitable for special applications, such as for instance space power, use liquid metals (e.g. Na, NaK) as the medium. Since base load power application is the background for the work in this report, liquid metals are not considered further. With a gaseous medium a high temperature is required and two cycles, shown in the figures 1.3 and 1.4, can be distinguished.

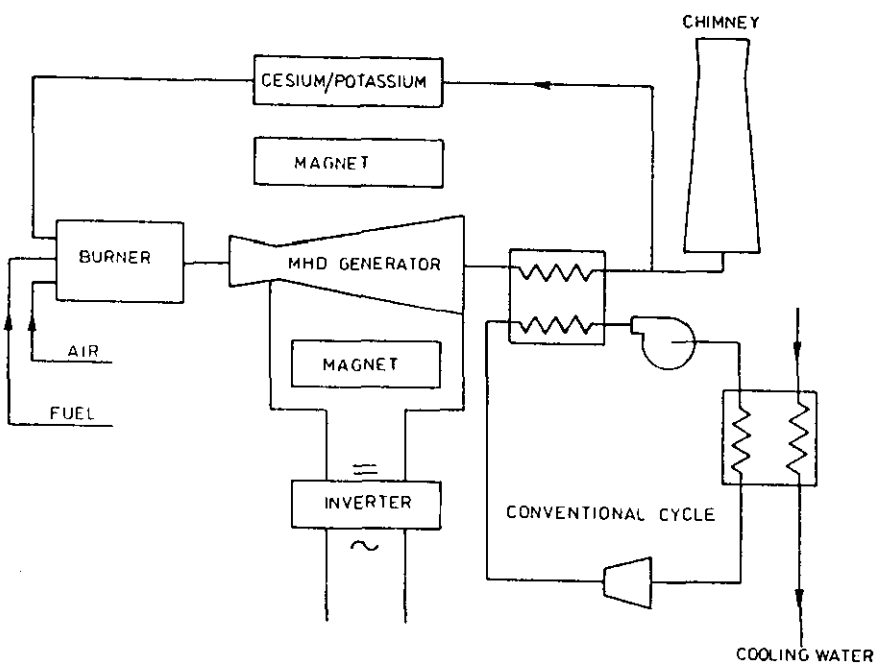

Figure 1.3 Open cycle MHD system.

In the open cycle system, combustion gases with a temperature up to 3000 K flow directly through the MHD generator and finally exhaust into the atmosphere. In order to increase the electrical conductivity K_2CO_3 is seeded through the medium. To reach satisfactory electrical

conductivity a minimum gas temperature of 2700 K is necessary. Further, a heat exchanger is installed downstream of the MHD generator, see figure 1.3, in which heat is transferred to a conventional steam cycle before the combustion gases are led to the stack.

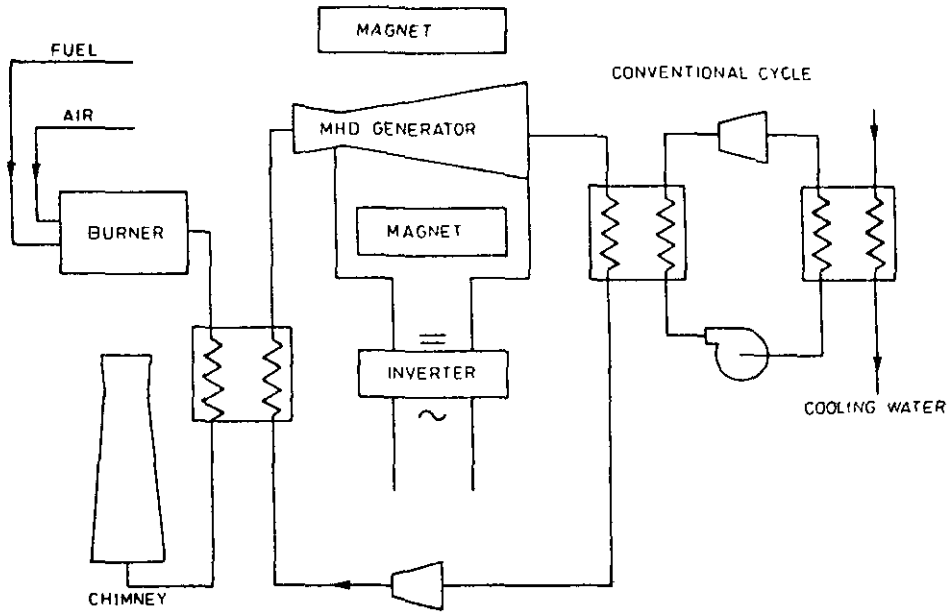

Figure 1.4 Closed cycle MHD system.

In the closed cycle system, the medium is an inert gas (Ar or He) to which a pure liquid metal (Cs or K) is added as seed in order to reduce the internal resistance. The cycle has to be closed because of the high cost of the medium in this case. As shown in figure 1.4 the heat obtained from the combustion of fossil fuels now has to be transferred through a heat exchanger to the medium. Since the medium is an inert gas, the electrons can behave independently of the heavy particle gas in this case. In other words the number of inelastic collisions between electrons and heavy particles is relatively low and therefore the electrons can have a higher temperature than the atoms. This is the reason that the maximum (inert gas) temperature can be considerably lower than in the open cycle situation namely about 2000 K. It will now be clear that four different systems have to be studied when the most important MHD base load power stations have to be compared.

The advantage of the MHD/steam cycle is that the addition of the MHD part can lead to an increase of the total plant (coal pile to busbar) efficiency from about 40 % to about 50 %. In a later stage when further refinements can be introduced and higher temperatures can be used even higher efficiencies up to 60 % are feasible. More details on this subject can be found in chapter 5 where the studies of the four commercial MHD systems are presented.

There is still one point in the comparison of the four MHD systems which has to be discussed at this moment, namely the various states of development. The open cycle system is in an advanced state of development especially in the USA and the USSR. In the USA the development is oriented entirely towards direct coal burning. In the

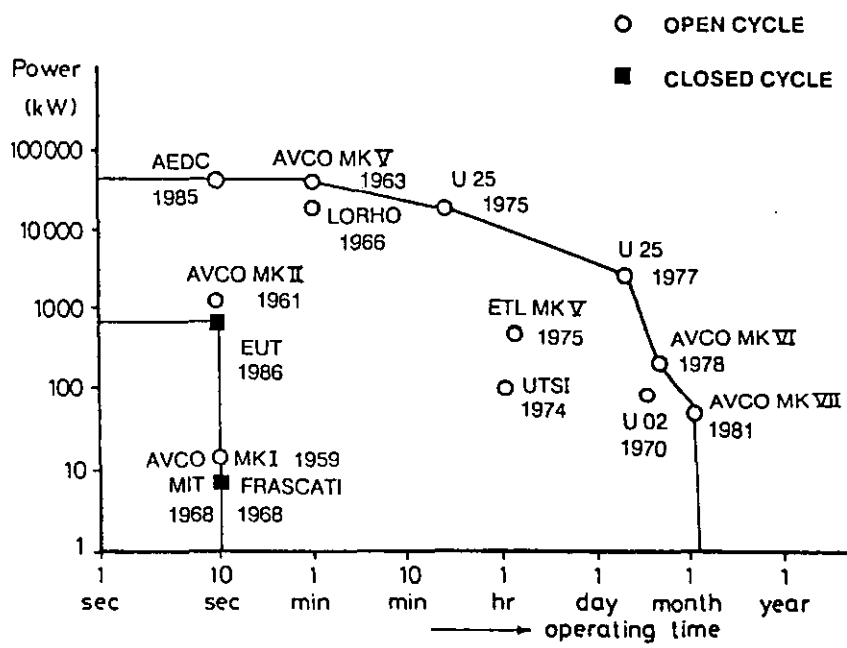

Figure. 1.5 Progress in the performance of major MHD generator experiments of the linear type. Note that the horizontal scale is nonlinear.

USSR the U-25 installation which uses natural gas firing, has produced power up to 20 MWe during 30 minutes and a power of 10 MWe during about 80 hours [1.1]. The progress in performance and operating time of experiments on linear MHD generators is illustrated in figure 1.5.

The difference in the state of development between the open cycle and the closed cycle systems is very remarkable in this figure. As mentioned above, the state of development of disk generators is not indicated in figure 1.5. However, the closed cycle disk generator experiments at the Tokyo Institute of Technology have yielded results that are quite comparable to those of the Eindhoven University of Technology linear generator [1.2]. The open cycle disk generator even lacks in state of development compared to the closed cycle systems. For disk generators providing power over a time scale from 1 to 10 seconds, the maximum electric power only equals 0.7 kWe at a thermal input of 2.1 MWt [1.3].

Since the present report concludes that disk generators can have certain advantages over linear generators, an experimental facility for investigating this type of generator is proposed.

Besides the MHD generator itself, the magnet system is a second important part of the complete installation. In principle one can use conventional magnets at low fields but usually superconducting magnets are applied because of the small power consumption, the possibility to generate large fields and to attain a more compact design.

Conventional copper magnets with iron cores can generate magnetic fields up to about 2 T maximum in a small volume. This limitation is caused by saturation of the iron core or yoke at this field level. Generation of higher fields is only possible with extremely high dissipation. The application of superconducting magnets limits the required power consumption almost to the refrigeration power, needed to cool down and to maintain the superconducting state of the magnet. Furthermore, for the magnet itself, only a low power high current supply is required. Due to the extremely high current density in superconductors, the winding volume can be reduced, thus a compact magnet system can be obtained. These advantages of superconducting magnets over conventional magnets drastically reduce the capital as well as the running costs. Therefore, application of superconducting magnets is inevitable in large systems especially when the magnetic field is stationary and when it has to be generated in a large volume as is the case with magnets for MHD and fusion plants.

In our case of an experimental, small size disk MHD system which should work as a facility for MHD research as well as a demonstration unit, we selected a magnetic field level of 9 T in stead of 5 T as in more conventional systems. This provides the possibility to gain experience with an advanced superconducting magnet system which also requires the use of Nb_3Sn technology.

2 THEORETICAL ASPECTS

In this report two viewpoints into the subject have been taken. The final goal of the work is to obtain a predesign of a 5-10 MWt facility in which disk MHD channels can be tested. Thus the operation of a 5-10 MWt disk generator has to be studied. In order to be able to compare the feasibility of disk generators with other MHD generators a system study of the four best known MHD systems has also been performed. A comparison of the four systems could also have been worked out at the 5-10 MWt scale but this does not lead to an optimum situation. At this power level the MHD generator is limited by unfavourable surface to volume ratios so that boundary layers play a very important role and the efficiencies are very much restricted. Thus a comparison at a larger power level is much more useful and therefore system studies have been performed at a power level of about 1000 MW (coal thermal input). Thus parts of this report run in parallel, i.e. the predesign calculations which are discussed in chapter 3 and similar system calculations which are presented in chapter 5. The basic equations which can be applied to both disk and linear MHD generators, both for open cycle and for closed cycle conditions are therefore presented in this chapter.

A comparable situation arises during the design process of the superconducting magnet. When this design is performed only at the 10 MWt scale it is possible that solutions for certain problems are chosen that cannot be applied in large scale systems. The support of the attractive forces between the coils is an example of this kind of problems. Thus the design of large scale superconducting magnets for disk generators also had to be studied for the present project. The general design philosophy which is also valid for large scale systems is therefore described in the second part of this chapter. The specific application, i.e. the predesign of the 5-10 MWt disk test facility is then discussed in chapter 3.

2.1 The MHD system

In this chapter the general theory concerning the MHD channel flow is

presented. Moreover the efficiencies describing the general performance of the MHD generator are discussed.

2.1.1 The channel

The behaviour of the plasma in the MHD channel is described by the following basic equations in which ion slip is neglected:

Heavy particles:

$$\text{Continuity equation: } \frac{\partial \rho}{\partial t} + \nabla\cdot(\rho\bar{v}) = 0 \tag{2.1}$$

$$\text{Momentum equation: } \rho\frac{\partial \bar{v}}{\partial t} + \rho(\bar{v}\cdot\nabla)\bar{v} = \tag{2.2}$$

$$= -\nabla\cdot\bar{\bar{P}} + en_i(\bar{E} + \bar{v}x\bar{B}) + n_e m_e(\bar{v}_e - \bar{v})(\nu_{ei}+\nu_{ea})$$

$$\text{Energy equation: } \frac{\partial}{\partial t}[n(\frac{3}{2}kT + \frac{1}{2}m\bar{v}\cdot\bar{v})] + \nabla[n(\frac{3}{2}kT + \frac{1}{2}m\bar{v}\cdot\bar{v})] + \nabla\cdot\bar{q} =$$

$$= -\nabla\cdot(\bar{v}\cdot\bar{\bar{P}}) - n_i e\bar{E}\cdot\bar{v} + n_e m_e \bar{v}\cdot(\bar{v}_e - \bar{v})(\nu_{ei}+\nu_{ea})$$

$$+ \frac{3}{2}\delta n_e m_e k(T_e - T)\sum_s \frac{\nu_s}{m_s} \tag{2.3}$$

Electrons:

$$\text{Continuity equation: } \frac{\partial}{\partial t} n_e + \nabla\cdot(n_e\bar{v}_e) = n_e n_a k_i - n_e^2 n_i k_r \tag{2.4}$$

Momentum equation:

$$0 = -\nabla(n_e kT_e) - en_e(\bar{E} + \bar{v}_e x\bar{B}) - n_e m_e(\bar{v}_e - \bar{v})(\nu_{ei}+\nu_{ea}) \tag{2.5}$$

$$\text{Energy equation: } \frac{\partial}{\partial t}[\frac{3}{2}n_e kT_e + n_i E_i] + \nabla\cdot[(\frac{3}{2}n_e kT_e + n_i E_i)\bar{v}_e] =$$

$$= -\bar{v}_e\cdot\nabla(n_e kT_e) - (n_e kT_e)\nabla\cdot\bar{v}_e - n_e e\bar{E}\cdot\bar{v}_e + n_e m_e\bar{v}\cdot(\bar{v} - \bar{v}_e)(\nu_{ei}+\nu_{ea})$$

$$-\frac{3}{2}\delta n_e m_e k(T_e - T)\sum_s \frac{\nu_s}{m_s} - \dot{R} - \nabla\cdot\bar{q}_e \tag{2.6}$$

Maxwell's equations: $\nabla\cdot\bar{E} = \frac{\rho_e}{\varepsilon}$ $\qquad$ $\nabla\cdot\bar{B} = 0$ $\qquad$ (2.7)

$$\bar{\nabla}x\bar{E} = -\frac{\partial\bar{B}}{\partial t} \qquad \bar{\nabla}x\bar{B} = \mu_o\bar{J} + \varepsilon_o\mu_o\frac{\partial\bar{E}}{\partial t}$$

For plasmas on laboratory scale the following assumptions are made:

- The magnetic Reynolds number R_m is much smaller than 1, i.e. the magnetic fields due to electrical currents in the plasma are negligible compared to the applied magnetic field;
- High frequency plasma oscillations are neglected. With this assumption the Maxwell relations reduce to:

$$\nabla\cdot\bar{B} = 0 \qquad \text{and} \qquad \nabla x\bar{E} = 0 \tag{2.8}$$

For simplicity we assume further:

- The inlet relaxation length is negligible in comparison with the generator length;
- The electrical space charge is assumed to be small. With this assumption, the Debye length is assumed to be the minimum characteristic length to be described;
- The collective kinetic energy of the electrons is negligible with respect to their thermal energy;
- Quantities vary only in one dimension. For the disk generator this is the radial direction and for the linear generator it is the axial direction.

In this one dimensional approach the heavy particle equations in the case of the disk generator reduce to the following ones (see fig.1.2):

Continuity: $$\frac{d}{dr}(\rho v_r A) = 0 \tag{2.9}$$

Momentum in radial direction: $$\rho v_r\frac{\partial v_r}{dr} + \frac{dp}{dr} = -\rho\frac{v_\vartheta^2}{r} - J_\vartheta B - W_r \tag{2.10}$$

Momentum in tangential direction: $$\rho v_r\frac{\partial v_\vartheta}{dr} = -\rho\frac{v_r v_\vartheta}{r} - J_r B - W_\vartheta \tag{2.11}$$

Energy:
$$\rho v_r \frac{dH}{dr} = J_r E_r - \dot{Q} \qquad (2.12)$$

Here v stands for $|\vec{v}| = \sqrt{v_r^2 + v_\vartheta^2}$, $\dot{Q}$ is the heat loss through the walls, W_ϑ and W_r are given by

$$W_\vartheta = c_f \frac{\rho v v_\vartheta}{z}, \qquad W_r = c_f \frac{\rho v v_r}{z},$$

and H is the stagnation enthalpy given by

$$H = h + \frac{v^2}{2}.$$

In the equations for the linear segmented Faraday generator the Coriolis term as well as the longitudinal component of the current density and the azimuthal gas velocity term vanish. Moreover all quantities referring to r now refer to the longitudinal direction x. In the linear generator, however, the electric power density in the energy equation equals $-J_y E_y$. At this point a distinction must be made between closed cycle and open cycle MHD. In an open cycle generator a strong coupling exists between the electron gas and the heavy particle gas due to inelastic collisions between the two species. In that case the electrical properties such as the Hall parameter and the electrical conductivity are entirely determined by the gas temperature and pressure.

In closed cycle conditions, however, due to the relative rareness of inelastic collisions between electrons and the noble gas atoms and ions, the temperature of the electron gas may rise above the heavy particle gas temperature. This leads to an increase of the conductivity and the Hall parameter.

In the following subparagraphs closed cycle and open cycle systems will be regarded separately.

2.1.1.1 Closed cycle systems

In the closed cycle MHD-generator equilibrium of the continuity and energy equations for the electrons is assumed. Hence the continuity equation is rewritten as the Saha equations for Argon and for Cesium. The energy equation reduces to the simple balance of energy lost due to elastic collisions and the energy gained due to the movement of the electrons in the electrical field W_{jh}. For a disk generator W_{jh} is written as:

$$W_{jh} = \frac{J_r^2 + J_\vartheta^2}{\sigma_{eff}} . \tag{2.13}$$

The momentum equations of the electron gas in the disk generator lead to:

$$J_r = \frac{\alpha_l}{\beta_{eff}} \sigma_{eff} v_r B \tag{2.14}$$

$$J_\vartheta = - \sigma_{eff} v_r B \, (1-\alpha_l) \tag{2.15}$$

$$E_r = - \beta_{eff} v_r B \left[1 + \frac{S}{\beta_{eff}} - \alpha_l - \frac{\alpha_l}{\beta_{eff}^2}\right] \tag{2.16}$$

where α_l is the loading parameter defined by Klepeis and Louis [2.1]:

$$\alpha_l = \frac{\beta_{eff} J_r}{\sigma_{eff} v_r B} \tag{2.17}$$

and the swirl S is given by v_ϑ / v_r.

The effective values of the electrical conductivity and Hall parameter are obtained from the quasi-linear plane wave theory of electrothermal waves in a plasma [2.2] according to:

$$\text{if } \beta < \beta_{crit} \text{ then } \sigma_{eff} = \sigma = \frac{n_e e^2}{m_e(\nu_{ei}+\nu_{ea})} \text{ and } \beta_{eff} = \beta = \frac{eB}{m_e(\nu_{ei}+\nu_{ea})}$$

$$\text{if } \beta > \beta_{crit} \text{ then } \sigma_{eff} = \frac{\beta_{crit}}{\beta}\,\sigma \text{ and } \beta_{eff} = \beta_{crit}. \tag{2.18}$$

The Hall parameter at the stability limit, β_{crit}, follows from the linearized plane wave theory and is calculated according to Nakamura and Riedmüller [2.3] and Massee [2.4].

In a linear generator W_{jh} is written as:

$$W_{jh} = \frac{j_y^2}{\sigma_{eff}} \tag{2.19}$$

and the momentum equation for electrons leads to:

$$j_y = -\sigma_{eff}\, v\, B\, (1-k_f) \quad \text{and} \tag{2.20}$$

$$E_y = k_f\, v\, B \tag{2.21}$$

where now v denotes the gas velocity in the axial direction.

The load factor k_f is given by:

$$k_f = \frac{R_l}{R_l + R_i} \tag{2.22}$$

where R_l is the external load resistance and the internal resistance $R_i = h/(\sigma_{app} w \cdot s)$. Here h is the channel height, w the channel width and s the distance between two adjacent electrodes. Due to segmentation losses, an apparent conductivity has to be introduced as:

$$\sigma_{app} = \frac{\sigma_{eff}}{1+\beta_{eff} s/h}\,. \tag{2.23}$$

This takes into account the bending of the electrical current lines in each generator segment. In the linear generator the critical Hall parameter is taken constant ($\beta_{crit} = 1.5$) and boundary layers are calculated in the one-dimensional approximation according to Massee [2.5].

In the way described above the effect of streamers (constricted discharges) has not been taken into account. The presence of streamers, which is in general observed experimentally, will reduce the performance of the generator. Neither has the fact been taken into account that the disk generator can also be operated under the condition of fully ionized seed. It has not yet been shown experimentally that a disk generator with large enthalpy extraction can fulfil this condition in the entire generator. On the other hand it has been shown before [2.6] that the advantage of the fully ionized seed condition over other loading conditions is probably limited.

Finally, in the calculations of the disk generator the following expressions for the wall friction coefficient and the heat flux are used:

$$c_f = 0.058\ Re^{-0.2} \tag{2.24}$$

$$\dot{Q} = \frac{2}{z}\,\dot{q} = \frac{2}{z}\,h_c\,(T_{aw} - T_w) \tag{2.25}$$

where h_c is the heat transfer coefficient, T_{aw} is the adiabatic wall temperature and T_w is the wall temperature

$$h_c = \frac{\lambda \cdot Nu}{r - r_0 + i_1}$$

$$T_w = T_{st} - 300\ K$$

$$T_{aw} = T + \frac{1}{2}\,Pr^{1/3}\,\frac{v^2}{C_p} \qquad (Pr = 2/3)$$

with Nu the Nusselt number which for a turbulent flow is assumed equal to:

$$Nu = 0.023\ (Re)^{0.8}$$

and Re is the Reynolds number

$$Re = \frac{\rho \cdot v \cdot (r - r_0 + i_1)}{\eta}\ .$$

In the case of an Argon plasma seeded with Cesium the gas constant for the Argon Cesium mixture R_{gas} is given by:

$$R_{gas} = \frac{R}{s_r \cdot m_{Cs} + (1 - s_r) \cdot m_{Ar}}$$

where m_{Cs} and m_{Ar} are the atomic masses of Cesium and Argon respectively, s_r is the seed ratio and R is the universal gas constant.

In case of a linear generator $r-r_0+i_1$ must be replaced by $x+i_1$ and $\frac{2}{z}$ by $\frac{2(w+h)}{w \cdot h}$.

2.1.1.2 Open cycle systems

The equations governing the flow of the plasma in an open cycle MHD generator are the same as those for closed cycle. However, due to the strong coupling between the electron gas and the heavy particles the electrical conductivity and the Hall parameter are entirely determined by the properties of the heavy particle gas. For the calculation of the flow of the combustion gas the values of the entropy s, enthalpy h, speed of sound c, ratio of specific heats γ, electrical conductivity σ and Hall parameter β are required. They are obtained from the NASA SP-273 chemical equilibrium computer code [2.7] and are approximated by a least squares curve fit as function of temperature and pressure in the general form:

$$\xi = \xi_0 + \xi_1 \left[\frac{p}{p_{ref}} \right]^{\xi_2} \left[\frac{T}{T_{ref}} \right]^{\xi_3} \qquad (2.26)$$

where p_{ref} and T_{ref} are reference values of the static pressure and temperature (p_{ref} = 1 bar, T_{ref} = 2500 K).

In the calculations segmentation losses and the effects of inhomogeneities are not explicitly taken into account and voltage drops are assumed to be constant over the length of the channel.

In the case of a disk generator the viscous and thermal losses are calculated using semi-empirical relations of the form:

$$c_f = (2.87 + 1.85 \log((r-r_0+i_1)/\varepsilon))^{-2.5} \text{ and} \qquad (2.27)$$

$$\dot{Q} = \frac{2}{z}\,\dot{q} = \frac{2}{z}\,h_c\,(T_{st} - T_w) \qquad (2.28)$$

with the wall roughness $\varepsilon = 0.001$ m, the heat transfer coefficient $h_c = \rho \cdot v \cdot \partial h/\partial T \cdot c_f/2$ and $T_{st} - T_w = 500$ K.

In the case of a linear generator (2.27) and (2.28) are also used but $r-r_0+i_1$ must be replaced by $x+i_1$ and $\frac{2}{z}$ by $\frac{2(w+h)}{w \cdot h}$.

2.1.2 Constraints

For all four generator types the constraint holds that the half angle between two opposite channel walls in the flow direction can not exceed 5° in order to prevent boundary layers to separate from the walls. This would greatly reduce the performance of the generator.

For both open cycle generators the pressure after the subsonic diffuser must be greater than 1.14 bar in order to withstand the atmospheric pressure when the gas is exhausted into the atmosphere.

The three supersonic channels (both disk channels and the closed cycle linear channel) must have a Mach number at the channel exit greater than 1.05 in order to prevent shock waves in the channel.

The closed cycle disk generator operates in the optimum loading mode, which means that the electrical efficiency is maximum at every point in the channel. This efficiency is defined as the ratio between the electrical power density and the work needed to push the gas through the channel against the Lorentz force, i.e.:

$$\eta_{el} = \frac{\bar{E} \cdot \bar{J}}{\bar{v} \cdot (\bar{J} \times \bar{B})} \,. \qquad (2.29)$$

To achieve this condition the load factor at the anode is adjusted. In the channel this condition is fulfilled by adjusting the local height.

The open cycle disk operates with a constant radial electric field, which is equal to the maximum field of 12 kV/m until which value

electrical breakdown does not occur [2.8]. This condition is fulfilled also by adjusting the load factor at the anode and the local height in the channel.

In the closed cycle channel the constant load factor is adjusted such that the Faraday current density equals at least 1500 A/m^2 at the inlet. The channel height and width are prescribed in this case.

In the open cycle linear channel the Mach number is kept constant at 0.9 and the constant load factor is such that the stagnation pressure at the exit of the subsonic diffuser is 1.14 bar. This situation is reached by local adjustment of both channel height and width.

In the closed cycle channel the wall temperature is assumed to be 300 K lower than the stagnation gas temperature. In the open cycle channel this temperature difference is taken at 500 K, since this channel has to be cooled more intensively.

2.1.3 Efficiencies

The performance of the channel can be described by the local electrical efficiency (section 2.1.2), the enthalpy extraction and the isentropic efficiency. The enthalpy extraction is defined by:

$$\eta_{ent} = \frac{\dot{m}(H_{in} - H_{out}) - P_{hl}}{\dot{m} H_{in}} = \frac{P_{el}}{\dot{m} H_{in}} \qquad (2.30)$$

and gives the fraction of the stagnation enthalpy at the inlet which is converted into electrical energy. For closed cycle systems H is the enthalpy relative to the enthalpy at 0 K but for open cycle systems H is relative to the enthalpy at 298 K.

The isentropic efficiency is the ratio of the actual electrical power and the electrical power that would have been generated if all processes occurred isentropically:

$$\eta_{is} = \frac{\dot{m}(H_{in} - H_{out}) - P_{hl}}{\dot{m}(H_{in} - H_{out,is})} \quad . \tag{2.31}$$

The isentropic efficiency can also take into account the loss of stagnation pressure in the nozzle and diffuser(s).

2.2 Superconducting magnet systems for disk MHD generators.

In this section we first provide a short introduction to superconductivity. Then the basic magnet configurations for disk MHD generators are discussed.

2.2.1 Brief introduction to superconductivity

The phenomenon of zero electrical resistivity which is observed for certain materials at temperatures far below 0 °C is called superconductivity. The change from the "normal" state into the "superconducting" state is quite abrupt and occurs at a characteristic temperature, called the critical temperature. Besides this critical temperature, there are two additional parameters which must not be exceeded in order to avoid transfer of the superconductor into the normal state, namely the critical current density and the critical magnetic field.

Superconductors can be classified into Type I and Type II. Pure metals which show superconductivity are often Type I superconductors. In the superconducting state this kind of conductor not only loses its electrical resistivity but also shows perfect diamagnetism. External magnetic fields induce superconducting currents in a surface sheath in such a way that all flux will be expelled out of the interior of the conductor. Exceeding the critical field B_{c1} leads to flux penetration into the conductor and transfer from the superconducting into the normal state. The critical values of magnetic field and current density are very low for Type I superconductors, thus they are not suitable for high magnetic fields.

Type II superconductors, often alloys such as NbTi and NbZr or compounds such as Nb_3Sn, NbGe or V_3Ga, show also perfect diamagnetism for fields smaller than B_{c1}. Beyond this value flux lines penetrate in clusters (fluxoids) surrounded by current vortices into the material. Outside these bundles, which possess a quantum unit of flux $\phi = h / 2e$, the material is still superconducting. This state of normal and superconducting regions (mixed state) will exist until the critical field B_{c2} is reached. Exceeding this field strength, no superconducting regions can persist so the material becomes normal conducting.

If a current is flowing through the conductor, Lorentz forces per unit volume $\bar{F}_v = \bar{J} \times \bar{B}$ will work on the fluxoids. Pinning forces created by lattice defects like boundaries, dislocations and precipitates in the

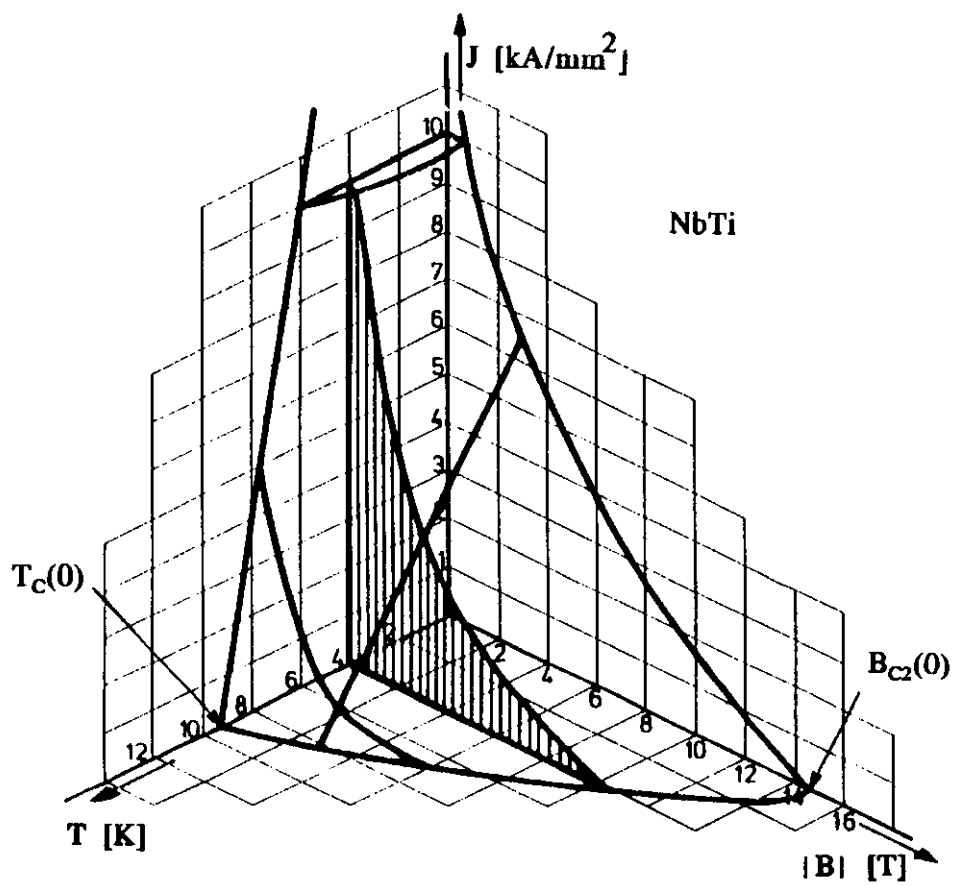

Figure 2.1 Phase diagram of a NbTi superconductor.

Type II superconductor prevent free motion of the fluxoids through the material and thus dissipation. Near the critical current density the Lorentz force equals the pinning force which can obviously be described by $\bar{F}_{pc} = \bar{B} \times \bar{J}_c$. Beyond J_c fluxoids will start to move and produce an electrical field over the conductor thus dissipation occurs. If this dissipation becomes larger than the cooling capacity, an abrupt transition to the normal state (quench) takes place. The critical current at a certain temperature and magnetic field is very sensitive to the number and strength of the pinning centres and thus to the metallurgical state after wire manufacturing. This is in contrast to the critical field and temperature, which are mainly determined by intrinsic material properties that can scarcely be influenced by the material composition. Type II superconductors possess large critical parameters as can be observed in the phase diagram of NbTi shown in figure 2.1. The superconducting state exists below the critical surface.

Besides the mentioned superconductors, nowadays often called the "classical" superconductors, there exists an other class of conductors the so-called high-T_c superconductors. These conductors, developed during the past 4 years, show zero resistance at the temperature of liquid nitrogen (80 K) instead of liquid helium. However, at this moment these superconductors are not important for magnet technology because the current density in the present bulk materials lies below 1 A/mm^2 when exposed to a moderate magnetic field. Moreover, these materials do not have isotropic properties and at present there exists no production process for a practical conductor that guarantees stable and reproducible results in combination with a required current density of 100 to 1000 A/mm^2 in a field range of 5 to 10 T. At this moment it is very uncertain whether all the efforts will lead to a technological success in the field of high T_c superconducting magnets.

In the following we will confine ourselves to the properties of type II superconductors, and more specifically to the practical NbTi and Nb_3Sn superconductors.

2.2.1.1 Practical superconductors

In figure 2.2 a cross-section of a practical multifilamentary wire is shown. The number of filaments in a wire varies from one (mono-filament) to hundreds or thousands, depending on the specific application. For a d.c. application a few dozen filaments embedded in a copper matrix is commonly used. Nowadays commercially available

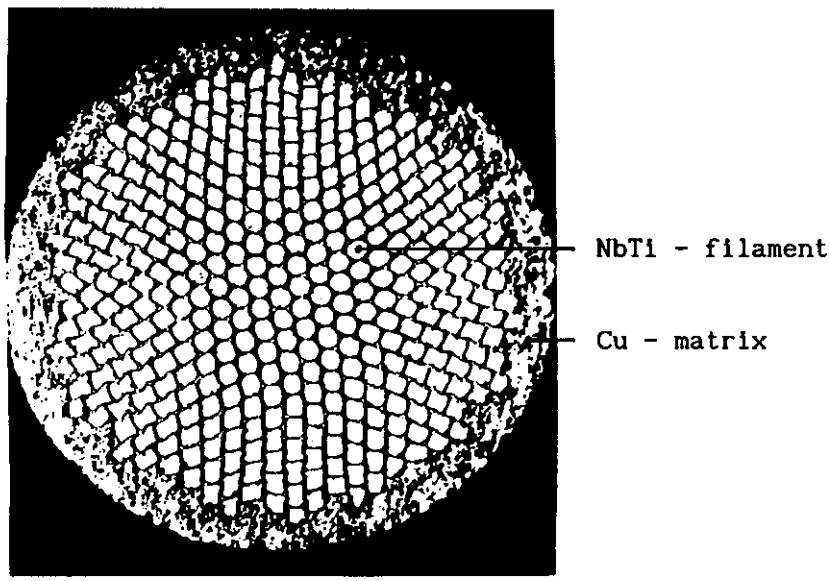

Figure 2.2 Cross-section of a multifilamentary superconducting wire. D_{wire}*=203 μm,* d_{fil}*=7 μm and* n_{fil}*=367.*

composite conductors are produced from NbTi and Nb_3Sn. The former is a ductile alloy, which can easily be fabricated into wires. NbTi is widely used in magnet technology for creation of magnetic fields up to 8 T at liquid helium temperature. In contrast with NbTi, Nb_3Sn is a brittle compound with is not easy to handle. Due to its high critical parameters this type of conductor is used to generate fields above 10 to 12 T or if the operating temperature departs from 4 K to higher levels. In the intermediate range of 8 to 11 T Nb_3Sn as well as NbTi could be used in practice. However, application of NbTi in this range requires a reduction of the operating temperature to about 2 K.

If high current capacity conductors are required, far more than the critical current of a single wire, several strands can be twisted or braided to form a cable. Such cables used in high current/high field magnets experience large Lorentz forces. The current carrying capacity

of superconductors reduces under strain conditions; especially Nb_3Sn is extremely strain sensitive. Filament fracture in this material occurs already at a tensile strain of 0.4 to 0.7 % . So in order to reduce the strain to an acceptable value, the cable must be combined with reinforcement material. Also additional material is necessary to enhance stability. Considerations concerning these problems and other design criteria will be dealt with in section 3.2.

2.2.1.2 Stability criteria

The enthalpy of superconducting material at liquid helium temperature is very small thus tiny energy releases due to mechanical, thermal, electrical or magnetical disturbances can be sufficient to raise the temperature above the critical value and to transfer the conductor into the normal state. In the early stage of superconducting magnet technology operating currents actually never reached the expected critical currents, since premature quenches occurred at much lower values. The superconducting state became unstable due to events that can be described to transient disturbances like flux jumps and wire motion. Flux jumps are sudden changes in the flux density profile in a superconductor caused by an arbitrary event that increases the temperature. As was described before, motion of flux lines is a dissipative event, thus due to the mentioned disturbances the temperature will rise further. A temperature increase reduces the critical current density which results in a further penetration of

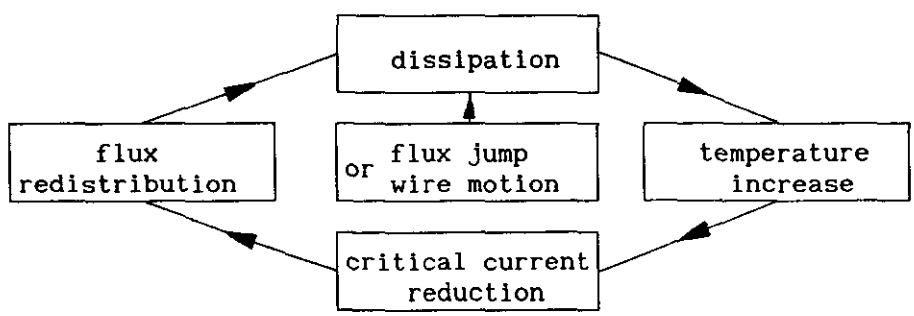

Figure 2.3 Schematic representation of a disturbance sequence leading to an instability.

flux in the superconductor. This chain reaction as visualized in figure 2.3 represents the occurrence of an instability.

Adiabatic stability

Because in the superconducting material like NbTi magnetic flux moves faster than heat, the stability criterion leads to a maximum allowable filament diameter under adiabatic conditions. Up to the filament diameter of

$$d_{fil} = \frac{1}{J_c} \left\{ \frac{3 \rho C_p (T_c - T_o)}{\mu_0} \right\}^{1/2}, \qquad (2.32)$$

the energy release after a small disturbance can be absorbed by the filament without reaching the critical temperature. In practice this means that filament diameters less than ~100 μm are necessary to prevent quenching due to flux jumps.

Dynamic stability

If many fine filaments are embedded in a matrix of copper, as is the case in almost all practical conductors, the process can not be considered as adiabatic anymore. In pure metals like copper the thermal diffusivity $k/\rho C_p$ is orders of magnitude larger than the magnetic diffusivity ρ_r/μ_0 thus the motion of the flux through the composite will slow down and conduction of heat through the copper away from the hot spot becomes important. The allowable filament diameter according to the dynamic stability criterion as given by:

$$d_{fil} < \frac{1}{J_c} \left\{ \frac{32\ k\ (1-\eta)}{\eta} \cdot \frac{(T_c - T_0)}{\rho_r} \right\}^{1/2} \qquad (2.33)$$

increases when the electrical conductivity of the matrix material increases and when the fraction of superconductor in the composite decreases.

Cryogenic stabilization

If the superconductor in the composite goes to a normal state, the highly conductive matrix material will take over the operating current. If it is possible during this time to reduce the temperature of the superconductor below T_c, recovery to the superconducting state will be obtained. To accomplish this so called full cryogenic stability, sufficient matrix material must be added to equal heat production in the matrix and heat transport to the coolant. The ratio of both terms

$$\alpha = \frac{\rho_r \, \eta^2 \, J_c^2 \, A}{(1-\eta) \, p \, h_c (T_c - T_0)} \quad , \tag{2.34}$$

is called the Stekly parameter, see bibliography 7. Thus, if $\alpha < 1$ full cryogenic stability is obtained and recovery of the magnet after a quench will take place. In fact when $\alpha = 1$ a copper coil is made having a superconducting short when sufficiently cooled.

Subdivision of the superconductor in filaments embedded in normal conducting material reduces the sensitivity to disturbances. However, application of a highly conductive normal matrix introduces all kinds of undesirable phenomena as for instance losses and magnetic coupling of the filaments. Treatment of these problems are beyond the scope of this brief introduction. The interested reader is referred to the text books of Wilson and Collings (see bibliography).

2.2.1.3 Critical parameters of NbTi and Nb_3Sn superconductors.

As mentioned before, the critical magnetic field B_{c2} and the critical temperature T_c are almost completely determined by intrinsic physical properties of the superconducting material and thus by the alloy composition. The latter varies for different applications and manufacturing processes between 45 and 55 weight % Ti in NbTi. The critical temperature at zero field lies between 9.0 and 9.3 K for the above-mentioned alloy compositions of technical interest. The critical field B_{c2} at 4.2 K lies between 10.4 and 11.5 T but is difficult to

measure. The baseline for NbTi (see figure 2.1) is described with a reasonable accuracy by:

$$B_{c2}(T) = B_{c2}(0)\ [1-\{\ T/T_c(0)\ \}^{1.7}],\quad (0<B<10T),\ \text{or} \tag{2.35}$$

$$T_c(B) = T_c(0)\ [1-\{\ B/B_{c2}(0)\ \}\ ]^{0.59},\quad \text{with} \tag{2.36}$$

$$T_c(0) = 9.2\ K;\quad B_{c2}(0) = 14.5\ K;\quad B_{c2}(4.2\ K) = 10.4\ K. \tag{2.37}$$

Besides the magnetic field, the transport current in the superconductor further reduces the allowable temperature in multifilamentary conductors to the so-called current sharing temperature T_{cs}, which is defined by:

$$T_{cs}(B,I) = T_0 + [T_c(B) - T_0]\ I/I_c, \tag{2.38}$$

where T_0 is the reference temperature (4.2 K), I the transport current and I_c the critical current of the conductor. At a temperature exceeding T_{cs} the composite conductor will start to show a resistive behaviour.

In contrast to B_{c2} and T_c, the critical current density J_c at a certain magnetic field and temperature is mainly determined by the metallurgical state of the final conductor, see 2.2.1. Its microstructure should have an optimum amount of flux pinning centres in order to allow a large field gradient in the superconductor. This determines the critical current density in accordance with Maxwell's relation, curl $\bar{B} = \mu_o \bar{J}$.

There is general acceptance of the linear relation between critical current density and temperature at constant magnetic field:

$$J_c(T) = J_c(B)\ [1-T/T_c(B)],\qquad (T>T_0 = 4.2\ K), \tag{2.39}$$

where $J_c(B)$ and $T_c(B)$ are respectively the critical current density at a lower reference temperature (e.g. 4.2 K), and $T_c(B)$ the critical temperature at the constant field B and at $J_c = 0$. There is no theoretical expression that describes the field dependence of the critical current density at constant temperature while covering the

entire range of 0 to 14.5 T. The region of 0 to 4 T in which low-field applications operate, can be described by the empirical relation:

$$J_c(B)_{T=constant} = J_0 \,/\, [1+|B|/B_0], \qquad (2.40)$$

where J_0 and B_0 are constants which are different for each wire since they are determined by the production process rather than by the intrinsic properties of NbTi. In the range between about 4 T and B_{c2} the critical current density usually decreases linearly with the magnetic field:

$$J_c(B)_{T=constant} = J_c(4)\ [B_{c2}-B]/[B_{c2}-4], \qquad (4<B<B_{c2}). \qquad (2.41)$$

The critical current density in Nb_3Sn compared to NbTi is shown in figure 3.7. The qualitative behaviour of the critical current density in both materials is the same. The critical current density versus magnetic field between 5 and 20 T can reasonably be described by Kramer's rule that states $J^{1/2}B^{1/4} \propto B$.

In section 3.2 we will use these properties to design the NbTi and Nb_3Sn coils of the disk MHD magnet system.

2.2.2 Magnet configurations

The number of practical configurations of superconducting magnets that can be used in disk-shaped MHD generators for large and small scale applications are limited. The coil systems found in the literature are solenoids and split-pair magnets, each having their own advantages and disadvantages.

2.2.2.1 Solenoids

One of the main arguments to use a single coil magnet is optimum accessibility of the MHD channel for maintenance and repair. A solenoid placed between combustor and generator channel, as shown in figure 2.4, is a practical solution [2.8-2.11].

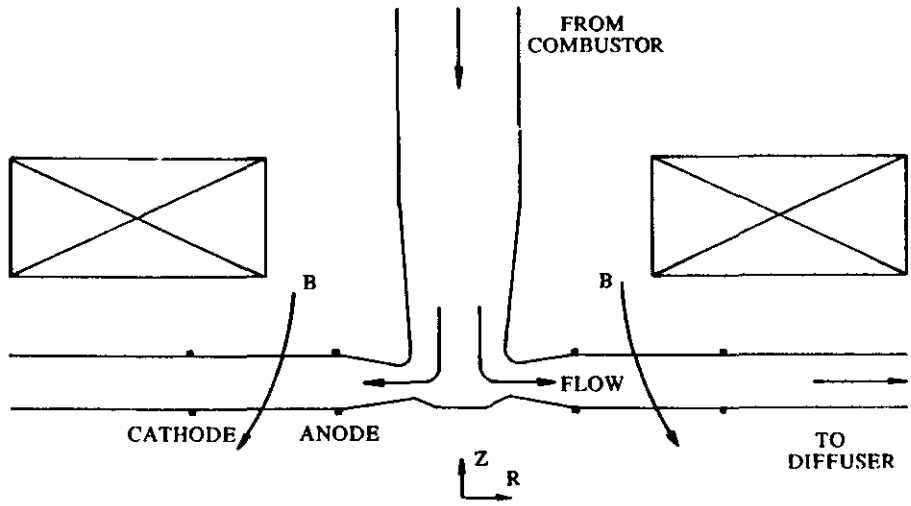

Figure 2.4 Schematic representation of an MHD channel with a single coil magnet.

In a disk MHD generator study Retallick [2.8] considered four slightly different open cycle generators working at a field of 7 T. In order to enhance the field uniformity, the magnet is split into two parts with respectively a low and a high current density. A nearly constant B_z-component between cathode and anode can thus be created. Marston [2.9] in his conceptual design of a space-based MHD generator also proposed a radially increasing current density by subdivision of the magnet in four sections. Optimum use of the magnetic field is obtained by placing an MHD channel at both sides of the magnet. In this case a reduction of weight is the main argument to use a single coil magnet.

A disadvantage of the concept of using a single solenoid is the relatively large component of the radial magnetic field in the MHD channel. This field component introduces undesirable nonuniformities in the plasma velocity in the generator. In order to overcome this adjustment of the channel configuration in such a way that the total field vector is perpendicular to the plasma flow was suggested [2.8]. However, the influence of a curved shape of the MHD channel on a supersonic plasma flow and thus on the performance of the generator has not yet been investigated thoroughly. Another solution to eliminate the radial field component is to place the MHD channel in the plane of symmetry of the single coil [2.10], as shown in figure

2.5. However, the magnetic field in the diffuser section and a large increase of coil volume are major drawbacks of this design.

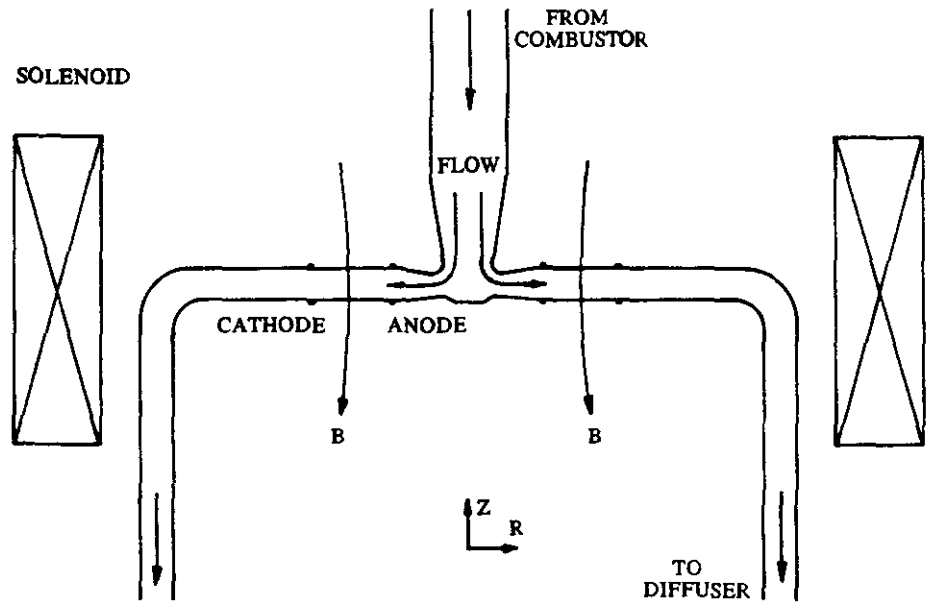

Figure 2.5 MHD channel in the plain of symmetry of a solenoid.

2.2.2.2 Split-pair Magnet

When using a split-pair magnet [2.10-2.12], the MHD channel is placed in the gap between the coils. So the plasma will flow in the radial direction as shown in figure 2.6. The main advantage of the split-pair magnet, compared to the single coil magnet, is the small radial component of the magnetic field in the MHD channel. Also the gradient in the magnetic field component B_z in the direction perpendicular to the plasma flow, is very small. Moreover, a considerably smaller volume of superconductor is required to produce the same field level in the active MHD volume as compared to the case with a single solenoid. This is also an important advantage of the split-pair magnet.

The main problem of using this coil configuration for an MHD disk generator is the support structure that has to handle the attracting electromagnetic forces between the coils. This structure has to penetrate through the disk channel. Therefore the introduction of obstructions in the plasma flow is inevitable. As a consequence, these

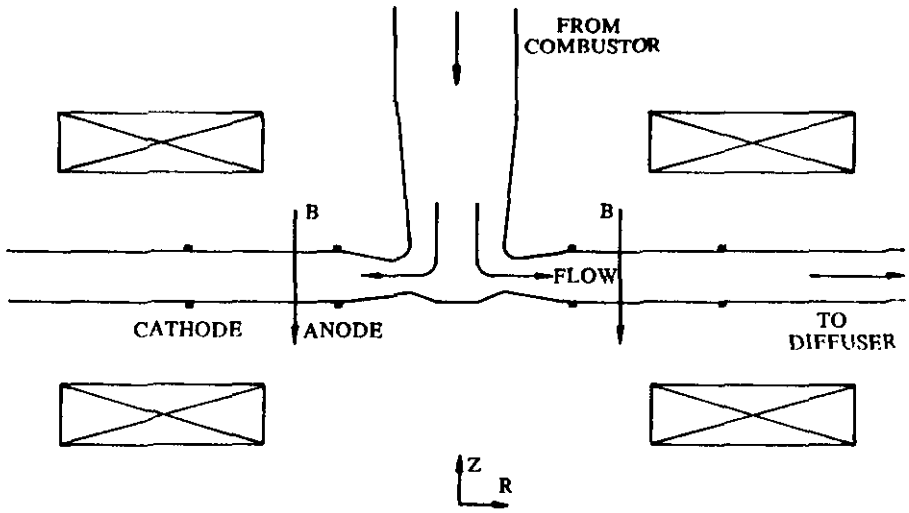

Figure 2.6 Schematic representation of an MHD channel with a split-pair magnet.

force containing structures are complicated and maintenance of the channel becomes more difficult. Besides this, the penetrating struts may enhance the heat load of the magnet cooling system considerably.

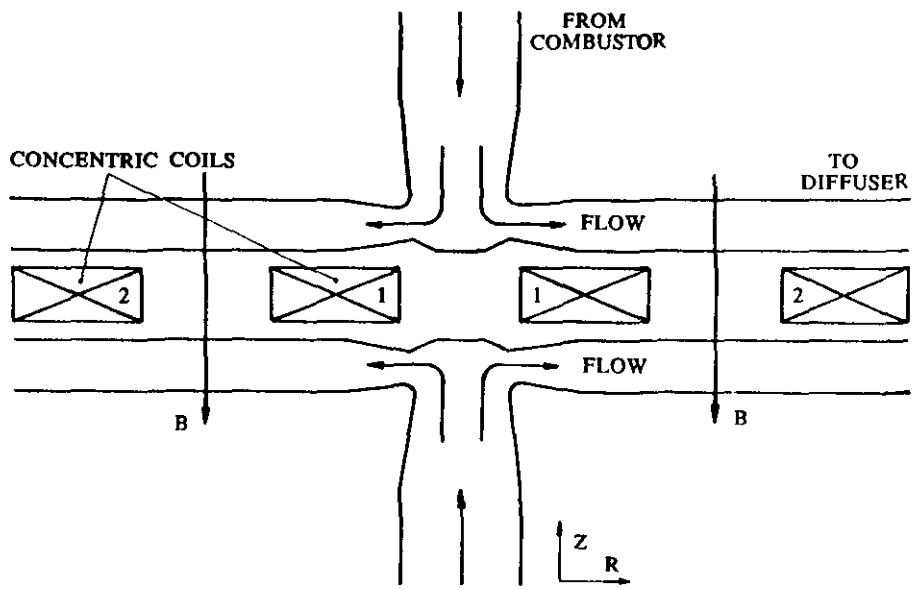

Figure 2.7 MHD channels with a pair of concentric coils.

2.2.2.3 Concentric coils between two channels.

Another solution that was suggested [2.13] is a pair of concentric coils placed between two MHD disk channels as shown in figure 2.7. The

radial field component of such a coil system is small in comparison to a single coil magnet. However, because the direction of the current in both coils has to be opposite, the coils repel each other and a mechanically unstable coil configuration has been created.

2.3 Summary

In this chapter the theoretical aspects of describing the flow through the various types of MHD generators has been discussed. Furthermore a brief introduction to superconducting materials, their properties and the basic magnet configurations for disk type MHD generators have been given.

The presentation can be summarized in the following points:

- the calculation of the flow through the MHD generator uses the same amount of detail for all four types (one-dimensional approximation),
- in all situations a system of coupled ordinary differential equations has to be solved simultaneously,
- the Maxwell equations needed for the calculation of the flow can be simplified drastically due to the MHD assumptions,
- constraints have to be fulfilled in order to obtain realistic solutions,
- applications of superconductors in magnet technology is inevitable for the creation of high magnetic fields,
- the creation of the magnetic field in disk shaped MHD generators can be provided by a single solenoid as well as by split-pair magnets.

3 PREDESIGN OF A DISK DEMONSTRATION UNIT

When this project was initiated it was anticipated that a facility for testing open cycle disk MHD generators could be proposed because this generator type needs the largest development. From the calculations of large MHD/steam systems presented in chapter 5 it turned out that the open cycle disk generator leads to the least attractive system when the coal to bus bar efficiency is considered and the closed cycle disk generator to the most attractive system. Therefore the predesign of a facility for testing a 10 MWt open cycle disk or a 5 MWt closed cycle disk generator will be presented in this chapter. It can be concluded at the same time, however, that further research will be required in order to determine more precisely what causes the limitations of the open cycle disk generator.

The line diagram of the open cycle facility is given in figure 3.1. As will be apparent from this figure an extensive infrastructure is required. It will be clear that this infrastructure is only partly visible from figure 3.1 since for instance the computer system that controls the operation of the facility and the diagnostic and data handling system are not included.

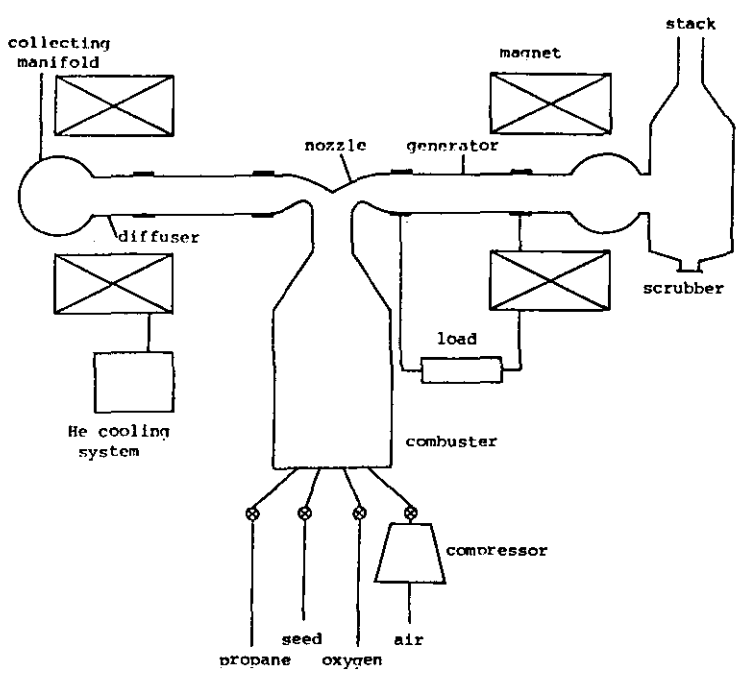

Figure 3.1 Line diagram of a 10 MWt open cycle disk MHD facility.

In the calculations of the 10 MWt open cycle system the fuel is assumed to be coal with directly preheated air. However, for technical simplicity of the test facility the high temperature, high pressure open cycle medium is obtained by the pressurized combustion of propane and oxygen. In a mature, fully developed system such as is considered in chapter 5, coal will be used as the fuel but for an experiment propane, which can be stored in liquid form, is more convenient. Further oxygen enriched air will be used to obtain the required high combustion temperature whereas in the fully developed system a heat exchanger will be used downstream of the MHD generator exhaust to preheat the combustion air.

In both cases the medium is seeded with for instance K_2CO_3 in order to increase the electrical conductivity of the combustion gases.

In the case of a 5 MWt closed cycle disk MHD facility the same line diagram of figure 3.1 can be used since the modifications are small. In the closed cycle case, where the medium is argon, the combustor in figure 3.1 has to be replaced by a regenerative heat exchanger to increase the enthalpy of the medium. In the closed cycle situation the seed material will be pure cesium injected in liquid form.

In both cases (open cycle and closed cycle) the disk generator is placed inside the same magnet. Also in both cases the medium is accelerated to supersonic speeds in a nozzle since the induced electric field and the electrical current are both proportional to the flow velocity. The electrical power which is produced by the disk generator can be dumped in a load resistance as long as the time duration of the experiment is limited. The operation of the disk generator should be such that the flow velocity is still supersonic at the generator exit. In order to convert the kinetic energy of the flow efficiently into potential energy, a diffuser system is then needed before the medium can be collected in a manifold and exhausted into the stack. It should be noted that the nozzle, diffuser system and collecting manifold are indicated in figure 3.1 in a simplified way. These items will be worked out in more detail later in this chapter.

Before the gases exhaust into the stack they are led through a scrubber to cool the gases down and to prevent emission of the seed into the atmosphere.

For the present test facility a superconducting magnet has been chosen which implies the application of a cryogenic system including a helium liquefier. In the remaining parts of this chapter the attention will be focused on the generator system and on the superconducting magnet system only. The remaining, more conventional parts of the infrastructure which have been briefly mentioned above will have to be worked out further in the next step of a detailed design study.

3.1 The disk MHD generator

In figure 3.2 some details of the generator with nozzle and diffusers are sketched. The triangular shapes form the side walls of the supersonic and subsonic diffuser. They also enclose the space through which the struts can support the coils of the magnet system. At the inlet, vanes are indicated to provide the required swirl. The exhausts of the diffusers are collected in a circular manifold. The wall construction which is given in a detail of cross section AA' is built up from ceramic pegs which are bolted to a water cooled glass fibre reinforced epoxy outer casing.

3.1.1 Optimization of the open cycle generator

As mentioned in the previous chapter the 10 MWt open cycle disk channel operates with a constant radial electrical field of 12 kV/m. In the calculations the magnetic field profile is approximated by two straight lines.

One series of calculations is performed with a stagnation temperature of about 2800 K giving very low values of the enthalpy extraction, This is due to the unfavourable surface to volume ratio and the low electrical conductivity . Therefore a second series of calculations is performed with a higher stagnation temperature (3060 K). This results

in higher electrical conductivity leading to higher enthalpy extraction. In each series of calculations the following parameters are varied: The Mach number at the channel inlet M_0 = 1.6, 1.8 and 2.0; the inlet swirl S_0 = 0.6, 0.8, 1.0, 1.5 and 2.0 and the pressure of the combustion air p_{cb} = 4, 5 and 6 bar. The results are given in table 3.1.

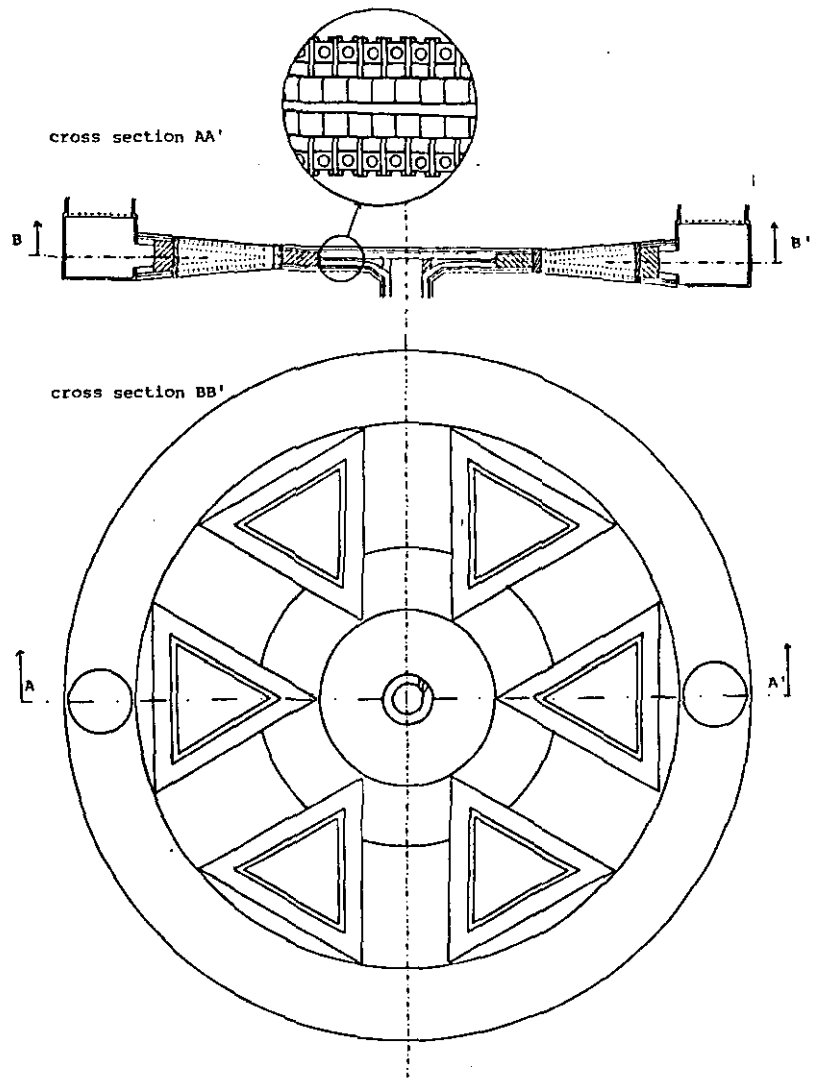

Figure 3.2 The channel (top view and cross section)

Two cases give the best results with respect to enthalpy extraction; one with M_0 = 1.8, S_0 = 0.6 and p_{cb} = 5 bar, and one with M_0 = 1.8, S_0 = 2.0 and p_{cb} = 4 bar, both with a stagnation temperature of about 3060 K. The latter case gives the highest isentropic efficiency of the channel including nozzle and diffusers, and is therefore chosen as the base case.

Table 3.1 Results of calculations performed on the 10 MWt open cycle disk channel. The anode radius is 0.11 m and the constant radial electrical field is 12 kV/m.

			$T_{st} \cong$ 2800 K					$T_{st} \cong$ 3060 K				
M_0 (-)	S_0 (-)	p_{cb} bar	h_0 (mm)	h_{out} (mm)	r_{out} (mm)	η_{ent} (%)	η_{is} (%)	h_0 (mm)	h_{out} (mm)	r_{out} (mm)	η_{ent} (%)	η_{is} (%)
1.6	0.6	4	22	8	390	3.1	18.6	16	9	270	6.2	36.1
		5	17	7	370	2.5	14.6	12	7	270	4.7	29.8
		6	15	6	330	1.8	11.2	10	6	250	3.6	24.3
	0.8	4	24	8	390	3.2	19.0	17	9	270	5.5	36.7
		5	19	7	350	2.3	14.4	14	7	250	4.1	29.7
		6	16	6	330	1.9	11.5	11	6	230	3.0	24.1
	1.0	4	26	8	370	3.2	19.2	19	9	270	5.6	37.0
		5	21	7	350	2.4	14.7	15	7	250	4.2	29.9
		6	18	6	310	1.7	11.2	13	7	210	2.5	23.5
	1.5	4	33	8	370	3.0	19.2	24	9	250	4.9	37.2
		5	27	7	330	2.2	14.5	19	8	230	3.6	30.1
		6	22	6	310	1.8	11.7	16	7	190	1.9	23.2
	2.0	4	41	8	370	3.1	19.5	30	9	230	4.2	37.1
		5	33	7	330	2.2	14.9	24	9	190	2.2	28.1
		6	28	7	290	1.6	11.4	20	8	170	1.3	21.4
1.8	0.6	4	27	11	430	3.0	13.7	18	10	370	8.1	35.2
		5	22	9	510	3.2	12.6	15	8	430	8.7	31.4
		6	18	8	550	3.2	11.2	12	7	430	7.3	26.4
	0.8	4	29	10	450	3.2	14.3	20	9	370	8.2	35.8
		5	24	9	510	3.3	12.8	16	8	410	8.3	31.4
		6	20	8	550	3.2	11.5	14	7	410	7.4	26.9
	1.0	4	32	10	450	3.2	14.6	22	9	370	8.3	36.4
		5	26	9	510	3.3	13.0	17	8	410	7.9	31.2
		6	22	7	570	3.3	11.7	15	7	410	7.1	26.8
	1.5	4	41	10	450	3.3	15.0	28	9	370	8.5	37.4
		5	33	9	510	3.4	13.5	23	8	390	7.5	31.4
		6	26	7	550	3.2	11.9	19	7	370	6.3	26.4
	2.0	4	51	10	450	3.3	15.3	35	9	370	8.7	37.9
		5	41	9	530	3.6	14.2	28	8	370	7.1	31.4
		6	35	7	530	3.1	11.8	24	7	350	5.9	26.5
2.0	0.6	4	35	16	350	1.7	7.4	23	13	350	5.8	24.4
		5	28	14	390	1.7	6.7	18	11	370	5.5	20.8
		6	24	12	430	1.7	6.1	15	11	410	5.7	19.0
	0.8	4	38	16	350	1.7	7.6	25	13	350	5.9	24.9
		5	31	13	390	1.7	6.8	20	11	390	6.0	22.1
		6	26	12	430	1.7	6.2	17	11	410	5.8	19.5
	1.0	4	42	16	350	1.7	7.7	28	13	350	6.0	25.4
		5	34	13	390	1.7	6.9	22	11	390	6.1	22.5
		6	29	12	430	1.8	6.3	19	11	410	5.9	19.8
	1.5	4	54	16	350	1.8	8.0	35	13	350	6.1	26.3
		5	44	13	410	1.9	7.4	28	11	390	6.3	23.3
		6	37	12	430	1.8	6.5	24	10	410	6.1	20.7
	2.0	4	67	16	350	1.8	8.2	44	12	350	6.3	27.0
		5	54	13	410	2.0	7.6	35	11	390	6.4	24.0
		6	45	12	430	1.9	6.7	30	10	410	6.2	21.3

In table 3.2 more details concerning the channel, diffusers and nozzle of the two best cases are given.

Table 3.2 Parameters of the 10 MWt open cycle disk MHD generator for the two cases with maximum enthalpy extraction. The case with the air pressure of 4 bar is the base case because η_{is} is higher.

Combustion parameters:*)				
Coal type	Illinois #6			
Mass flow coal	0.21 kg/s			
Mass flow air	1.8 kg/s			
Mass flow seed (K_2CO_3)	0.04 kg/s			
Air pressure	4	bar	5	bar
Anode parameters:				
Radius	0.11	m	0.11	m
Load factor	0.84		0.88	
Mach	1.8		1.8	
Swirl	2.0		0.6	
Channel height	0.035	m	0.01	m
Electrical conductivity	14.8	1/Ωm	13.2	1/Ωm
Hall parameter	8.9		7.2	
Stagnation temperature	3060	K	3072	K
Static temperature	2568	K	2577	K
Stagnation pressure	3.54	bar	4.42	bar
Static pressure	0.83	bar	1.03	bar
Cathode parameters:				
Radius	0.37	m	0.43	m
Mach	1.1		1.0	
Swirl	0.2		0.0	
Channel height	0.009	m	0.008	m
Electrical conductivity	18.0	1/Ωm	16.6	1/Ωm
Hall parameter	8.6		7.6	
Stagnation temperature	2779	K	2740	K
Static temperature	2589	K	2576	K
Stagnation pressure	1.31	bar	1.24	bar
Static pressure	0.73	bar	0.75	bar
Channel:				
Radial electrical field	-12	kV/m	-12	kV/m
Heatloss through walls	0.74	MW	0.98	MW
Enthalpy extraction	8.7	%	8.7	%
Subsonic diffuser exit:				
Pressure	1.15	bar	1.07	bar
Isentropic efficiency**)	37.9	%	31.4	%

*) Calculations are performed with coal as fuel. In the demonstration unit, however the fuel will be propane.

**) Of generator including nozzle and diffusers.

Also calculations are performed with the constraint that the decrease of the radial Mach number when going through the channel is constant.

In that case the radial electrical field at the anode could be made equal to 12 kV/m by adjusting the load factor. Between the anode and the cathode, however, the field rose up to values above 40 kV/m, which is not allowed due to breakdown.

In figure 3.3 the channel height and various parameters as function of the channel radius are given. In figure 3.4 the influence on the performance of varying parameters around the base case is given. Apparently, the enthalpy extraction is mainly affected by the stagnation temperature.

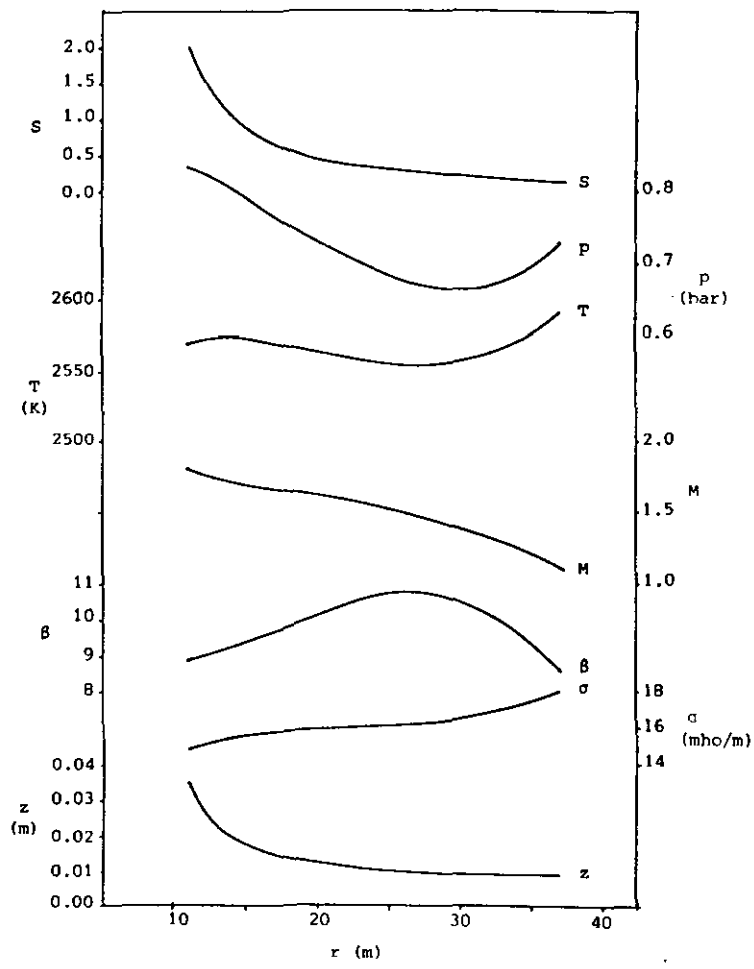

Figure 3.3 Variation of the parameters with the radius for the base case.

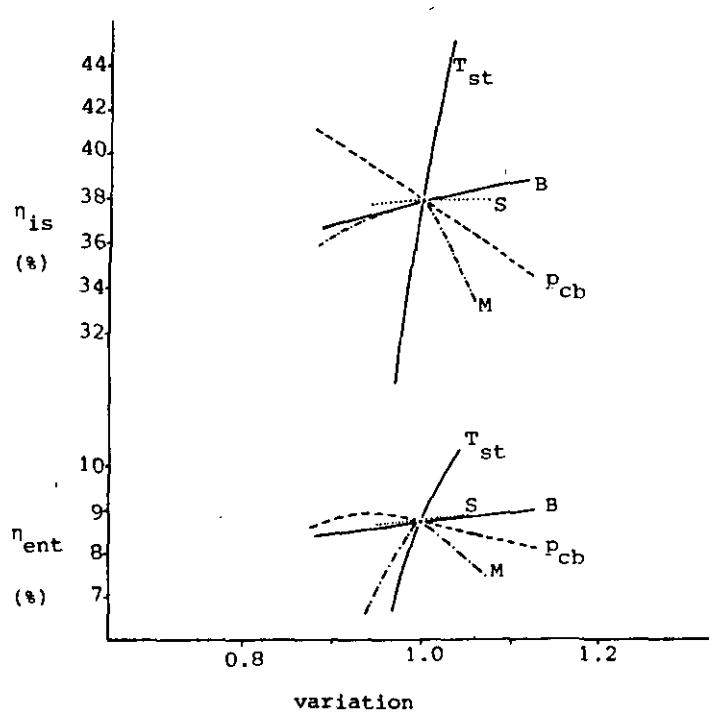

Figure 3.4 Influence of the variation of several parameters on the enthalpy extraction and the isentropic efficiency of the channel including nozzle and diffusers. Horizontally the relative variations of the parameters are given.

3.1.2 Optimization of the closed cycle generator

Besides calculations on an open cycle disk demonstration unit also calculations on a channel for a closed cycle disk generator are performed. The main goal was to compare the performance with the open cycle channel when the dimensions are comparable. The magnetic field is the same as used for the calculations on the open cycle channel, while further constraints are mentioned in section 2.1.2.

Calculations are performed with seed ratios of $5 \cdot 10^{-5}$ and 10^{-4}, inlet stagnation pressures of 5, 6, 7 and 8 bar, inlet swirls of 1.0, 1.5 and 2.0 and inlet Mach numbers of 2.2, 2.4 and 2.6. The results are

given in table 3.3. The highest enthalpy extraction is reached in the configuration with $s_r = 10^{-4}$, $S_0 = 1.0$, $M_0 = 2.2$ and $p_{st,0} = 8$ bar.

Table 3.3 Results of calculations performed on the 5 MWt closed cycle disk channel. The anode radius is 0.11 m. Optimum loading mode ($\alpha = \alpha_{opt}$ for each radius).

				$s_r = 0.00005$				$s_r = 0.00010$			
S_0 (-)	M_0 (-)	p_{st} bar	h_0 (m)	h_{out} (m)	r_{out} (m)	η_{ent} (%)	η_{is} (%)	h_{out} (m)	r_{out} (m)	η_{ent} (%)	η_{is} (%)
1.0	2.2	5	0.029	0.011	0.42	26.2	57.5	0.015	0.29	31.1	67.4
		6	0.024	0.009	0.45	27.5	56.7	0.013	0.31	33.1	67.2
		7	0.020	0.008	0.42	24.5	53.1	0.012	0.32	32.3	65.1
		8	0.028	0.007	0.43	24.6	51.7	0.011	0.32	31.5	63.2
	2.4	5	0.033	0.012	0.39	25.5	55.8	0.017	0.27	29.8	65.2
		6	0.027	0.011	0.43	27.7	56.1	0.015	0.30	33.7	67.0
		7	0.023	0.009	0.45	28.4	55.4	0.014	0.32	35.7	67.1
		8	0.020	0.008	0.45	28.0	53.9	0.013	0.33	35.0	65.5
	2.6	5	0.038	0.013	0.36	24.3	53.2	0.019	0.26	29.5	63.1
		6	0.031	0.012	0.40	26.9	54.5	0.016	0.28	32.3	64.7
		7	0.027	0.010	0.44	29.2	55.3	0.015	0.30	34.8	65.8
		8	0.023	0.009	0.44	28.1	53.5	0.014	0.32	37.0	66.4
1.5	2.2	5	0.036	0.010	0.45	26.2	58.0	0.014	0.31	31.6	68.1
		6	0.030	0.008	0.44	24.4	54.8	0.012	0.33	32.8	66.7
		7	0.026	0.007	0.45	24.6	53.1	0.010	0.32	29.4	62.7
		8	0.023	0.006	0.45	23.8	50.8	0.009	0.34	30.3	61.4
	2.4	5	0.042	0.011	0.42	26.1	57.4	0.015	0.29	31.2	67.4
		6	0.035	0.009	0.45	27.3	56.5	0.013	0.32	34.1	67.8
		7	0.030	0.008	0.45	26.6	54.4	0.012	0.33	33.1	65.5
		8	0.026	0.007	0.45	25.4	52.2	0.011	0.34	33.2	64.0
	2.6	5	0.048	0.012	0.39	25.5	55.9	0.017	0.27	29.9	65.3
		6	0.040	0.010	0.44	28.2	56.5	0.015	0.30	33.6	66.9
		7	0.034	0.009	0.45	28.2	55.3	0.013	0.32	35.4	66.9
		8	0.030	0.008	0.45	27.6	53.6	0.012	0.34	36.9	66.6
2.0	2.2	5	0.045	0.008	0.45	24.1	56.4	0.012	0.33	30.8	66.6
		6	0.038	0.007	0.45	23.0	53.3	0.011	0.35	30.1	63.6
		7	0.032	0.006	0.45	21.9	50.4	0.009	0.31	25.8	58.5
		8	0.028	0.005	0.44	20.1	47.1	0.008	0.28	21.6	53.4
	2.4	5	0.052	0.009	0.45	25.9	57.7	0.014	0.31	31.3	67.6
		6	0.043	0.008	0.45	25.1	55.0	0.012	0.34	33.2	66.6
		7	0.037	0.007	0.45	24.3	52.6	0.011	0.35	31.8	63.7
		8	0.032	0.006	0.45	23.3	50.1	0.009	0.35	30.4	60.8
	2.6	5	0.059	0.010	0.43	26.4	57.6	0.015	0.29	30.8	67.1
		6	0.049	0.009	0.45	26.8	56.1	0.013	0.32	33.6	67.2
		7	0.042	0.008	0.45	26.1	54.0	0.012	0.34	34.7	66.2
		8	0.037	0.007	0.45	25.4	52.0	0.011	0.35	33.5	63.8

More details of this configuration are given in table 3.4. In these calculations it has been taken into account that the closed cycle disk demonstration unit has to be operated as a blow down facility. Therefore the pressure downstream of the diffusers has to equal 1.14 bar.

Table 3.4 Parameters of the optimal 5 MWt closed cycle disk MHD generator.

Thermal input power			4.68	MW	
Mass flow			4.50	kg/s	
Seed ratio			0.0001		
Channel:	Anode			Cathode	
Radius	0.11	m		0.32	m
Height	0.023	m		0.014	m
Mach number	2.6			1.6	
Swirl	1.0			0	
Stagnation pressure	8.0	bar		1.4	bar
Static pressure	0.42	bar		0.29	bar
Stagnation temperature	2000	K		1246	K
Static temperature	615	K		660	K
Electron temperature	4645	K		4753	K
Effective conductivity	91	1/Ωm		122	1/Ωm
Effective Hall parameter	10			20	
Radial electrical field	-1045	V/m		-599	V/m
Load factor	0.96			0.96	
Subsonic diffuser exit:					
Pressure			1.15	bar	
Overall parameters:					
Enthalpy extraction:			37.0	%	
Generated el. power			1.7	MW	
Isentropic efficiency*)			66.4	%	
Heatloss through generator walls			27	kW	

*) of generator including nozzle and diffuser system

In figure 3.5 various parameters as function of the channel radius are given. The influence of the variation of parameters on the enthalpy extraction and on the isentropic efficiency is shown in figure 3.6. When the high value of the effective Hall parameter in table 3.4 is considered too optimistic, the value can be decreased by an increase of stagnation pressure.

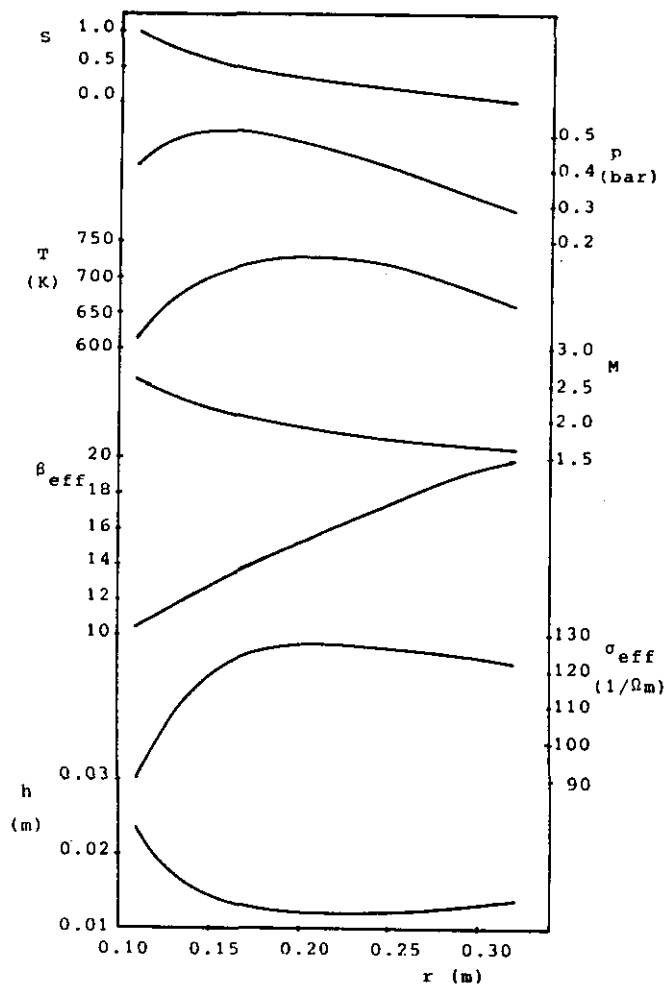

Figure 3.5 Channel height and various parameters as function of the channel radius for the base case.

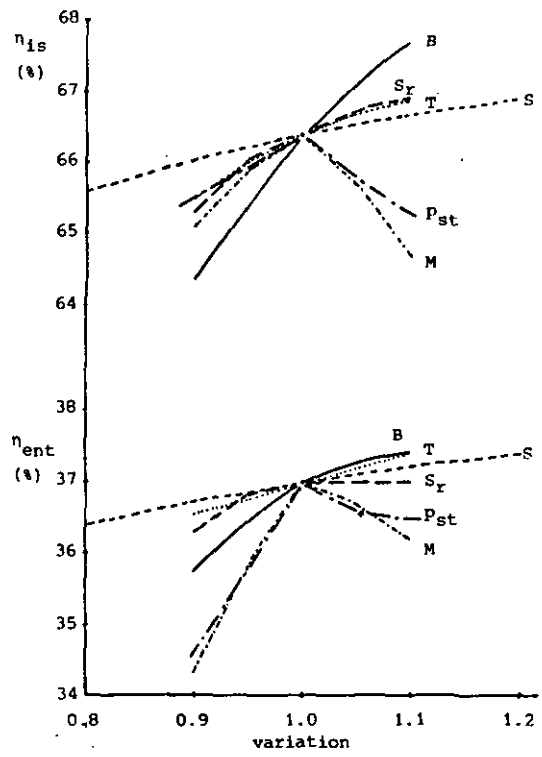

Figure 3.6 Influence of the variation of several parameters on the enthalpy extraction and the isentropic efficiency of the channel including nozzle and diffusers. Horizontally the relative variations of the parameters are given.

3.2 The superconducting magnet system.

In this section we describe the predesign of the coil including the optimization process used . After that we continue with the field analysis, the stress and the strain calculations. Finally basic solutions for the construction of the magnet and its cryostat are presented.

3.2.1. High field superconductors.

Due to the advantages as mentioned in 2.2.1, the split-pair magnet was selected as the most suitable coil configuration. To attain the

desired field strength of 9 T in the active volume of the MHD channel, a magnet system based on NbTi as well as Nb_3Sn technology can be used. Figure 3.7 shows the maximum current density of both superconductors as a function of the applied magnetic field. Cooling down the NbTi to

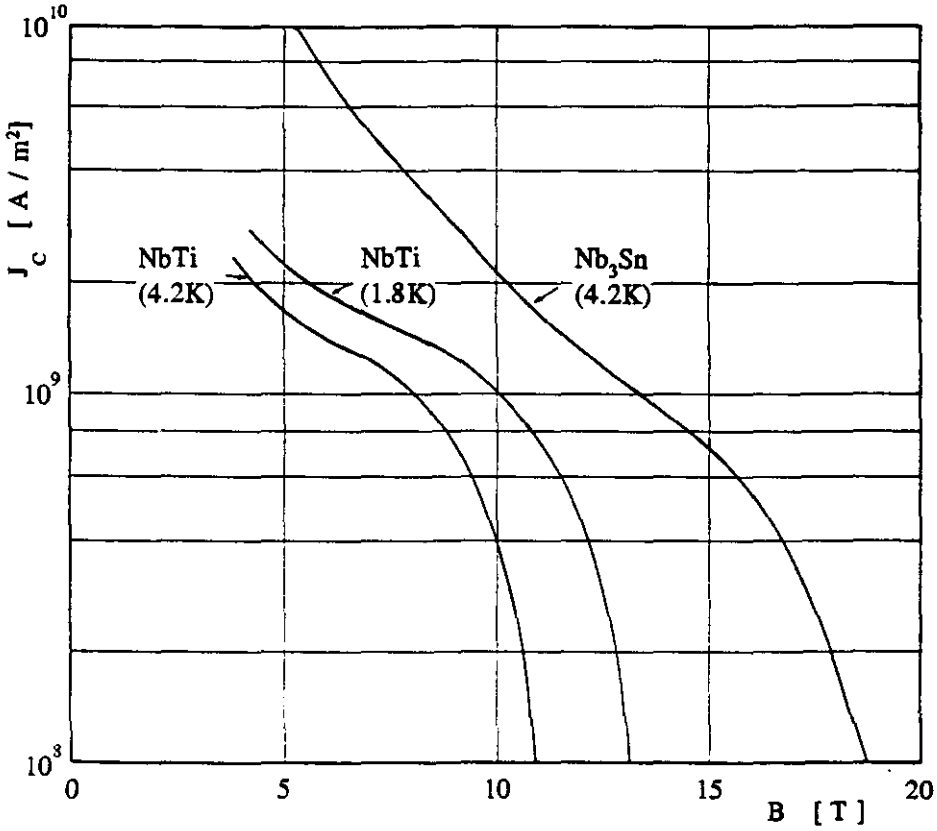

Figure 3.7 Critical current density as function of the magnetic field for NbTi and Nb_3Sn.

1.8 K will increase the critical current density roughly by an order of magnitude in the field range of interest. However this value of critical current density is still about a factor 2 smaller than Nb_3Sn at 4.2 K. Application of NbTi at the mentioned reduced temperature will also put high quality demands on the used superconductor to prevent enhanced cooling power. Nevertheless refrigeration costs will still increase because an additional cooling level is necessary which gives an increased power consumption of 30 to 50 %. We prefer to use 4.2 K cooling which has the consequence that Nb_3Sn has to be used in the high field part of the coil volume.

3.2.2 Coil optimization

The design parameters of the magnet are determined mainly by the dimensions of the channel and the thickness of both the channel insulation and cryostat thermal insulation. Therefore the minimum inner radius and the distance between the split-pair coils are 0.3 and 0.4 m respectively. To attain the desired field strength in the active volume of the MHD channel, the magnet will be split into two sections, a coil of NbTi providing the background field and an insert coil of Nb_3Sn that will enhance the field in the MHD channel up to 9 T. A distance between both coils in the radial direction of 0.03 m is required for the clamping structure of the Nb_3Sn coil and the connections of the helium cooling tubes. The winding volume is determined now by the outer radius of the NbTi part and the coil thickness. The distribution of the winding volume among both sections will introduce an additional parameter. Due to the difference in the costs of the NbTi and Nb_3Sn conductors this parameter can have a large impact on the manufacturing costs of the magnet.

Optimum coil dimensions with respect to minimum conductor costs can be calculated. Here a difference of a factor four between the costs per

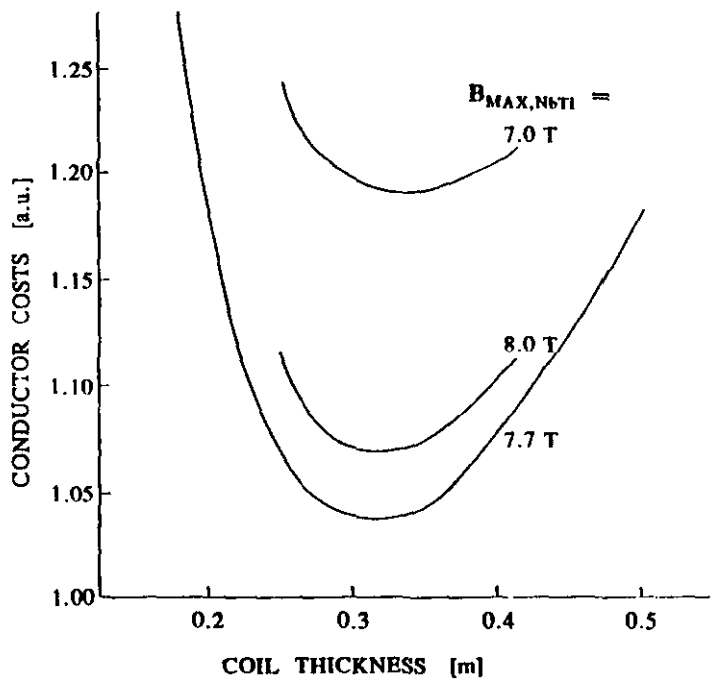

Figure 3.8 Conductor costs versus coil thickness.

unit volume of the composite Nb_3Sn and NbTi conductors has been assumed The mentioned coil parameters are optimized in order to minimize a function including both the design field in the MHD channel and the allowable field $B_{max,NbTi}$ at the inner windings of the outer coil section. The variation of the total conductor costs as a function of the coil thickness thus obtained is shown in figure 3.8. The overall current density in the NbTi coil will decay from 47 A/mm^2 to 33 A/mm^2 for a $B_{max,NbTi}$ varying from 7.0 T to 8.0 T. Here a linear relationship between current density and magnetic field has been assumed. The overall current density in the insert coil is held constant at a conservative value of 31 A/mm^2. A minimum in conductor costs is obtained with a coil thickness of 0.32 m. This value is almost independent of the maximum field at the windings of the NbTi coil. The minimum conductor costs will change dramatically with $B_{max,NbTi}$ as indicated in figure 3.9. A sharp minimum appears at a

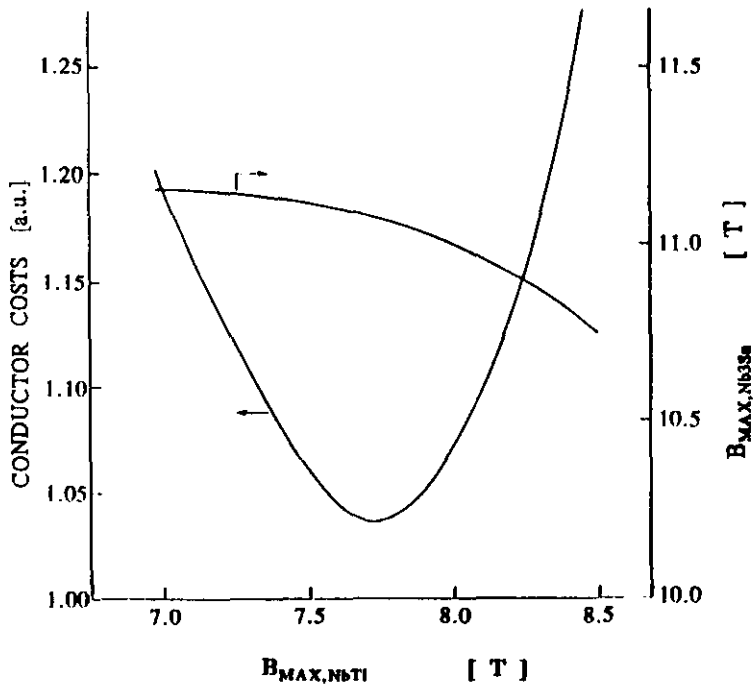

Figure 3.9 Conductor costs versus maximum field at outer coil winding.

value of 7.7 T at an overall current density in this coil section of 37 A/mm^2. This minimum in conductor costs shift to smaller $B_{max,NbTi}$ values if the difference in composite conductor costs between NbTi and Nb_3Sn reduces.

The maximum field at the windings of the insert coil is also included in figure 3.9. A value of 11.1 T at $B_{max,NbTi}$ of 7.7 T is determined and a small decay with increasing maximum field at the background coil windings can be noticed.

3.2.3 Conductor design.

When using Nb_3Sn in the high field section of the magnet, a forced flow cooling with supercritical helium is preferred above bath cooling in order to get a compact rigid coil construction that can handle the high stresses we are dealing with. Additional advantages of this type of cooling are:

- The improved mechanical stability will reduce the possibility of an energy release due to an arbitrary event that can lead to a quench.
- A reduced risk on shorted turns. Due to the internal cooling method the insulation of the conductor will not influence the heat transfer to the coolant.
- Less coolant is necessary in comparison with cooling by immersion.
- Using supercritical helium, the thermal stability will be improved because no reduction of heat transfer to accumulated helium gas in contact with the conductor can occur.

The react-and-wind concept for Nb_3Sn coil fabrication is foreseen because with this method insulation problems of the composite conductor are not to be expected. Furthermore, this method of fabrication prevents degradation of mechanical properties of the composite conductor constituents.

The concept of internally cooled Nb_3Sn and NbTi conductors is adopted after considering the requirements mentioned above. Conductors with forced flow cooling can be classified in tube-cooled and cable-in-conduit conductors. The latter consists of a number of fully transposed strands encapsulated in a stainless steel jacket. A direct contact between strands and coolant provides good heat transfer. In the tube-cooled concept the superconducting cable is in electrical and thermal contact with one or more tubes that will often serve as

conduit and additional stabilization/reinforcement material. Due to the react-and-wind technique, as adopted for this project, bending strain in the Nb_3Sn multifilamentary conductors will be introduced. To limit this strain contribution, the Nb_3Sn layer in the composite conductor must be located at the neutral axis of the conductor and its thickness must be as small as possible. Therefore the tube-cooled conductor in combination with cabled strands in the Rutherford geometry seems more suitable. A good behaviour of these composite conductors is obtained if the cross section has two right-angled symmetry axes so that tension builds up symmetrically [3.1]. Many composite conductor designs that satisfy this conductor profile have been described in the literature [3.2-3.5].

The design values of current density are rather conservative in order to achieve reliable magnet operation. With the winding cross-section of an optimized Nb_3Sn section of 0.32 x 0.194 m^2 and an operating current of 6.13 kA, the deduced dimensions of the composite conductor are 26.7 x 7.5 mm^2. The distribution of available space among the constituents of the composite conductor, as listed in table 3.5, is dictated by the current carrying capacity, the cryogenic stability and the maximum allowable stress in the materials used.

Table 3.5 Distribution of composite conductor constituents.

Composite conductor		Nb_3Sn	NbTi
cross section	[mm^2]	200	165
strand material	[mm^2]	22	25
stability material	[mm^2]	86	85
stainless steel reinforcement	[mm^2]	50	-
coolant	[mm^2]	20	25
insulation	[mm^2]	17	15
solder	[mm^2]	5	15

With the mentioned overall current density in the Nb_3Sn section, the hoop stress in the additional stabilization material of hard copper is limited to 2/3 of its tensile yield strength.

Multifilamentary Nb_3Sn wires of 1.0 mm diameter produced by the "ECN powder technique" [3.6] show an exceptionally high current density. Using this conductor as an example, the thickness of the Rutherford

cable can be limited to 1.8 mm. Application of 28 strands results in a maximum critical current of 13 kA at 4.2 K and 11 T, if no degradation of current carrying capacity occurs. Furthermore as result of the manufacturing process, the stability of this wire is increased in comparison with wires produced by the bronze process, due to the absence of the bronze among the filaments.

The layout of the proposed Nb_3Sn conductor is shown in figure 3.10a. The cable and the copper stabilization parts will be soldered together and encapsulated by a stainless steel conduit with a thickness of 0.8 mm. In order to preserve symmetry the coolant surface is distributed over two channels of 5.3 x 1.8 mm^2 each and is located at both thin edges of the superconducting cable. These channels will be formed by stabilization and stainless steel reinforcement material. The wetted perimeter p of the composite conductor is 28.1 mm and the hydraulic diameter D = 4 A / p will be 2.7 mm.

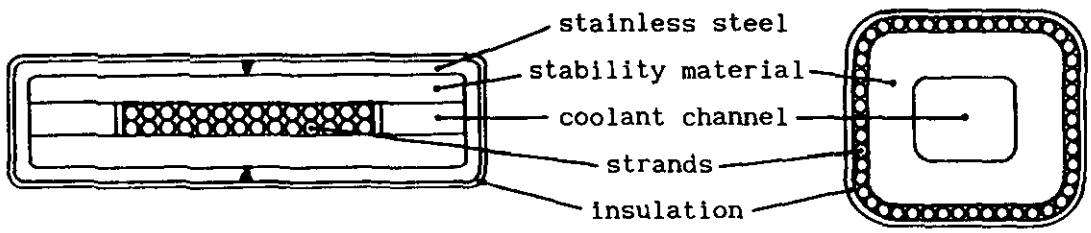

Figure 3.10 Layout of the proposed Nb_3Sn (a) and NbTi (b) composite conductor.

Figure 3.10b shows the internal layout and table 3.5 contains the characteristics of the proposed NbTi conductor. The outer sizes of the composite conductor are 13.3 x 12.4 mm^2. A conduit of cold worked copper with a wall thickness of 3.7 mm, creating a helium channel of 5.7 x 4.8 mm^2, also provides the function of stabilization and reinforcement material. With the given conductor layout, the stress in the stabilization material will not exceed the maximum allowable value assuming no support of the outer windings. Thus additional reinforcement material is not necessary.
Application of 50 strands in the composite conductor, using a common NbTi multifilamentary wire with a diameter of 0.85 mm and a strand

critical current of 250 A at 7.7 T and 4.2 K, leads to a cable critical current of 12.5 kA. At an operating temperature of 4.5 K, this value will be reduced to $I_c(4.5)$ = 10.3 kA. These strands will be twisted and soldered to the outer surface of the copper conduit. The wetted perimeter and hydraulic diameter for this conductor are 21 mm and 5.2 mm respectively.

3.2.4 Magnetic field distribution.

The decay of the axial field component B_z in the radial direction, when both sections are energized, is shown in figure 3.11. In the centre of the MHD channel this field is 9.05 T. At the anode of the disk generator this field is 9.0 T and will decrease to about 7 T at

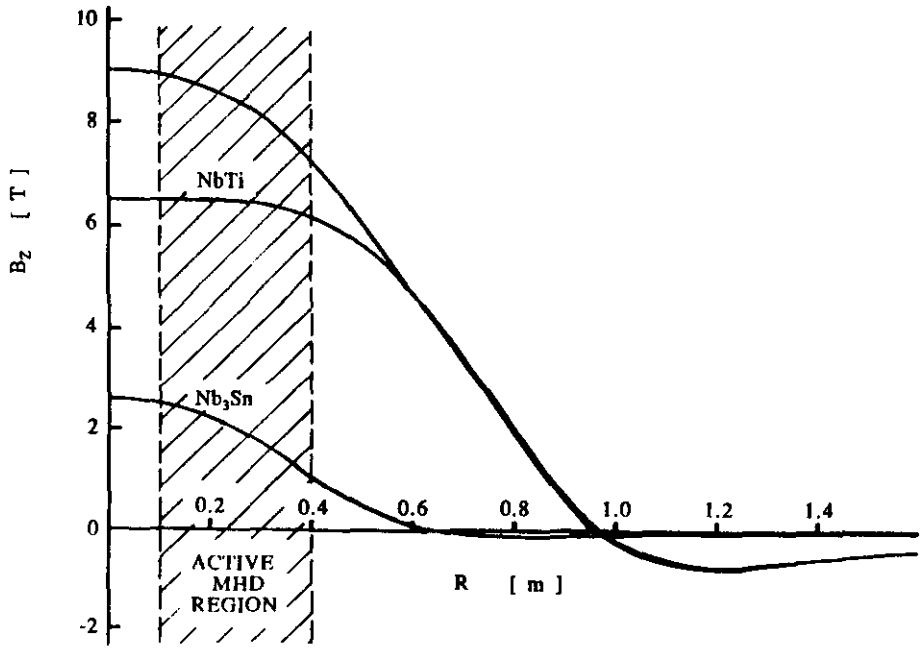

Figure 3.11 Field distribution as a function of radius in the centre of the MHD channel.

the position of the cathode. The maximum radial field component that will occur in this part of the MHD channel, is limited to 0.2 T. The field distribution due to the separate sections is also shown in figure 3.11. The contribution of the NbTi section to the total axial field component between anode and cathode shows only a small reduction of 4.8 %. Thus energizing the sections separately, provides the

possibility to investigate the influence of the field inhomogeneity on the performance of the disk generator.

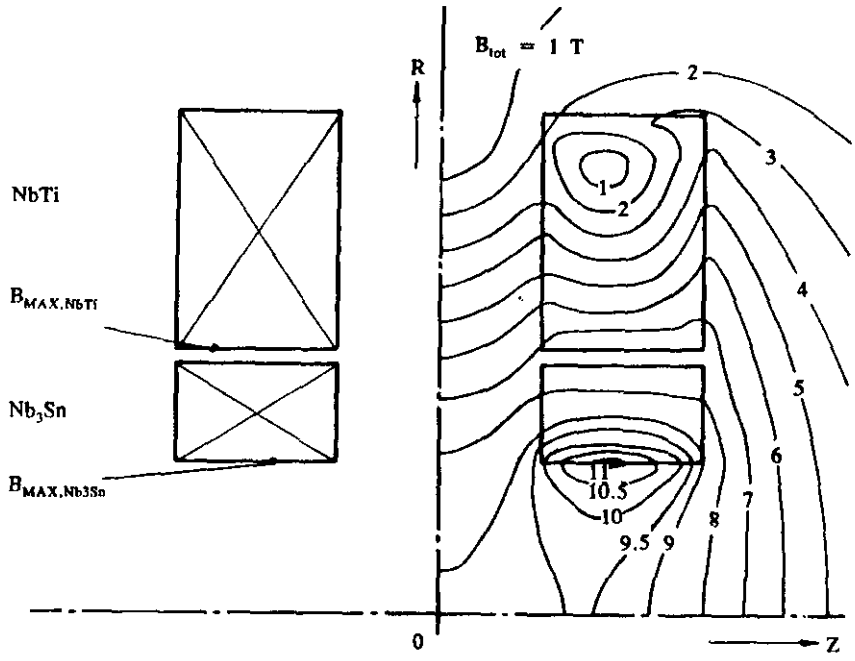

Figure 3.12 Magnetic field distribution at operating current.

The lines of constant magnetic field in the coil sections and the surroundings are shown in figure 3.12. The peak field in the Nb_3Sn section of the split pair magnet is 11.1 T. This field occurs near to the centre of the innermost windings and decays to 7.0 T at the outer edge of this section. The maximum magnetic field at the NbTi coil is 7.7 T and occurs also at the inner windings as indicated.

3.2.5 Stress behaviour.

One of the major disadvantages of using multifilamentary Nb_3Sn in magnet technology is that the current carrying capacity is affected considerably by strain. This degradation effect will be enlarged with increasing magnetic field as is shown in figure 3.13. Uniaxial strain in the superconducting windings will mainly be caused by pre-tension of the conductor during coil fabrication, by radial expansion and mutual attraction of the coil parts due to Lorentz forces and by internal forces. The latter are introduced by fabrication of the

conductor and by differences in thermal contraction of the composite materials after cooling the magnet down to liquid-helium temperature. This internal stress is compressive for the superconducting filaments which usually results in a prestrain in the range 0.1 to 0.3 % [3.7].

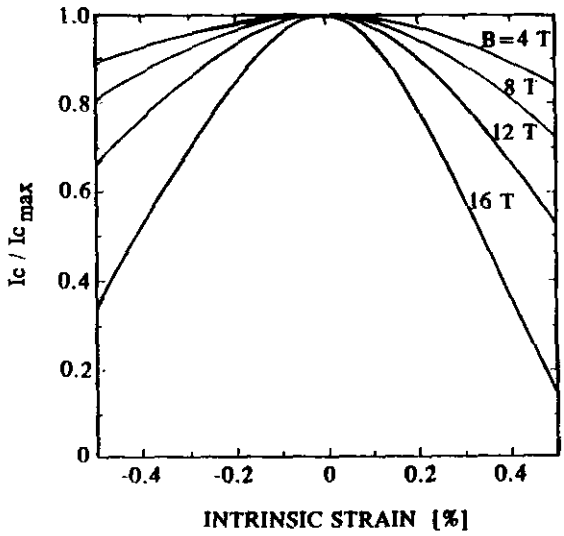

Figure 3.13 Reduction of the critical current in multifilament Nb_3Sn versus the intrinsic strain as function of the magnetic field.

The windings of the sections experience a Lorentz force that will be balanced by a tensile force in tangential direction of $F = I \cdot B \cdot R$. From the calculated fields and sizes of the Nb_3Sn section it becomes clear that the forces acting on the windings are almost constant going from the inside to the outside of the coil section, so the inner turns will not be supported by the outer turns. The tangential stress caused by the radial Lorentz force was calculated using a layer model [3.8]. The composite conductor is modelled by layers alternately carrying current. A cable thickness (current carrying layer) of 1.8 mm and a stabilizer /reinforcement layer (non current carrying layer) of 5.7 mm was assumed. When using the following material properties

- $E_{\text{stainless steel}}$ = 210 GPa,
- $E_{\text{cold worked copper}}$ = 154 GPa,
- $E_{\text{Nb3Sn multifilamentary conductor}}$ = 60 GPa,
- Poisson ratio = 0.33,

a stress level in the Nb_3Sn cable of 110 MPa was found. The calculated

stress in the additional copper stabilizer is 260 MPa which is roughly 2/3 of the tensile yield strength of cold-worked copper. The stress in the stainless steel reinforcement layer is 360 MPa. The maximum strain due to the hoop stress is limited to 0.17 %.

The attracting body force between the coil parts of the split-pair magnet as a function of the radius is shown in figure 3.14. The total force that has to be absorbed by the containment structure is 28 MN. For global computation of the bending of the side flanges of the magnet, which are part of the containment structure, the body force is assumed to act at a distance R = 0.72 m.

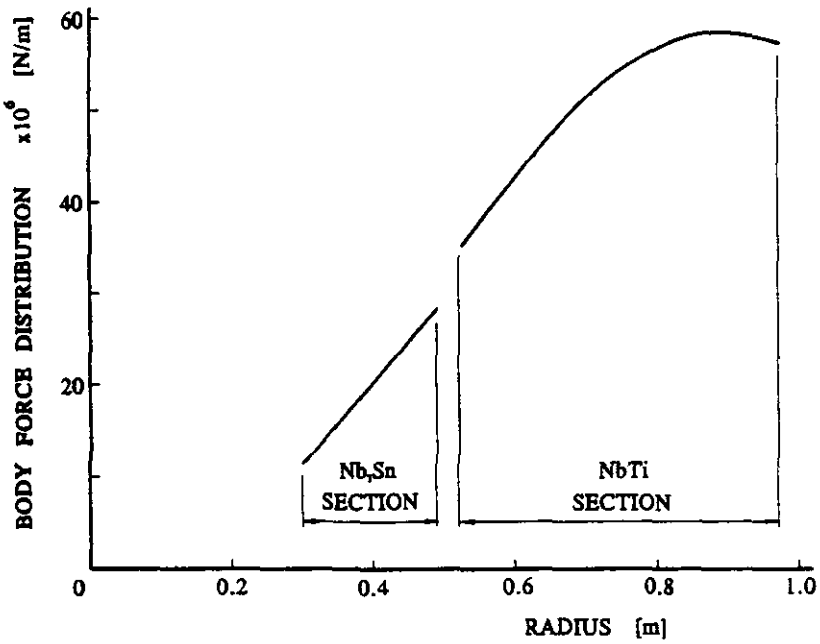

Figure 3.14 Attracting body force between the coil parts as function of the radius.

Solving the Saint-Venant's equations for a curved beam [3.9] the displacement out of its initial plane of these side flanges can be found. This displacement can introduce an additional stress in the conductor. The strain as function of the thickness of the stainless steel flanges and the number of supporting rods N is shown in figure 3.15. A rectangular cross section of the side flanges has been assumed for this calculation.

The total uniaxial strain in the conductor when the magnet is energized is a combination of the mentioned effects. We attempt to

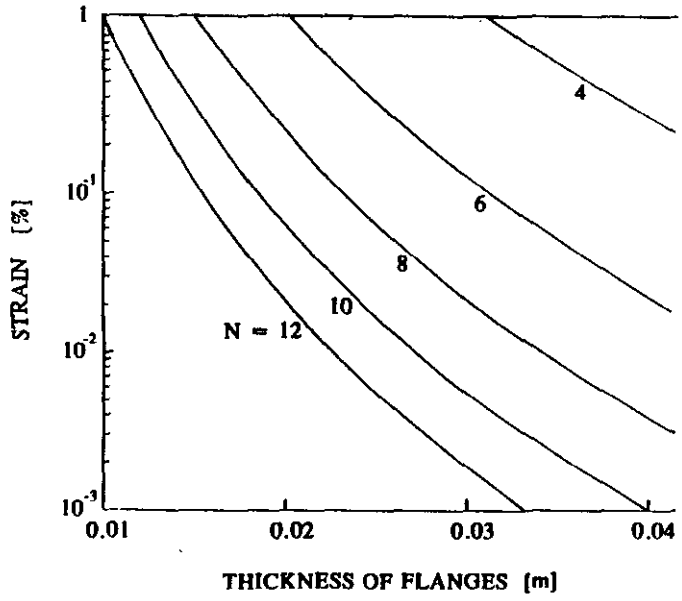

Figure 3.15 Strain introduced by bending of the side flanges due to attractive body force as function of the flange thickness.

reach a situation in which the sum of these strain effects is negligibly small because, at a field of 11 T, a uniaxial intrinsic strain of 0.2 % reduces the maximum current density of Nb_3Sn multifilamentary conductors with 10 % . Besides this, an increase of strain with 0.1 % will cause an additional degradation in the current carrying capacity of roughly 10 %. Due to filament fraction the irreversible strain point above which permanent degradation occurs is reached between 0.4 and 0.7 % [3.7].

Maximum bending strain ε_b will appear at the inner windings and can be given by the relation $\varepsilon_b = h / (2 R_{in})$, where h is the cable thickness and R_{in} the inner radius of the coil. If bending strain is present, the maximum in the characteristics shown in figure 3.13, can not be achieved. This situation is not changed if the tensile component of the uniaxial strain is compensated by the compressive part. In this case degradation of the critical current density in the conductor is inevitable. The extent of this reduction is also dependent on magnetic field as becomes obvious in figure 3.16. Here I_c degradation is shown as function of magnetic field and bending strain. With the assumed cable thickness a bending strain of 0.3 % is calculated for our coil

design. The maximum field at the windings is 11.1 T so we have to accept a degradation of the critical current of at least 5 %.

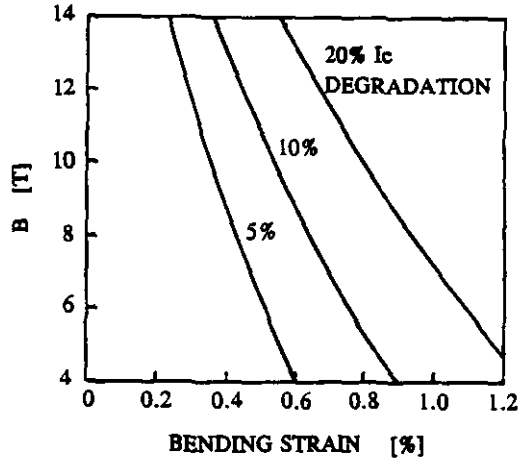

Figure 3.16 Reduction of critical current due to bending strain in Nb_3Sn filaments as a function of magnetic field [3.7].

An additional source of stress related current degradation in Nb_3Sn is transverse stress. The impact of this stress component on the maximum current carrying capacity of multifilamentary Nb_3Sn conductors is investigated in the last four years [3.10-3.11]. It has been shown that transverse compressive stress of about 70 MPa can lead to a reduction of the critical current of approximately 10 % at 10 T and about 30 % at 100 MPa. This degradation effect is field dependent and almost reversible. In comparison to critical current degradation due to axial stress, this effect is about an order of magnitude larger. In our design a maximum transverse stress in the Nb_3Sn section of roughly 10 MPa will be created by the attractive body force at the outer radius, as can be calculated from the body force distribution curve in figure 3.14. This stress value will lead to a negligible current degradation of less than 1 %. In general, transverse stress is not dominating and degradation effects due to this component, in small magnets wound from single wired multifilamentary conductors, will therefore be limited. However, in large magnets where cabled conductors must be used, large stress concentrations at cross-over points can occur. The impact of these local stress centres on the current carrying capacity of the superconducting cable has not yet been investigated.

The effects of strain on NbTi due to bending stress and uniaxial stress are relatively small. For instance, a uniaxial strain of 1 % in a NbTi multifilamentary conductor leads to a critical current degradation of 5 % maximum only. Transverse compressive stress also causes a very limited current reduction [3.12]. Therefore, stress effects in magnets using NbTi technology are in general not a serious problem. Due to this limited sensitivity of NbTi to strain, no stainless steel as reinforcement material is applied. Instead, the copper conduit will be used for strengthening the composite conductor. Lorentz forces introduce now a maximum hoop stress in this conduit of 200 MPa. This value is rather pessimistic since it will be reduced because the outer windings support the inner layers. Using the mentioned value, the yield strength of the copper must be enhanced to 300 MPa by cold work (>7 %).

3.2.6 Coil construction

To generate a field strength of 9 T in the centre of the MHD channel, the optimized Nb_3Sn and NbTi coil sections need $3.8 \cdot 10^6$ and $10.6 \cdot 10^6$ ampere-turns respectively. Coil dimensions and supplementary parameters of the split-pair magnet, defined at the operating current level of 6.13 kA are collected in table 3.6. Both conductors have their operating point substantially below the critical current, thus reliable long term operation can be expected.

Using forced flow cooling, it is advantageous to apply the double pancake winding technique. With this winding method the coil is build up from relative small modules that can be handled easily.

Nb_3Sn-section

The number of windings in this section of each coil part will be 312. Using the dimensions of the conductor and an optimized winding volume, the Nb_3Sn section will be composed of 6 identical double pancakes consisting of 26 layers each. The total length of conductor used for one double pancake is 131 m.

Table 3.6 Parameters of the magnet system for the MHD disk generator.

Section		Nb_3Sn	NbTi
Winding inner radius	[m]	0.300	0.524
Winding outer radius	[m]	0.494	0.972
Coil thickness	[m]	0.320	0.320
Number of turns per coil		312	864
Mean current density	[A/mm^2]	31	37
Maximum field	[T]	11.1	7.7
Operating current	[kA]	6.13	6.13
Self inductance of each pair	[H]	1.445	
Mutual inductance between coil pair	[H]	0.377	
Self inductance coil system	[H]	3.644	
Stored energy total magnet	[MJ]	68.5	
Number of double pancakes		12	24
Number of layers		26	36
Weight of bare magnet	[kg]	11. 10^3	
Weight of cold mass	[kg]	13. 10^3	

Electrical joints located at the outer radius of the section will inter connect the pancakes. The resistance of one joint is estimated at 1 nΩ, thus the contribution of these joints to the total resistance in the electrical circuit will be 14 nΩ.

NbTi-section

All sections are connected in series thus the operating current in the Nb_3Sn and NbTi section will be the same. Therefore, each NbTi section must contain 864 turns in order to obtain the required number of ampere-turns. These turns will be distributed over 12 double pancakes with 36 layers with a total conductor length of 4062 m. A total of 26 joints in both NbTi sections will add 26 nΩ to the total electrical resistance.

3.2.7 Support struts

The entire magnet will be supported by six struts. These struts have to carry the weight of the magnet and the containment structure. The total weight of the cold mass is estimated at $13 \cdot 10^3$ kg. To reduce the heat leak, the thermal path must be as long as possible. The realization of this demand in combination with a limited height of the

struts can be obtained by using two concentric cylinders of G-10 fiber glass epoxy interconnected by a third cylinder of stainless steel, as shown in figure 3.17. The G-10 cylinders are connected between the temperature intervals 300-80 K and 80-4.5 K. The G-10 cylinders will only be exposed to compressive stress. The N_2-radiation shield is connected to the stainless steel cylinder. In order to minimize the heat conduction through the G-10 material into the cold mass, the position of this shield in the strut is calculated. A ratio of 0.45 is found for the length of both G-10 cylinders. The assumed thicknesses of the G-10 cylinders is 5 mm.

3.2.8 Steady-state heat load

The cold mass which consists of the coils, the containment structure and the circular helium dewar, will be located in a vacuum vessel. The cold mass is surrounded by a thermal shield as shown in figure 3.17 in order to intercept conducted and radiated heat coming from the MHD channel, the walls of the vessel and the supporting struts.

The heat load estimated for the thermal shield, which is cooled by liquid nitrogen flowing through cooling tubes in close contact with this shield, is 180 W. A refrigeration flow of liquid nitrogen of 0.9 g/s is necessary to achieve a continuous and stable cooling of the shield at 80 K.

The magnet will be energized by a current supply located outside the vacuum vessel; thus current leads connected between the cold mass and the surroundings have to transport the magnet current. Besides the heat load due to conduction there is also ohmic dissipation in the current leads. Both mechanisms have contradictory demands with respect to the cross section of the leads. The minimum heat load at the cold terminal of commercially available counter flow current leads is about 1 W/kA thus leading to a heat load of 12 W minimum. These leads have to be cooled by a helium gas flow rate of 0.3 g/s.

The steady state thermal loads for the cold mass are collected in table 3.7. The contribution of the current leads to the total heat

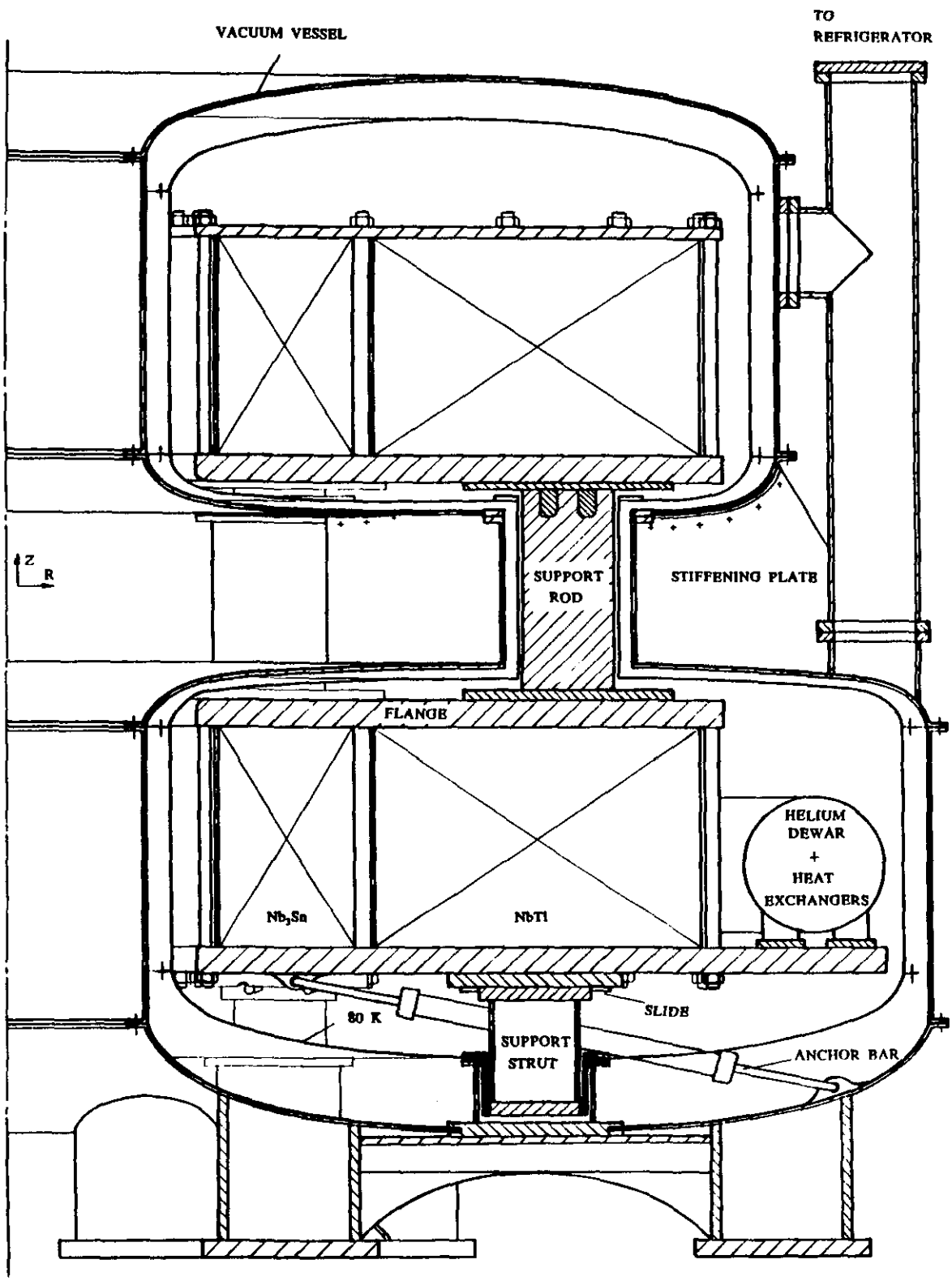

figure 3.17 Location of the cold mass in the vacuum vessel (cross sectional view).

load is considerable. In order to limit these cryogenic losses, it is desirable to avoid application of more than one pair of vapour cooled current leads, thus all coil sections are connected in series. The current leads are connected to the NbTi-section. Thus the heat flux into the helium from the NbTi and Nb_3Sn sections are approximately 90 and 60 mW/m^2 respectively. Starting from the estimated dissipation a cooling power of 20 W at 4.5 K should be sufficient.

Table 3.7 Sources of cryogenic loss at 4.5 K.

Current leads	12.0 [W]
Radiation from LN2-shield	1.3 [W]
Joints	1.4 [W]
G-10 supporting struts	1.4 [W]
Others	2.0 [W]
Total loss at 4.5 K	18.1 [W]

3.2.9 Cooling technique

Supercritical helium circulates through the coils and through the heat exchangers. The latter ones, used to recool the coolant, are positioned in a circular dewar which contains liquid helium at 4.5 K. A helium flow from the upper coils to the heat exchangers is obtained by a cryogenic transfer line connected to both parts of the vacuum vessel. Downstream, the helium will expand in a Joule-Thomson valve and liquid and vaporized helium return to the circular helium dewar.

Both conductors include hydraulically smooth tubes. In this case the Fanning friction factor as a function of the Reynolds number $Re = \rho uD/\eta$ can be described by [3.13]

$$f = 0.079\ Re^{-0.25}. \qquad (3.1)$$

It can be shown that the pressure and temperature gradient over the length of the tube, under steady state conditions and for flow velocities of the compressible helium of less than 10 m/s, can be written as [3.13]:

$$\frac{dp}{dx} = \frac{-2\ G^2\ f}{\rho\ D} + \frac{4\ q\ G\ \beta}{\rho\ D\ C_p}\ , \qquad (3.2)$$

$$\frac{dT}{dx} = \frac{4\ q}{G\ D\ C_p} - \frac{2\ G^2 f\ (\psi + u^2\kappa/C_p)}{\rho\ D}\ , \qquad (3.3)$$

where G is the specific mass flow rate, q is the heat flux, β is the expansion coefficient, κ is the compressibility and ψ is the Joule-Thomson coefficient. With a mass flow rate of the supercritical helium through the Nb_3Sn and NbTi section of 2.0 and 4.7 g/s respectively, the pressure drop is 0.30 kPa per meter of channel for both sections.

NbTi-section

When connecting 6 double pancakes hydraulically in series, the total pressure drop will be 0.6 MPa. A total of 4 parallel cooling channels in both NbTi sections are foreseen. Each channel starts at the plane of symmetry at the outer radius of a section. The inlet pressure is 1.5 MPa at a temperature T_0 of 4.5 K.

In order to limit the dissipation in the coils, the temperature should not exceed the current sharing temperature of 4.86 K as given by equation 2.38. Beyond this temperature the multifilamentary conductor exhibits a resistive behaviour. This means that in each flow channel interim cooling has to take place after passing two double pancakes. Before entering into the heat exchangers, both channels of a section will be joint together.

Nb_3Sn-section

All pancakes of the Nb_3Sn section are connected hydraulically in series. The conductor length is 1560 m and the pressure drop is 0.47 MPa. Interim cooling of the helium to 4.5 K takes place three times. Supercritical helium of 4.5 K will enter at the midplane of the section. Inlet and outlet connections are located at the outer radius of the coil section.

3.2.10 Stability and current margin.

The cryogenic stability parameter α as formulated by the Stekly criterion is determined by application of the Dittus-Boelter turbulent heat transfer correlation [3.13]. With the assumed mass flow rate and the resistivity for cold work copper used in the NbTi and Nb_3Sn conductor of 5.6 and $9.4 \cdot 10^{-10} \Omega m$, values of 4.8 and 1.9 for the NbTi and Nb_3Sn coils respectively are found. Especially the calculated α-parameter for NbTi indicates a substantial deviation from cryogenic stability. However, because no axial heat conduction is included, the Stekly criterion leads to a very conservative design. As a consequence, many medium size magnets work far below the level of full cryostability of α=1, see (2.34).

Figure 3.18 shows the load lines of the magnet. The critical current data for the Nb_3Sn composite conductor are based on the short sample characteristics of the proposed conductor. To obtain the characteristic of the assumed NbTi composite conductor, a common value of 2.0 kA/mm^2 for the critical current density at 5 T and 4.2 K is used.

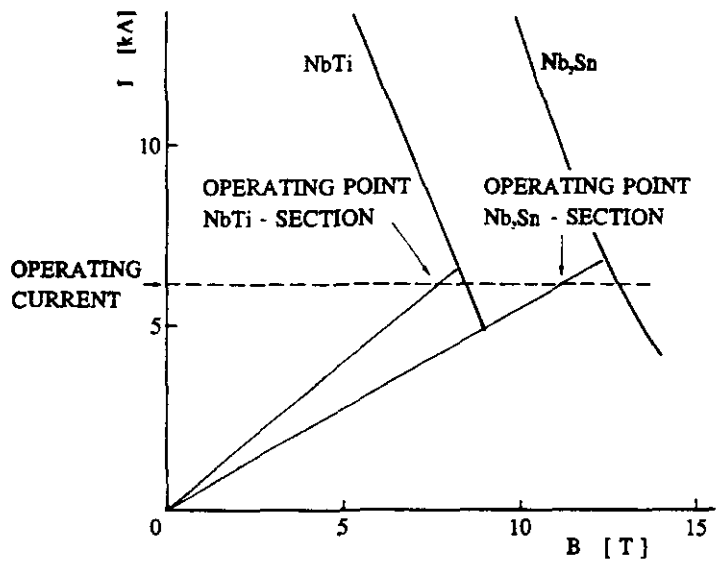

Figure 3.18 Load lines of the magnet.

When the magnet is energized, the ratios of the nominal current to the critical current for the NbTi section and Nb_3Sn section are 0.72 and 0.62 respectively. A degradation of the critical current due to stress effects and cable manufacturing of 20 % is assumed for both conductors.

3.2.11 Electrical circuit diagram

The magnet requires a power supply of 60 kVA. At a maximum voltage of 10 V the time needed to energize the magnet is about 0.6 hr. During operation of the MHD demonstration unit this supply unit is connected to the magnet. In figure 3.19 the electrical circuit of the magnet system is shown. In the case of a quench, protection of the magnet is

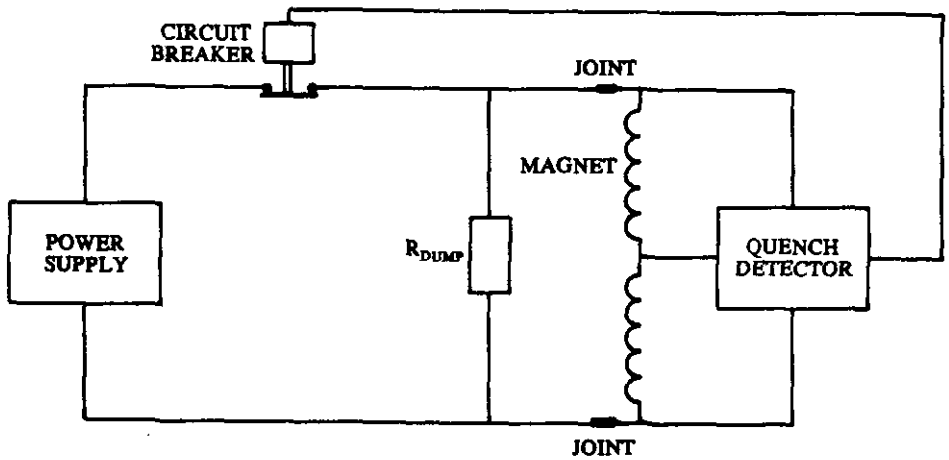

Figure 3.19 Electrical circuit.

obtained by disconnecting the power supply from the magnet system. This is obtained by a circuit breaker that will be activated by a quench detector. After disconnecting the power supply the magnet will be discharged over a water cooled dump resistor of 0.8 Ω located outside the vacuum vessel. The peak discharge voltage that will appear during a quench is limited to 5 kV.

3.2.12 Coil assembly

The Nb_3Sn and NbTi pancakes will be vacuum impregnated separately with epoxy resin. The coil sections will be formed by the pancakes stacked upon a stainless steel cylinder. At the outer radius of the Nb_3Sn section a clamping structure is foreseen. After connecting the pancakes electrically in series, both concentric sections are clamped between two stainless steel flanges. The flanges in face of the MHD channel are part of the containment structure. In the lower part of the vacuum vessel the supporting rods of the containment structure are

welded to the magnet flange. In the upper part of the vacuum vessel the connections between the supporting rods and magnet side flange will be made by dowel pins. Access to the MHD channel can be realized by removing the upper coil part.

The cold mass will be anchored by a total of four anchor bars connected between the lower magnet flange and the vacuum vessel. Springs in these anchor bars facilitate thermal shrinking. The connection between the magnet flange and the struts are made by means of sliding contacts.

The anchor bars of the coil parts form, together with the current leads and the struts, the connections between the cold mass and the vacuum vessel at 300 K.

Figure 3.20 shows an impression of the outside of the vacuum vessel. Rigidity will be enhanced by stiffening plates located at the sides of each MHD channel outlet.

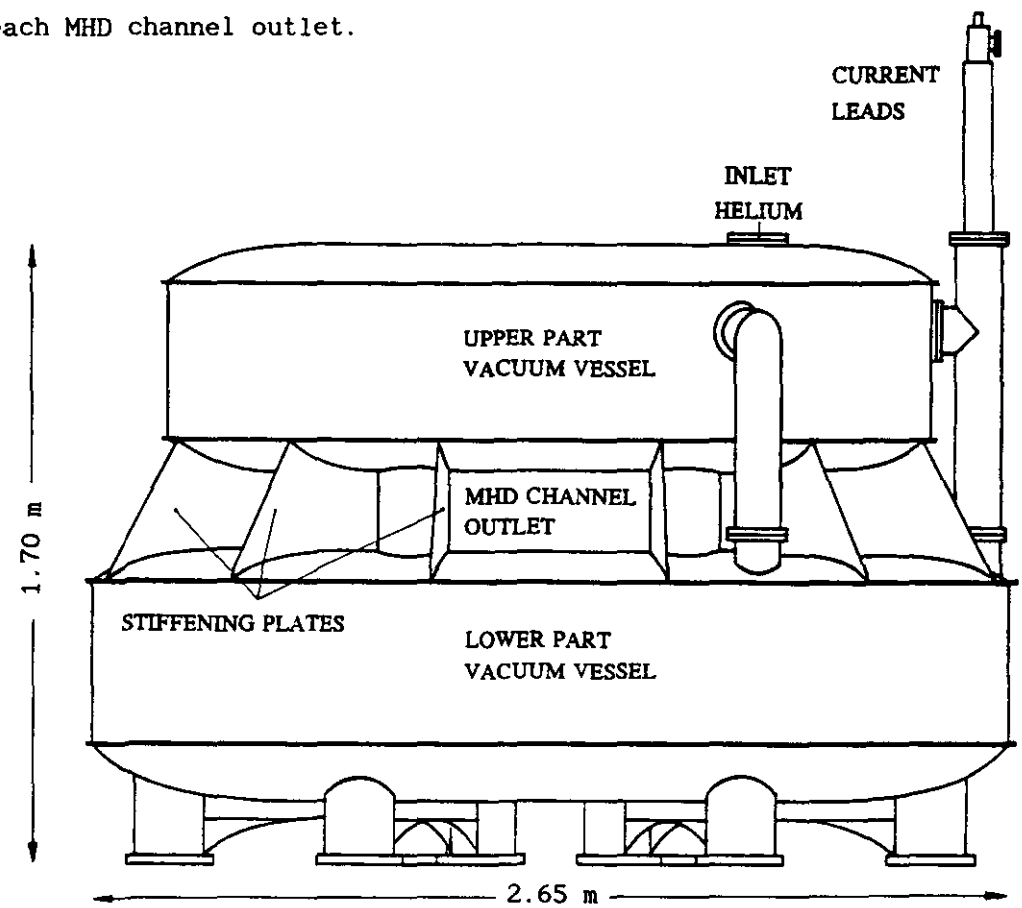

Figure 3.20 Outside view of the vacuum vessel.

3.3 Summary

In this chapter the predesign of an experimental MHD disk facility has been worked out. Both open cycle and closed cycle disk generators have been considered since the first type needs further development efforts but the second type is the most attractive MHD system with respect to efficiency (see chapter 5). A superconducting magnet for the experimental facility has been designed according to the same principles that could hold for commercial (1000 MWt) systems. An iterative procedure has been followed in designing the open cycle disk generator and the required superconducting magnet. After that the size of the warm bore of the superconducting magnet has been used as a constraint in designing the closed cycle disk generator. The calculations have led to the following conclusions:

- in order to reach reasonable enthalpy extractions for the open cycle disk generator at the 10 MWt scale the stagnation temperature had to be increased significantly from 2800 to 3060 K (table 3.1),
- an increase in isentropic efficiency is obtained by a decrease in pressure from 5 to 4 bar (table 3.2),
- despite the optimization, the enthalpy extraction of the open cycle disk is limited to 8.7 % and the isentropic efficiency to 37.9 %,
- the closed cycle disk is tested also in a blow down mode and therefore also fulfills the constraint that the pressure downstream of the diffusers equals 1.14 bar,
- the closed cycle disk leads to much better performance i.e. an enthalpy extraction of 37.0 % and an isentropic efficiency of 66.4 %,
- the split-pair magnet was selected as the most suitable coil configuration,
- due to the high field value of 9 T in the centre of the MHD channel the magnet volume will be split into a NbTi and a Nb_3Sn section,
- optimization with respect to minimum conductor costs has been worked out,
- cooling of the magnet to 4 K will be realized by forced flow of supercritical helium, and
- full cryogenic stability is not pursued for both sections. Stekly parameters of 4.8 and 1.9 for the NbTi and Nb_3Sn sections are obtained.

4 FEASIBILITY STUDY OF THE DISK MHD FACILITY

In this chapter the practical realization of the experimental disk MHD facility will be discussed. While the predesign of the facility is discussed in the previous chapter, problems which might impede the realization will be discussed in this chapter. This area consists of technical problems in the construction or operation of the facility and obtaining the financial support from external sources that is required to realize the proposed facility. The aim of the proposed disk MHD facility is the practical realization of high enthalpy extraction in a generator type that is less developed than the open cycle linear MHD generator. At the same time the construction and operation of such a facility would imply a very useful continuation of the dutch MHD efforts, which have received large recognition in the world.

4.1 Technical problems

From the line diagram shown in figure 3.1 and from the introduction to chapter 3 an impression can be obtained of the infrastructure that is required for testing of an open cycle or closed cycle disk MHD generator. Essential parts such as the high temperature combustor or regenerative heat exchanger and the liquid helium and liquid nitrogen system for the cooling can be obtained from subcontractors, if necessary according to our specifications. The swirl is introduced by swirl vanes. These vanes are either constructed from ceramic material which makes them rather vulnerable or they are made of stainless steel and they should be heavily water cooled which implies a reduction of the thermal input to the generator channel.

The construction of the walls of the disk generator and the diffuser may require a special development effort but much can be learned from the extensive expertise built up with linear MHD generators. Perhaps the wall construction may limit the lifetime of the generator in the beginning but development during the operation of the facility can be expected to solve this problem. The best wall construction is probably similar to that used by AVCO in linear MHD generators [4.1]. Here the

ceramic inner wall is split up into rather small tiles that are individually connected by means of bolts to a glass fiber reinforced supporting structure (see figure 3.2). The advantage of this approach is that cracking of the ceramic tiles due to thermal stress can be avoided and that curved inner walls can be constructed rather easily.

A component that will need special development is the diffuser. A lot of information about the shape of the diffuser is available from experiments in linear MHD generators. In general, however, the optimization has to be done experimentally since predictive calculational techniques are lacking. In the field of disk generators not much experience on diffusers is available and the translation from the field of linear generators is not straightforward. In fact a relatively large MHD disk facility at the Tokyo Institute of Technology had such large problems with the diffuser system that a large vacuum sphere downstream of the system had to be installed.

From the viewpoint of the design of the magnet and the cryogenic system, possible problem areas are the force containing structure between both coils in the magnet system. The huge Lorentz forces have to be handled by supporting struts which have to stick through the MHD channel. Furthermore the relatively low level of experience with large superconducting coils made of Nb_3Sn conductor with its specific problems of brittleness means a true challenge for the detailed design and manufacturing of these coils.

4.2 An estimate of the required financial support

The financial costs of the construction and the operation of the facility which will be given below have an accuracy of only 20 %. For a more accurate specification of the costs a detailed design will be necessary. In the specification of the estimated costs (table 4.1 and 4.2) it is assumed that the oxygen is present in high pressure storage cylinders and the propane is stored in liquid form so that an evaporator suffices to obtain the required inlet pressure to the combustor. It is further assumed that one experimental run will last at most 2 minutes and that a total of 100 runs have to be performed in

a period of 2 years after the construction and shake down tests of the facility have been completed which will take 3 years.

In estimating the costs it was further assumed that the facility will be placed in an existing building and that the costs of personnel can be based on salaries paid in the public sector.

Table 4.1 Estimated investment costs of the 5-10 MWt test facility over 5 years (in kfl in year 1990).

	open cycle	closed cycle
Combustor (including air compressor)	2000	
Reg. heat exchanger (incl. vacuum system)		2000
Seed supply system	50	
Generator, nozzle, diffuser	2000	
Magnet system (including cooling system)	4500	
Scrubber, stack	50	
Electrical load	50	
Data acquisition and control system	250	
Diagnostics	400	
Propane system	50	
Technical provisions	500	
Consumption of propane	50	
oxygen	280	
potassium carbonate	20	
argon		500
cesium		200
liquid He, N_2	200	
Unanticipated costs	1000	
	——— +	——— +
Total	11400	11800

Table 4.2 Estimated costs of personnel over 5 years (in kfl in year 1990)

Academic people	1800
Technicians	250
Design engineers	1500
Travel and accomodation expenses	100 +
Total	3650

4.3 Possibilities for realization within Europe

The interest for MHD within the countries of the european communities (EC) is again growing. The prospects of MHD for the EC has been evaluated by a special working group which included representatives of various industries and public utilities of the different countries. Based on the recommendations of this working group two contracts of limited extend have been awarded by the EC to investigate a few crucial items. One of these problem areas is the prolonged lifetime testing of open cycle linear generators. When the answers to the crucial items are positive the EC considers to start a large scale MHD program. In the latter case it is quite reasonable to expect that the EC will also consider financial support of a disk MHD test facility as outlined in this report.

4.4 Summary

In this chapter the feasibility of the predesign has been considered leading to the following statements:

- no large problems are foreseen with the channel since there is a lot of experience with linear MHD generators and even with a closed cycle disk generator at Tokyo Institute of Technology,
- concerning the required magnet system for the disk generator there are no fundamental or technological problems foreseen,
- the financial costs do not depend much on the choice for open cycle or closed cycle operation and equal a total of about 15 million dutch guilders (1990) for a total period of 5 years, and
- due to the new development within the European Communities the possibilities for realization within the EC seem to be a bit optimistic.

5 STUDY OF 1000 MWt SCALE COMMERCIAL SYSTEMS

In this chapter some aspects of 1000 MWt scale commercial systems are presented. In chapter 5.1 the MHD and system calculations will be discussed of four different MHD/steam systems and in chapter 5.2 a discussion of the results will be presented.

5.1 Four MHD/steam systems

In this chapter results of calculations of four different commercial size MHD/steam systems will be presented. This study includes linear and disk type generators for both closed and open cycle MHD. Figure 5.1. shows the plant arrangement schematic of the closed cycle MHD/steam plant and figure 5.2 shows it for the open cycle MHD. All systems are direct coal fired and use two stage cyclone combustors burning Illinois #6 as coal. A two stage cyclone combustor is chosen because it has a high slag rejection factor. The advantages due to this high slag rejection factor are an increase of the electrical conductivity, a decrease in losses of potassium by reaction with slag and a lot of components are less aggravated by the slag. In table 5.1 the specification of Illinois #6 coal is given. Before the coal is used it is dried by a part of the exhaust gases to a moisture content of 2 %.

5.1.1 The two stage cyclone combustor

To accomplish a high slag rejection factor the process conditions have to be chosen such that in the first stage as little as possible slag evaporates. For the selected coal type the minimum stoichiometric factor to transform all the carbon into carbon monoxide is 0.39. Combustion of the coal with a stoichiometric factor of 0.39 and preheated air with a temperature of 1800 K results in a temperature of intermediate combustion products of about 2100 K. At this temperature about 15 % of the mineral fraction of the coal is in the gaseous phase and also about 85 % of the slag can be rejected in the cyclone. In the second stage preheated air with a temperature of 1800 K is used for

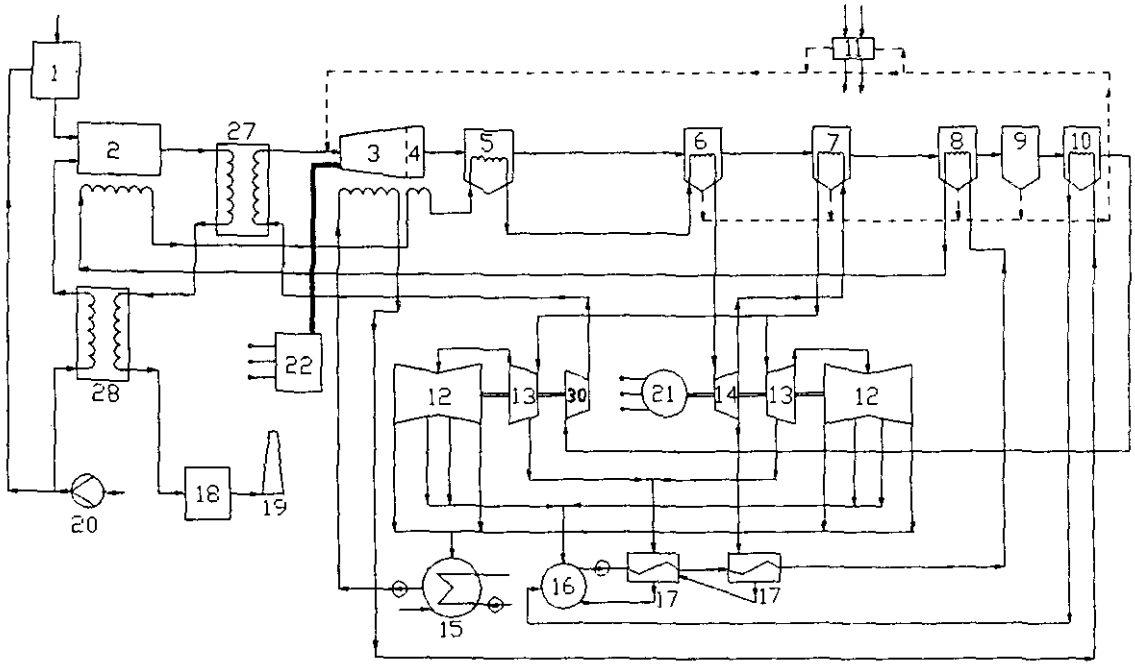

Figure 5.1 Plant arrangement schematic of the closed cycle MHD/steam plant.

The numbers have the following significance: 1. coal treatment; 2. combustor; 3. MHD generator; 4. diffuser; 5. radiant boiler; 6. super heater; 7. reheater; 8. high temperature economizer; 9. gas cleanup equipment; 10. low temperature economizer; 11. seed treatment; 12. low pressure steam turbine; 13. medium pressure steam turbine; 14. high pressure steam turbine; 15. condenser; 16. degas equipment; 17. water preheaters; 18. coal dryer; 19. stack; 20. air compressor; 21. generator; 22. dc-ac inverter; 27. high temperature argon heater; 28. air preheater; 30. argon compressor.

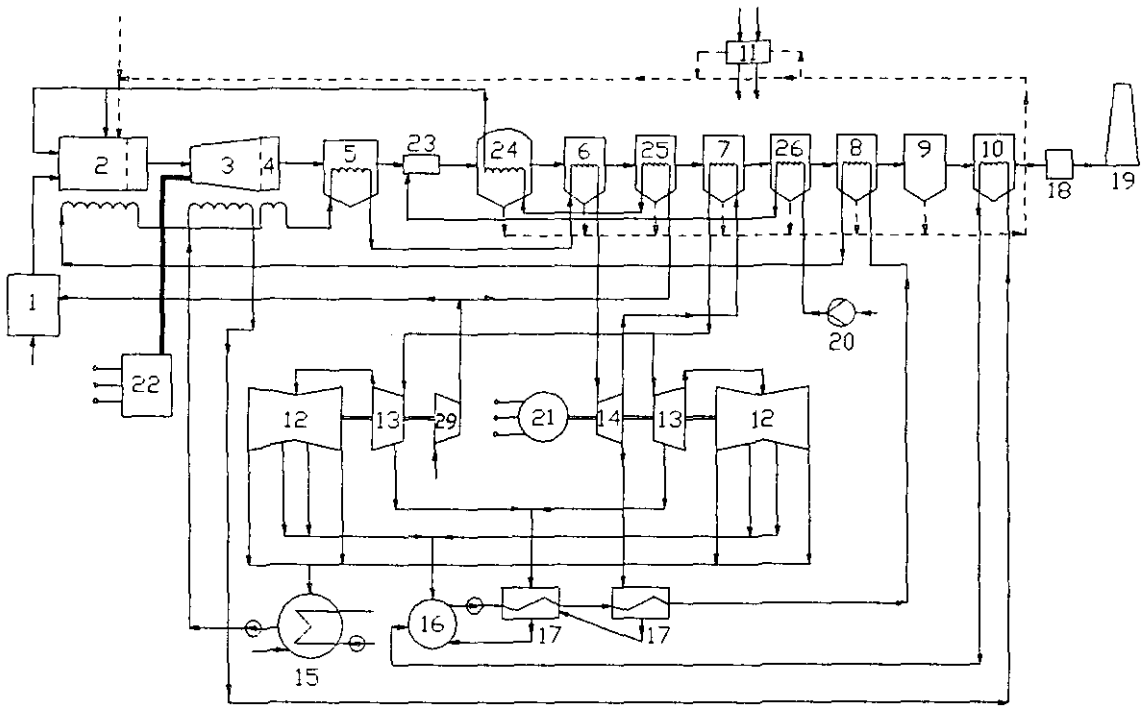

Figure 5.2 Plant arrangement schematic of the open cycle MHD/steam plant.

The numbers have the following significance: 1. coal treatment; 2. combustor; 3. MHD generator; 4. diffuser; 5. radiant boiler; 6. super heater; 7. reheater; 8. high temperature economizer; 9. gas cleanup equipment; 10. low temperature economizer; 11. seed treatment; 12. low pressure steam turbine; 13. medium pressure steam turbine; 14. high pressure steam turbine; 15. condenser; 16. degas equipment; 17. water preheaters; 18. coal dryer; 19. stack; 20. air compressor; 21. generator; 22. dc-ac inverter; 23. secondary combustor; 24. intermediate and high temperature air heater; 25. low temperature air heater; 26. secondary air preheater; 29. air compressor.

Table 5.1 Specification of the Illinois #6 coal.

Type: Illinois #6			
Proximate analysis (as received), wt %			
Fixed carbon	41.7		
Volatile matter	38.0		
Ash	11.4		
Moisture	8.9		
Higher heating value	28.8 MJ/kg		
Lower heating value	26.2 MJ/kg		
Ultimate analysis (as received), wt %		Ash analysis wt %	
C	62.40	Al_2O_3	21.26
H	4.41	CaO	5.95
O	8.39	Fe_2O_3	24.56
N	1.20	MgO	0.33
S	3.30	SiO_2	45.59
Ash	11.40	K_2O	2.31

the combustion. In the open cycle systems the K_2CO_3 seed is injected in this second stage. The stoichiometric factor is chosen at 0.93 to limit the formation of NO_x. For the open cycle systems this also leads to a high electrical conductivity. The combustion gas has at the inlet of the generator a stagnation temperature of about 2830 K when preheated air of 1800 K is used. For the closed cycle MHD system the combustion gas temperature can be limited to about 2250 K. This can be reached with an air preheat temperature of 400 K. This means that even slag rejection factors of nearly 100 % can be obtained. The oxidation process is completed by injecting air in a secondary combustor. For the open cycle systems secondary combustion is performed between the radiant boiler and the high temperature air preheater; for the closed cycle systems between the high temperature argon heater and the air preheater. The stoichiometric factor for the secondary combustion is 1.05 and the combustion takes place at a temperature level where no new NO_x can be formed. The required cooling power of the two stage cyclone combustor is assumed to be 3 % of the total thermal input. As indicated in 2.1.1.2 the composition of the combustion gas as well as the values of enthalpy, entropy, speed of sound, ratio of specific

heats, electrical conductivity and Hall parameter are obtained from the NASA SP-273 chemical equilibrium computer code [5.1]. This code is also used for calculations of the different stages of the combustion process.

5.1.2 Closed cycle MHD/steam plant description

The closed cycle MHD generator is included in a loop which is shown in figure 5.1. The system configuration of a coal burning closed cycle MHD/steam plant can be divided into three subsystems:

- an open cycle coal combustion system to heat up the argon by means of ceramic regenerative heat exchangers,
- a closed cycle argon system with the previously mentioned heat exchangers, the MHD generator and diffusers, components for heat transfer to the steam cycle and an argon compressor, and
- a steam cycle.

A disadvantage of the closed cycle MHD system is that the total heat flux has to be supplied to the argon by means of a system of ceramic regenerative heat exchangers which has a negative effect on the investments. The combustion gases which leave the regenerative heat exchangers are used to preheat the combustion air and to dry the coal. The combustor is cooled with feed water from the high temperature economizer. The argon which is heated in the regenerative heat exchangers to a temperature of 2000 K is accelerated in the nozzle to obtain the desired Mach number and flows through the MHD duct. The flow which is still supersonic at the generator exit is decelerated in a diffuser system and the remaining heat is transferred to the steam system by means of several heaters and boilers. The argon compressor operates without intercooling and is driven by a steam turbine.

The cesium is injected in the high temperature argon before it enters the nozzle. Removal of the cesium from the argon is accomplished by condensation of the cesium vapour. The recovered seed is purified, mixed with make-up seed and passed to a liquid metal pump before reinjection into the argon cycle. To keep the contamination level of the argon low, a gas cleanup system is desired.

A supercritical steam cycle of 230 bar/823 K/823 K is used as bottoming cycle. The cycle rejects heat to surface water through a 0.027 bar condenser and yields a thermodynamic efficiency of 43.2 % [5.2]. In the performance analysis, channel cooling with low temperature feed water is assumed.

The components in the loop are specified by efficiencies which are listed in table 5.2. The design parameters needed to specify the burner system, MHD generator and the steam bottoming plant are specified in table 5.3. These numbers make the calculation of the performance of the argon cycle straightforward once the enthalpy extraction, the isentropic efficiency and the heat losses of the MHD generator plus nozzle and diffusers have been determined. The specification of the burner system is very simple since the constant stack temperature implies constant stack losses. This also implies a constant efficiency of the combustion system which can be calculated from the relevant equations [5.3] and equals 0.966 for a stack temperature of 393 K.

Table 5.2 Efficiencies of components valid for both open cycle and closed cycle and for both linear and disk generators.

Radiative boiler	0.99
Convective apparatuses	0.99
Thermodynamic efficiency of the steam bottoming plant	0.432
Mechanical efficiencies	0.99
DC-AC converter	0.96
AC generator	0.998
Internal electricity consumption	0.03
Compressor efficiency	0.82
Isentropic efficiency of nozzle	0.99
Isentropic efficiency of subsonic diffuser	0.9
Correction factor for non ideal shock supersonic diffuser	0.9
Pressure drops per component	0.02
Heat for seed recovery	0.03*)
Heat for coal drying	0.01*)
pressure loss of combustion air system	0.10
pressure loss of burner system	0.10

*) related to coal thermal input

Table 5.3 Assumed design parameter for closed cycle studies (both disk and linear MHD generator).

Enthalpy flux at generator entrance	1200 MWt
Coal type	Illinois #6
Burner system	
Stoichiometry	0.95
Cooling power related to coal thermal power	0.03
Stack temperature	393 K
Efficiency of the burner system	0.966
MHD generator	
Medium	Ar + Cs
Magnetic induction (constant)	5 T
Stagnation temperature-wall temperature	300 K
Voltage drop per electrode pair (linear segmented Faraday type only)	150 V
Cooling	feed water
Total pressure drop argon loop	0.12

5.1.3 Closed cycle design constraints and optimization results

For the calculations of both types of closed cycle MHD generators the thermal input at the inlet of the generator is 1200 MWt. A supersonic flow in the generator is assumed and heat losses in the generator are based on the assumption that the difference in stagnation and wall temperature is constant and equals 300 K. The following general constraints have to be fulfilled:

- the Mach number at the generator exit must be larger than 1.05 in order to avoid shock waves inside the channel, and
- the half divergence angle between the channel walls must be smaller than 5 degrees in order to avoid separation of the flow from the wall [5.3].

Following Retallick [5.4] the closed cycle disk MHD generator is designed to work in the optimum loading mode. In this mode the loading parameter α equals the optimum value α_{opt} for each value of the radius r for which purpose the channel height z is accommodated at each location. The optimum loading parameter α_{opt} is easily calculated and leads to the maximum value of the local electrical efficiency η_L

[5.5]. Both α_{opt} and η_L depend on the value of the swirl S and on the value of the effective Hall parameter β_{eff}. It has been shown before [5.5] that the optimum loading mode may be preferred for an unstable plasma i.e. for a plasma which will not be in the condition of fully ionized seed over a large range of the expansion.

For the base case of the disk generator the Mach number at the inlet M_0 = 2.2, the inlet stagnation pressure p_{st} = 7 bar, the seed ratio $s_r = 5 \times 10^{-5}$, the inlet swirl So = 1.5 and the magnetic induction B = 5 T. Various parameters such as the swirl S, the static pressure p, the static temperature T, the Mach number M, the effective Hall parameter β_{eff}, the effective electrical conductivity σ_{eff} and the height z are given for the base case as a function of the channel radius in figure 5.3. For the optimization of the performance of the disk generator about 200 calculations have been performed.

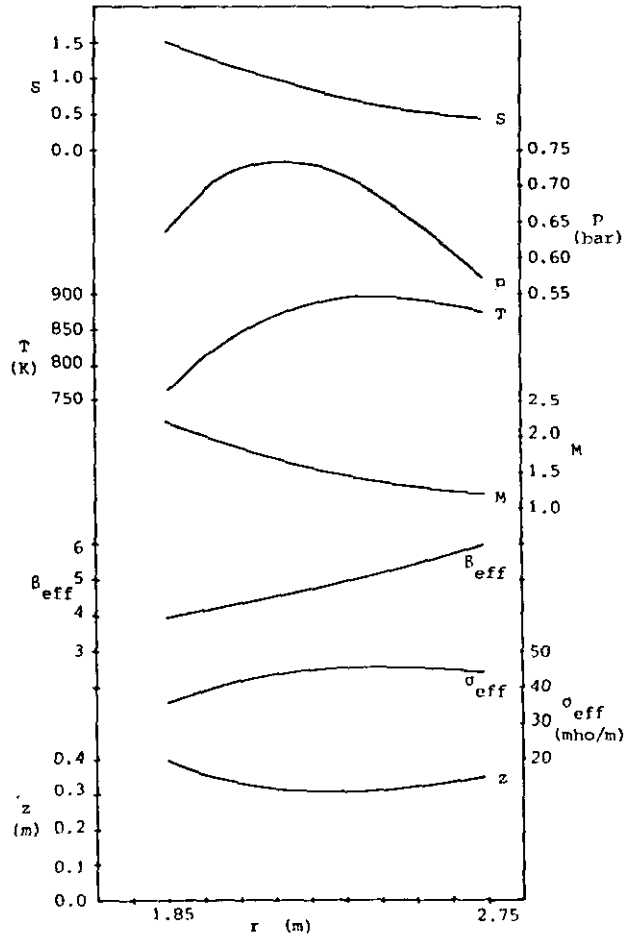

Figure 5.3 Variation of parameters with channel radius.

For this the inlet parameters have been varied in the following way: Mach number M_0 = 1.8, 2, 2.2 and 2.4; stagnation pressure p_{st} = 4, 6, 7 and 8 bar; seed ratio s_r = 10^{-5}, 5 x 10^{-5}, 10^{-4}, 5 x 10^{-4} and 10^{-3} and inlet swirl S_0 = 0.75, 1, 1.5 and 2. The most significant results have been collected in table 5.4 and the influence of the variation of parameters on efficiencies is illustrated in figure 5.4.

Table 5.4 Summary of most significant results for the closed cycle disk MHD generator. Seed ratio = 5 x 10^{-5}, B = 5 T, $T_{s,in}$ = 2000 K and inlet radius = 1.85 m. Optimum loading mode ($\alpha = \alpha_{opt}$ for each radius).

S_0 (-)	M_0 (-)	$p_{st,0}$ (bar)	η_{ent} (%)	η_{is} (%)	η_{cb} (%)	P_{MHD} (MW)	P_{comp} (MW)	P_{steam} (MW)	P_{net} (MW)
2.0	2.4	4	30.3	71.8	49.4	363	183	271	424
		6	30.3	68.5	48.6	363	198	271	409
		7	30.2	66.8	48.1	362	206	272	401
		8	30.2	65.1	47.6	363	216	271	391
	2.2	4	30.3	72.4	49.6	363	180	271	426
		6	30.1	67.7	48.4	361	200	272	406
		7	30.2	65.5	47.7	362	213	272	394
		8							
1.5	2.4	4	30.1	70.5	49.1	361	187	272	419
		6	30.3	68.5	48.6	364	199	271	409
		7	30.3	67.3	48.3	363	204	271	403
		8	30.3	66.1	47.9	363	211	271	397
	2.2	4	30.3	72.5	50.0	364	181	271	426
		6	30.3	69.2	48.8	364	195	271	412
		7	30.3	67.5	48.3	363	203	271	404
		8	30.3	65.8	47.8	363	212	271	395

The comparison which can be made from table 5.4 is at a constant enthalpy extraction of 30 % and a seed ratio of 5 x 10^{-5}. At a seed ratio of 10^{-5} an enthalpy extraction of 30 % is only obtained in four situations. At a seed ratio of 10^{-4} or larger an enthalpy extraction of 30 % has not been reached at all. The limiting factor in most cases is the half divergence angle becoming too large, which also leads to some empty lines in table 5.4. It is apparent from figure 5.4 that the best coal to busbar efficiency is obtained at the lowest inlet stagnation pressure, the largest value of the magnetic induction and the highest enthalpy extraction which have been considered.

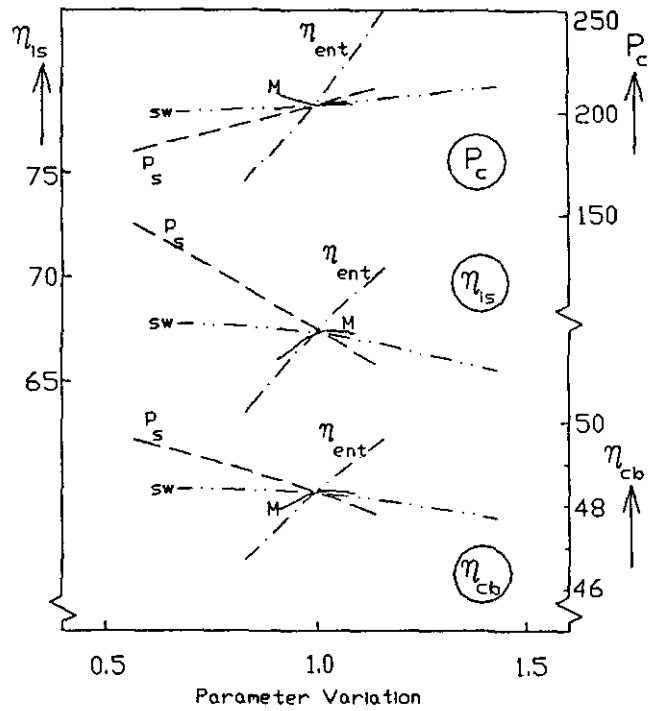

Figure 5.4 Effect of parameter variation on compressor power P_c, isentropic efficiency η_{is} and on the coal to busbar efficiency η_{cb}. Closed cycle disk MHD/steam system. Base case conditions for the reference point: $p_{s,in}$ = 7 bar, M_{in} = 2.2, S_{in} = 1.5, SR = 5 x 10^{-5}, B = 5 T and η_{ent} = 30 %. Under these conditions: r_{in} = 1.85 m, z_{in} = 0.33 m, r_{out} = 2.58 m, z_{out} = 0.4 m, $\beta_{eff,in}$ = 4.0, $\beta_{eff,out}$ = 5.6, $\sigma_{eff,in}$ = 36 1/Ωm, and $\sigma_{eff,out}$ = 45 1/Ωm.

The optimum inlet Mach number appears to be 2.2 and the optimum inlet swirl 0.75. The best operation of the disk generator has been obtained for the inlet conditions M_0 = 2.4, p_{st} = 4 bar, s_r = 5 x 10^{-5} and S_0 = 2 (B = 5 T). At an enthalpy extraction of 35 % this leads to an isentropic efficiency (of generator plus nozzle and diffusers) η_{is} of 75.5 % and a coal to busbar efficiency η_{cb} of 51.3 %. Comparison with the corresponding numbers in table 5.4 shows an increase of 3.7 percentage points in η_{is} and 1.9 percentage points in η_{cb} due to the increase in enthalpy extraction from 30 to 35 %. At a magnetic induction B = 6 T the best operation of the disk generator has been obtained for the inlet conditions M_0 = 2.2, p_{st} = 4 bar,

$s_r = 5 \times 10^{-5}$, $S_0 = 2$ and $\eta_{ent} = 35$ %. This leads to $\eta_{is} = 76.8$ % and $\eta_{cb} = 51.6$ % which is only a limited gain compared to the case mentioned above. The variation in compressor power P_{comp} is also shown in figure 5.4 because this can explain the variation of η_{cb}. At constant enthalpy extraction the electric power from the MHD generator and from the steam bottoming plant are both constant.

Following Geutjes and Kleyn [5.3] the closed cycle linear MHD generator is designed with straight channel walls under the maximum divergence angle and operates at constant Faraday load factor k_f. It has been shown in [5.3] that closed cycle linear MHD generators with subsonic flow do not have attractive part load behaviour so that supersonic flow has been chosen.

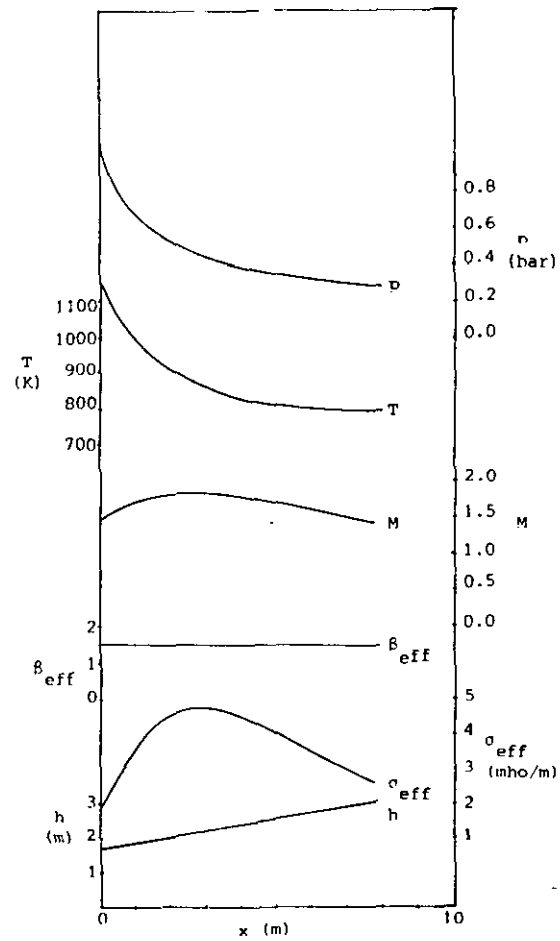

Figure 5.5 Variation of parameters with channel length.

For the base case of the linear generator the Mach number at the inlet M_0 = 1.45, the inlet stagnation pressure p_{st} = 4 bar, the seed ratio $s_r = 10^{-3}$ and the magnetic induction B = 5 T. Various parameters such as the static pressure p, the static temperature T, the Mach number M, the effective Hall parameter β_{eff}, the effective electrical conductivity σ_{eff} and the height of the channel h are given for the base case as a function of the channel length in figure 5.5. For the optimization of the performance about 50 calculations have been performed. For this the inlet parameters have been varied in the following way: M_0 = 1.2, 1.45, 1.7 and 2; p_{st} = 4, 6, 7 and 8 bar and $s_r = 10^{-4}$, 5 x 10^{-4} and 10^{-3}. The most significant results have been collected in table 5.5 and the influence of the variation of parameters on efficiencies is illustrated in figure 5.6.

Table 5.5 Summary of most significant results for the closed cycle linear MHD generator (segmented Faraday type). Seed ratio = 10^{-3}, B = 5 T, $T_{s,in}$ = 2000 K, voltage drop = 150 V and Faraday load factor k_f = constant.

M_0 (-)	$p_{st,0}$ (bar)	k_f (-)	η_{ent} (%)	η_{is} (%)	η_{cb} (%)	P_{MHD} (MW)	P_{comp} (MW)	P_{steam} (MW)	P_{net} (MW)
1.20	4	0.845	30.3	70.4	47.6	362	188	271	417
	6	0.815	30.3	67.4	46.9	363	204	270	402
	7	0.805	30.2	66.0	46.4	361	209	271	396
	8	0.790	30.1	64.8	46.0	360	215	271	389
1.45	4	0.865	30.3	68.9	47.3	362	195	271	410
	6	0.840	30.3	66.2	46.5	363	210	270	396
	7	0.825	30.8	65.7	46.4	369	219	267	390
	8	0.815	30.7	64.5	45.9	366	224	268	384
1.70	4	0.880	30.3	66.8	46.7	362	207	270	399
	6	0.855	30.1	64.2	45.8	360	219	271	386
	7	0.845	30.2	63.3	45.5	360	226	271	379
	8	0.835	30.2	62.4	45.2	360	231	271	374
2.00	4	0.890	30.3	64.5	45.9	362	220	270	386
	6	0.875	30.4	61.3	44.7	363	243	270	364
	7	0.865	30.9	61.2	44.5	369	251	267	359
	8	0.855	30.3	60.1	44.1	362	252	270	355

The comparison which can be made from table 5.5 is at a constant enthalpy extraction of 30 % and a seed ratio of 10^{-3}. The influence of the seed ratio on the isentropic efficiency and on the coal to busbar efficiency is minute and is therefore not shown in figure 5.6.

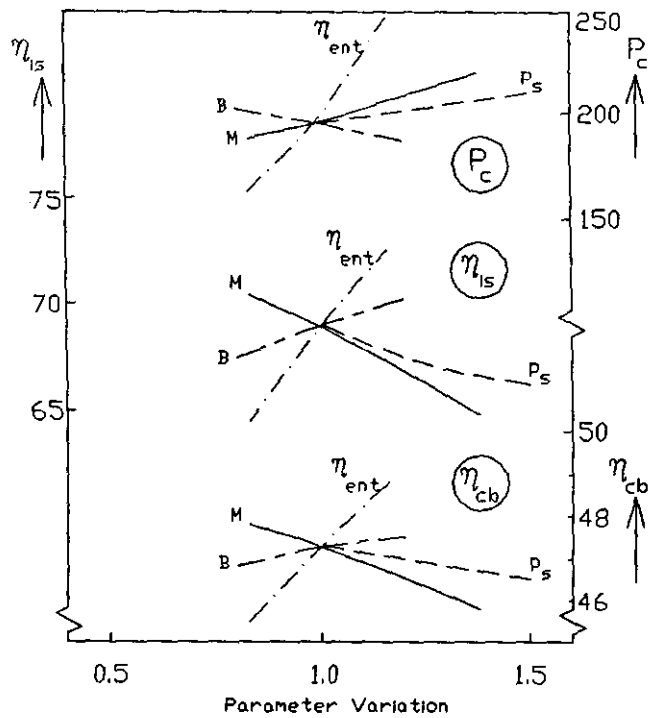

Figure 5.6 Effect of parameter variation on compressor power P_c, isentropic efficiency η_{is} and on the coal to busbar efficiency η_{cb}. Closed cycle linear MHD/steam system. Base case conditions for the reference point: $p_{s,in}$ = 4 bar, M_{in} = 1.45, SR = 10^{-3}, B = 5 T and η_{ent} = 30 %. Under these conditions: $h_{in} = b_{in}$ = 1.70 m, $h_{out} = b_{out}$ = 2.92 m, l = 7 m, $\sigma_{app,in}$ = 1.7 1/Ωm, and $\sigma_{app,out}$ = 3 1/Ωm.

It has been observed from the calculations that boundary layer separation quite often prevents an enthalpy extraction of 35 % to be reached at the Mach numbers 1.2 and 1.45 and at an inlet stagnation pressure larger than 4 bar. It is apparent from figure 5.6 that the best coal to busbar efficiency is obtained at the lowest inlet stagnation pressure, the smallest Mach number and the largest enthalpy extraction which have been considered. The gain which can be obtained by increasing the magnetic induction from 5 to 6 T is very limited. The best operation of the linear generator is thus obtained for the inlet conditions M_0 = 1.2, p_{st} = 4 bar and s_r = 10^{-3} (B = 5 T). At an enthalpy extraction of 35 % this leads to an isentropic efficiency (of

generator plus nozzle and diffusers) η_{is} of 73.4 % and a coal to busbar efficiency η_{cb} of 49.1 %. Comparison with the corresponding numbers in table 5.5 shows an increase of 3 percentage points in η_{is} and 1.5 percentage points in η_{cb} due to the increase in enthalpy extraction from 30 to 35 %.

5.1.4 Open cycle MHD/steam plant description

The open cycle MHD generator is included in a loop which is shown in figure 5.2. The system configuration can be divided into two subsystems:

- an open cycle coal combustion system, MHD generator and diffusers and components for the heat transfer to the steam cycle, and
- a steam cycle.

Compared with the closed cycle system the main difference in the combustion system is the location of the combustion air preheater. In the closed cycle system it is located downstream of the high temperature ceramic regenerative heat exchangers and in the open cycle it is located downstream of the radiant boiler. The seed in the form of dry potassium carbonate is added to the combustor in such an amount that the plasma will contain 1 % of potassium by weight. The combustion gases are accelerated through a nozzle to the desired Mach number. In the MHD channel enthalpy is extracted in such a way that the stagnation pressure leaving the subsonic diffuser is 1.14 bar. From the subsonic diffuser the combustion gases enter the heat recovery/seed recovery system, including a steam generator, air heaters, gas clean up equipment and coal dryers.

The steam cycle is supposed to be the same as for the closed cycle system. From the calculations of nozzle, generator channel and diffusers enthalpy extraction and isentropic efficiency have been determined. The heat which is carried off by cooling the burner, nozzle, channel and diffusers can be used in the steam bottoming cycle. Given the specific efficiencies of the cycle components (table 5.2) and the assumed design parameters for the open cycle system (table 5.6) the coal to busbar efficiency can be calculated.

Table 5.6 Assumed design parameters for open cycle studies (both disk and linear MHD generator).

Coal thermal input to combustor	1000 MWt
Coal type	Illinois #6
Air preheat system	direct
Preheat temperature	1800 K
Seed	dry K_2CO_3, 1% wt K
Burner system	2 stage cyclone
Stoichiometry	0.95
Cooling power incl. nozzle related to coal thermal input	0.04
Slag rejection	0.85
MHD generator	
Magnetic induction (constant)	5 T
Stagnation temperature - wall temperature	500 K
Voltage drop per electrode pair (linear segmented Faraday type only)	150 V
Cooling	feed water
Downstream pressure subsonic diffuser	1.14 bar

5.1.5 Open cycle design constraints and optimization results

For the calculations of both disk and linear types of open cycle MHD generators the coal thermal input is 1000 MWt. Heat losses in the generator are based on the assumption that the difference in stagnation and wall temperature is constant and equals 500 K.

Following Retallick [5.4] the open cycle disk generator has been designed for constant radial electric field (E_r = 12 kV/m) since this leads to the most compact configuration. In order to keep E_r at this maximum allowable value the channel height is adjusted at each location. It has been shown [5.4] that variation of the value of E_r does not have a large influence on the results. For the optimization of the performance about 80 calculations have been executed. For the base case of the disk generator the Mach number at the inlet M_0 = 1.8, the inlet stagnation pressure p_{st} = 4.5 bar, the inlet swirl S_0 = 1 and the magnetic induction B = 5 T. Various parameters such as the swirl S, the static pressure p, the static temperature T, the Mach

number M, the Hall parameter β, the electrical conductivity σ and the height z are given for the base case as a function of the channel radius in figure 5.7.

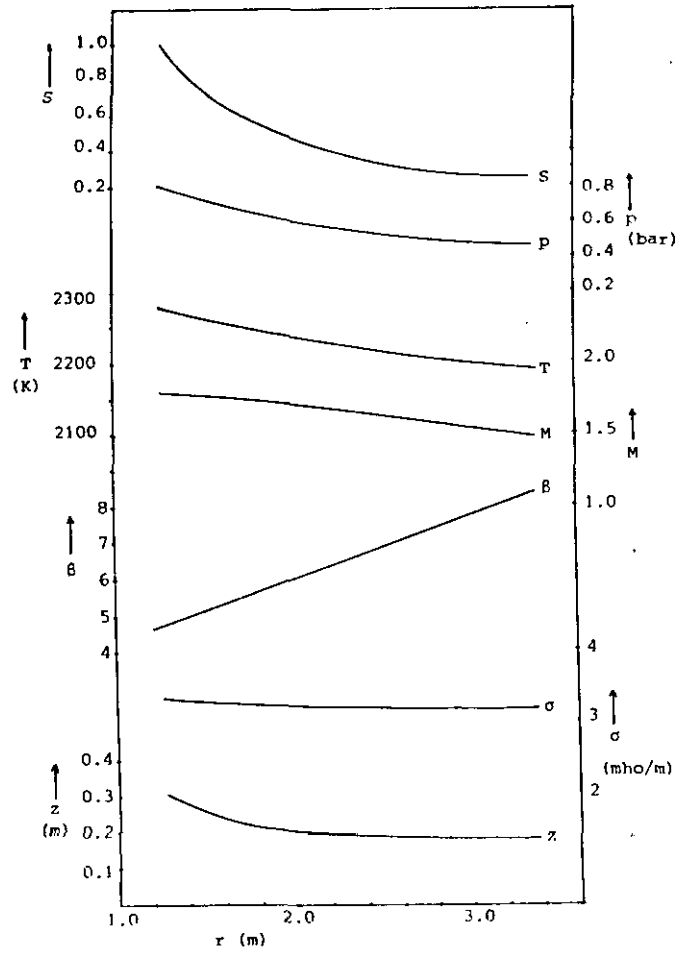

Figure 5.7 Variation of parameters with channel radius; base case of open cycle disk MHD generator.

For the optimization the inlet parameters have been varied in the following way: M_0 = 1.7, 1.8, 1.9 and 2; p_{st} = 4.5, 5.4, 6.3 and 7.2 bar and S_0 = 0.5, 0.75, 1, 1.5 and 2. The most significant results have been collected in table 5.7 and the influence of the variation of parameters on efficiencies is illustrated in figure 5.8. The comparison which can be made from table 5.7 is at a swirl S_0 = 1. It is apparent from figure 5.8 that the best coal to busbar efficiency is obtained at the lowest Mach number, the smallest inlet stagnation pressure and the largest value of the magnetic induction which have been considered. The optimum swirl appears to be S_0 = 1.5 but the effect of swirl is limited. The latter is connected with the fact that

losses due to the inlet swirl vanes have not been taken into account [5.4]. The best operation of the disk generator is obtained for the inlet conditions M_0 = 1.7, p_{st} = 4.5 bar and S_0 = 1 (B = 5 T). At a magnetic induction B = 7 T this leads to η_{ent} = 20.8 % (related to the coal thermal input), η_{is} = 69.8 % (of MHD generator only) and η_{cb} = 44.5 %. These efficiencies are limited by the fact that the pressure downstream of the diffusers must always equal 1.14 bar. Comparison with the corresponding numbers in table 5.7 shows an increase of 3.5 percentage points in η_{ent}, of 7 percentage points in η_{is} and 1.7 percentage points in η_{cb} due to the increase in magnetic induction from 5 to 7 T. A further increase of the magnetic induction to 9 T leads to a maximum coal to busbar efficiency η_{cb} = 45.5 % under the inlet conditions M_0 = 1.8, p_{st} = 6.3 bar and S_0 = 0.5. The other corresponding efficiencies in this case are η_{ent} = 24.6 % and η_{is} = 67.4 %. When the difference in unit size is taken into account the quoted values of efficiencies are comparable to those given by Retallick [5.4] and Simpson [5.6].

Table 5.7 Summary of most significant results for the open cycle disk MHD generator. Inlet swirl S = 1, B = 5 T and constant electric field (E_r = 12 kV/m). The character M in the last column indicates that the expansion had to be stopped because a Mach number = 1.05 was reached.

M_0 (-)	$p_{st,0}$ (bar)	η_{ent} (%)	η_{is} (%)	η_{cb} (%)	P_{MHD} (MW)	P_{comp} (MW)	P_{steam} (MW)	P_{net} (MW)	
2.0	4.5	15.0	64.1	41.6	150	65.5	363	416	
	5.4	16.2	59.5	41.7	161	74.5	362	417	
	6.3	16.6	55.4	41.5	166	82.5	364	415	
	7.2	16.5	51.6	41.1	166	89.8	367	411	
1.9	4.5	16.4	64.1	42.3	164	65.5	357	423	
	5.4	17.4	59.8	42.3	175	74.5	357	423	
	6.3	17.9	56.6	42.2	179	82.5	358	422	
	7.2	17.8	53.0	41.7	178	89.8	362	417	
1.8	4.5	17.1	63.5	42.6	170	65.5	354	426	
	5.4	18.0	59.5	42.6	180	74.5	354	426	
	6.3	18.3	56.5	42.3	183	82.5	357	423	
	7.2	7.1	26.0	36.3	71	89.8	407	363	M
1.7	4.5	17.3	62.8	42.8	172	65.5	353	428	
	5.4	7.4	32.7	37.3	74	74.5	399	373	M
	6.3	7.1	28.3	36.7	71	82.6	404	367	M
	7.2	6.5	24.0	36.0	65	89.8	410	360	M

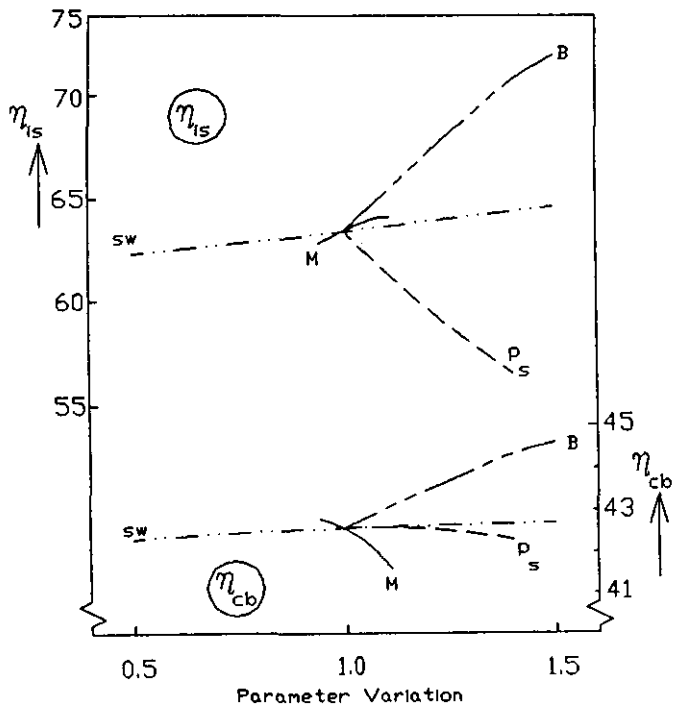

Figure 5.8 Effect of parameter variation on isentropic efficiency η_{is} and on the coal to busbar efficiency η_{cb}. Open cycle disk MHD/steam system. Base case conditions for the reference point: $p_{st,it}$ = 4.5 bar, M_{in} = 1.8, S_{in} = 1, and B = 5 T. Under these conditions: r_{in} = 1.27 m, z_{in} = 0.31 m, r_{out} = 3.37 m, z_{out} = 0.18 m, β_{in} = 4.8, β_{out} = 8.4, σ_{in} = 3.4 1/Ωm, and σ_{out} = 3.2 1/Ωm.

The linear channel is loaded in the segmented Faraday mode and the Mach number is kept constant at 0.9. The voltage drop is constant (150 V) and the load factor is constant for the whole generator and is adjusted such that the stagnation pressure at the exit of the subsonic diffuser is constant and equals 1.14 bar. To satisfy these conditions the square cross-section of the generator is adjusted. To prevent boundary layer separation the half divergence angle between the channel walls is checked and may not exceed 5 degrees.

For the base case of the linear generator the inlet stagnation

pressure p_{st} = 7.2 bar, the magnetic induction B = 5 T and the length l = 20 m. Due to the decrease of the plasma temperature the electrical conductivity changes under base case conditions from 7.4 1/Ωm at the inlet to 2.1 1/Ωm at the exit of the channel. The maximum Hall parameter amounts 5.3 at the exit. The maximum electrical field in the axial direction is 4370 V/m and in the Faraday direction 3140 V/m. The inlet cross section is 0.8 x 0.8 m^2, the exit cross section is 1.96 x 1.96 m^2 and the heat loss of the channel is 63 MWt. For the base case the isentropic efficiency η_{is} amounts 74.8 % (of generator plus nozzle and diffusers) and the coal to busbar efficiency η_{cb} = 49.0 %. Various parameters such as the static pressure p, the static temperature T, the Mach number M, the Hall parameter β, the electrical conductivity σ and the diameter d (b = h = d) are given for the base case as a function of the channel length in figure 5.9.

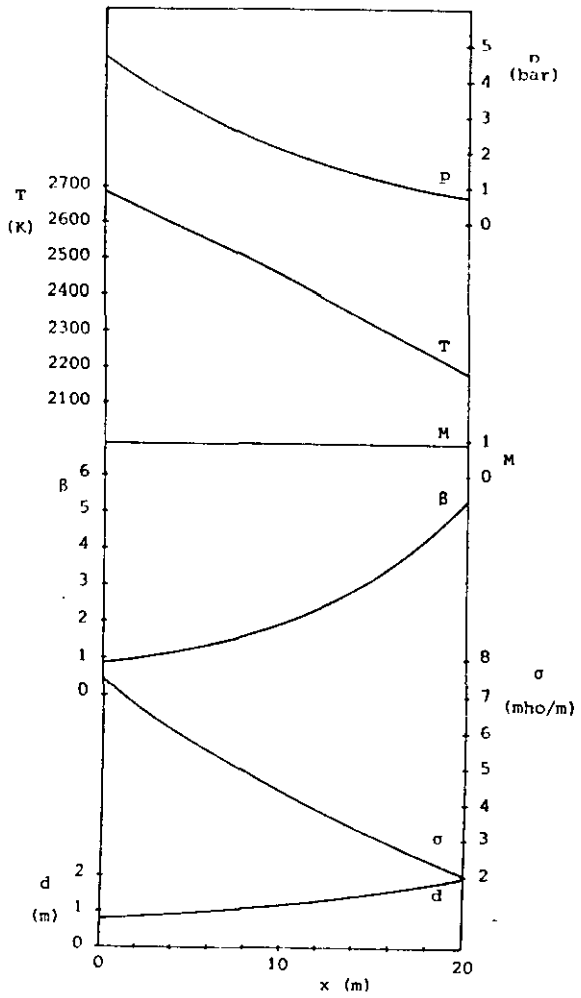

Figure 5.9 Variation of parameters with channel length; base case of open cycle linear MHD generator.

For the optimization the inlet parameters have been varied in the following way: p_{st} = 5.4, 6.3 ,7.2, 8.1 and 9.0 bar and the length of the channel l = 16, 20 and 24 m. The most significant results have been collected in table 5.8 and the influence of the variation of parameters on efficiencies is illustrated in figure 5.10.

Table 5.8 Summary of most significant results for the open cycle linear MHD generator (segmented Faraday type). Mach number = constant (M = 0.9), B = 5 T, voltage drop = 150 V and Faraday load factor k_f = constant.

$p_{st,0}$ (bar)	l (m)	k_f (-)	η_{ent} (%)	η_{is} (%)	η_{cb} (%)	P_{MHD} (MW)	P_{comp} (MW)	P_{steam} (MW)	P_{net} (MW)
5.4	16	0.84	29.8	78.9	48.6	298	75	305	486
5.4	20	0.86	30.4	80.7	48.9	304	75	302	489
5.4	24	0.88	30.8	81.6	49.1	308	75	300	491
6.3	16	0.79	30.7	75.5	48.6	307	83	304	486
6.3	20	0.82	31.7	77.9	49.1	317	83	300	491
6.3	24	0.84	32.2	79.3	49.4	322	83	298	494
7.2	16	0.74	30.9	71.9	48.4	309	90	306	484
7.2	20	0.78	32.2	74.8	49.0	322	90	301	490
7.2	24	0.81	33.0	76.7	49.4	330	90	297	494
8.1	16	0.69	30.7	68.1	47.9	307	96	310	479
8.1	20	0.73	32.3	71.6	48.7	323	96	303	487
8.1	24	0.77	33.3	73.8	49.2	333	96	299	492
9.0	16	0.65	30.1	64.3	47.3	301	102	315	473
9.0	20	0.70	32.0	68.2	48.2	320	102	307	482
9.0	24	0.73	33.2	70.8	48.8	332	102	302	488

Comparison of the calculations shows that an increase of the length of the channel from 16 to 24 m results in an increase of 4.8 percentage points in η_{is} and 1.0 percentage points in η_{cb}. The influence of the magnetic induction is more pronounced. An increase in B from 4 to 6 T results in an increase of 15.4 percentage points in η_{is} and 2.7 percentage points in η_{cb}.

Variation of the stagnation pressure at the inlet of the generator from p_{st} = 5.4 to 9.0 bar results in a decrease in η_{is} of 12.5 percentage points but the effect on η_{cb} is only 0.9 percentage points and a maximum is reached for $p_{st} \approx 6.5$ bar. In table 5.9 data are collected

for variation of voltage drop, difference between stagnation and wall temperature, heat losses in the burner and nozzle and air preheat temperature. The voltage drop is varied from 50 to 250 V which results in a decrease in η_{is} and η_{cb} of respectively 3.2 and 0.7 percentage points. The difference between the stagnation and the wall temperature is varied from 400 to 600 K. Due to the larger heat loss in the generator this results in an decrease in η_{is} and η_{cb} of respectively 1.6 and 0.4 percentage points. The heat losses in burner and nozzle are varied from 4.05 to 4.95 % of the coal thermal input. The influence on the efficiencies is rather small. With increasing heat losses the decrease in η_{is} and η_{cb} is respectively 0.6 and 0.4 percentage points. For one case the air preheat temperature is decreased from 1800 to 1650 K. This results in a lower stagnation temperature (2775 K) and also a lower value for the electrical conductivity (5.8 1/Ωm at the inlet). This effect lowers η_{is} and η_{cb} with respectively 3.2 and 1.5 percentage points.

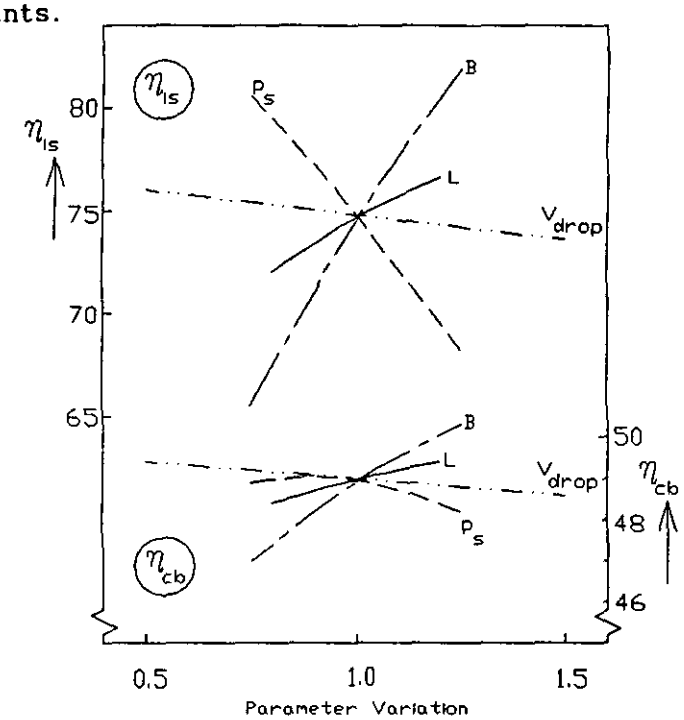

Figure 5.10 Effect of parameter variation on isentropic efficiency η_{is} and on the coal to busbar efficiency η_{cb}. Open cycle linear MHD/steam system. Base case conditions for the reference point: $p_{st,in}$ = 7.2 bar, M_{in} = 0.9, and B = 5 T. Under these conditions: $h_{in} = b_{in}$ = 0.92 m, $h_{out} = b_{out}$ = 1.96 m, l = 20 m, β_{in} = 0.9, β_{out} = 5.3, σ_{in} = 7.4 1/Ωm, and σ_{out} = 2.1 1/Ωm.

Table 5.9 Summary of sensitivity study by variation of voltage drop, difference in stagnation and wall temperature, heat losses in burner and nozzle and air preheat temperature.

$p_{st,0}$ (bar)	k_f (-)	η_{ent} (%)	η_{is} (%)	η_{cb} (%)	P_{MHD} (MW)	P_{comp} (MW)	P_{steam} (MW)	P_{net} (MW)	*)
7.2	0.78	32.2	74.8	49.0	322	90	301	490	bc
7.2	0.78	32.9	76.4	49.4	329	90	298	494	Vd-
7.2	0.78	31.5	73.2	48.7	315	90	304	487	Vd+
7.2	0.79	32.6	75.6	49.2	326	90	299	492	Tw-
7.2	0.77	31.9	74.0	48.8	319	90	302	488	Tw+
7.2	0.78	32.5	75.1	49.2	325	90	299	492	hl-
7.2	0.77	31.9	74.5	48.8	319	90	302	488	hl+
7.2	0.72	29.3	71.6	47.5	293	90	314	475	Ta-

*) bc : base case

Vd- : voltage drop = 50 V

Vd+ : voltage drop = 250 V

Tw- : $T_{st} - T_{wall}$ = 400 K

Tw+ : $T_{st} - T_{wall}$ = 600 K

hl- : heat loss in combustor and nozzle 10 % lower than base case

hl+ : heat loss in combustor and nozzle 10 % higher than base case

Ta- : preheat air T_{air} = 1650 K

When the difference in unit size is taken into account the comparison of the calculated efficiencies with the corresponding numbers of the ECAS study [5.7] shows a good agreement.

5.1.6 Additional constraints for the linear MHD generator

In the previous results concerning the linear open cycle MHD generator no restrictions were taken into account regarding maximum electric field, current density and Hall parameter. With the constraints of maximum Faraday field = 4 kV/m, maximum Hall field = 3 kV/m, maximum current density = 10 kA/m^2 and maximum Hall parameter = 4 a series of calculations have been carried out, but only the behaviour of nozzle, MHD channel and subsonic diffuser has been studied. In these calculations the magnetic induction is 6 T. If the constraints for electric field, current density or Hall parameter are not satisfied

the magnetic induction is decreased to fulfil the constraints. In these calculations the load factor is kept constant over the length of the generator and the length is increased in steps of 0.5 m (to a maximum of 200 m) until the stagnation pressure at the exit of the diffuser becomes less than 1.16 bar. The voltage drop is taken constant over the length of the channel and equals 150 V. The cross section is considered to be square and is adjusted such that the load factor is constant. To compare these results with available results from a study of the Netherlands MHD Association [5.8] the heat losses through the wall are based on a constant temperature difference of 430 K between the stagnation temperature of the gas and the wall. The main results are collected in tables 5.10, 5.11 and 5.12 for load factors of respectively 0.75, 0.8 and 0.85.

In these tables P_{in} is the total thermal input, P_{MHD} is the electrical power output of the MHD generator, P_{comp} is the power consumption of the combustion air compressor and P_{wall} is the heat loss of the MHD generator.

The remaining parameter variations are:
- stagnation pressure at the entrance of the nozzle p_{st} = 4, 6, 8, 10 and 12 bar;
- thermal input P_{in} = 1620, 1800 and 1980 MW; and
- mass flow rate $\dot{m}$ = 396, 440 and 484 kg/s.

From these calculations the following general conclusions can be drawn:
- higher load factors result in longer channels, higher enthalpy extractions and higher isentropic efficiencies;
- a higher stagnation pressure also results in longer channels and higher enthalpy extraction and higher isentropic efficiencies;
- an increase of mass flow rate results in a minor increase in channel length and enthalpy extraction and higher isentropic efficiencies. This effect is larger for higher stagnation pressures;
- higher stagnation temperatures result in shorter channels and lower isentropic efficiencies but have not much influence on the enthalpy extractions. This is caused by the fact that higher stagnation temperatures result in higher electrical conductivities leading to

Table 5.10 Summary of most significant results for the open cycle linear MHD generator. Mach number is constant (M = 0.9), B_{max} = 6 T, $|E_{x,max}|$ = 3 kV/m, $|E_{y,max}|$ = 4 kV/m, β_{max} = 4, Voltage drop = 150 V and Faraday load factor k_f = 0.7.

$\dot{m}$ kg/s	P_{in} MW	p_{st} bar	T_{in} K	P_{MHD} MW	P_{wall} MW	P_{comp} MW	l m	d_{in} m	d_{out} m	p_{dif} bar	η_{ent} (%)	η_{is} (%)
396	1620	4	2835	281.8	16.0	59.4	5.0	1.16	2.18	1.07	17.4	69.8
		6	2857	355.9	26.4	81.6	8.0	0.95	2.14	1.11	22.0	72.5
		8	2872	403.6	41.3	98.9	12.5	0.82	2.12	1.14	24.9	73.7
		10	2884	440.4	62.1	113.4	19.0	0.74	2.13	1.14	27.2	74.1
		12	2894	464.6	86.9	125.9	27.0	0.67	2.14	1.14	28.7	73.9
	1800	4	2972	276.4	26.4	59.4	7.5	1.16	2.12	1.14	15.4	62.5
		6	2995	363.8	39.1	81.6	10.0	0.95	2.12	1.13	20.2	65.6
		8	3011	437.1	51.4	98.9	12.5	0.83	2.19	1.06	24.3	68.0
		10	3023	472.8	62.7	113.4	14.5	0.74	2.15	1.10	26.3	69.0
		12	3034	503.4	74.7	125.9	17.0	0.68	2.14	1.11	28.0	69.8
	1980	4	3098	295.0	45.1	59.4	13.0	1.17	2.20	1.06	14.9	56.7
		6	3122	368.6	64.8	81.6	16.5	0.96	2.13	1.12	18.6	59.0
		8	3139	425.1	82.0	98.9	19.0	0.83	2.11	1.14	21.5	60.6
		10	3152	468.6	97.6	113.4	21.0	0.74	2.11	1.15	23.7	61.8
		12	3163	517.9	112.3	125.9	23.0	0.68	2.18	1.07	26.2	63.2
440	1620	4	2701	283.7	19.4	66.0	7.0	1.22	2.25	1.13	17.5	74.9
		6	2722	363.0	42.3	90.6	15.5	1.00	2.25	1.14	22.4	76.9
		8	2736	409.6	73.0	109.9	27.5	0.87	2.25	1.15	25.3	77.1
		10	2748	438.1	112.4	126.0	44.5	0.78	2.26	1.15	27.0	76.2
		12	2757	453.2	162.6	139.9	70.0	0.71	2.27	1.15	28.0	74.3
	1800	4	2835	313.2	16.9	66.0	5.0	1.22	2.30	1.07	17.4	70.0
		6	2857	396.6	27.8	90.6	8.0	1.00	2.26	1.11	22.0	72.7
		8	2872	450.3	43.6	109.9	12.5	0.87	2.24	1.14	25.0	73.9
		10	2884	492.4	65.5	126.0	19.0	0.78	2.25	1.13	27.4	74.5
		12	2894	520.5	91.7	139.9	27.0	0.71	2.26	1.13	28.9	74.3
	1980	4	2959	343.3	27.1	66.0	7.5	1.23	2.39	0.98	17.3	64.7
		6	2981	399.3	39.2	90.6	9.5	1.00	2.21	1.16	20.2	66.4
		8	2997	480.6	51.8	109.9	12.0	0.87	2.28	1.09	24.3	68.8
		10	3010	516.2	63.5	126.0	14.0	0.78	2.22	1.15	26.1	69.7
		12	3020	558.6	77.0	139.9	17.0	0.71	2.25	1.12	28.2	70.7
484	1620	4	2582	285.8	32.3	72.6	13.5	1.29	2.34	1.16	17.6	79.0
		6	2602	365.8	73.9	99.7	33.5	1.05	2.38	1.14	22.6	80.0
		8	2616	402.7	134.5	120.9	68.0	0.91	2.39	1.15	24.9	78.1
		10	2627	405.3	241.0	138.6	158.0	0.82	2.43	1.14	25.0	72.4
		12	2636	330.8	326.0	153.9	200.0	0.75	2.04	1.64	20.4	62.9
	1800	4	2714	314.3	19.3	72.6	6.5	1.28	2.35	1.13	17.5	74.6
		6	2734	406.1	42.4	99.7	14.5	1.05	2.37	1.13	22.6	76.8
		8	2749	459.3	72.9	120.9	25.5	0.91	2.37	1.14	25.5	77.3
		10	2761	492.0	111.4	138.6	40.5	0.82	2.37	1.15	27.3	76.7
		12	2770	511.3	159.6	153.9	62.0	0.75	2.38	1.15	28.4	75.3
	1980	4	2835	345.0	17.7	72.6	5.0	1.28	2.41	1.07	17.4	70.1
		6	2857	437.1	29.2	99.7	8.0	1.05	2.37	1.11	22.1	72.9
		8	2872	497.3	45.7	120.9	12.5	0.91	2.35	1.14	25.1	74.2
		10	2884	544.5	68.7	138.6	19.0	0.82	2.36	1.13	27.5	74.8
		12	2894	571.1	95.6	153.9	26.5	0.75	2.34	1.15	28.8	74.6

Table 5.11 Summary of most significant results for the open cycle linear MHD generator. Mach number is constant (M = 0.9), B_{max} = 6 T, $|E_{x,max}|$ = 3 kV/m, $|E_{y,max}|$ = 4 kV/m, β_{max} = 4, Voltage drop = 150 V and Faraday load factor k_f = 0.75.

$\dot{m}$ kg/s	P_{in} MW	p_{st} bar	T_{in} K	P_{MHD} MW	P_{wall} MW	P_{comp} MW	l m	d_{in} m	d_{out} m	p_{dif} bar	η_{ent} (-)	η_{is} (-)
396	1620	4	2835	295.8	15.3	59.4	5.0	1.16	2.15	1.10	18.2	74.7
		6	2857	377.9	30.6	81.6	10.0	0.95	2.14	1.12	23.3	77.1
		8	2872	426.6	52.0	98.9	17.0	0.82	2.12	1.14	26.3	77.8
		10	2884	462.4	79.0	113.4	26.5	0.74	2.14	1.13	28.5	77.8
		12	2894	481.6	110.6	125.9	38.0	0.67	2.13	1.16	29.7	76.9
	1800	4	2972	326.4	22.8	59.4	6.5	1.16	2.24	1.01	18.2	68.9
		6	2995	386.8	33.4	81.6	18.5	0.95	2.09	1.17	21.5	70.8
		8	3011	450.1	44.9	98.9	11.0	0.83	2.09	1.17	25.0	72.7
		10	3023	503.8	58.4	113.4	14.5	0.74	2.13	1.12	28.0	74.1
		12	3034	534.4	73.8	125.9	18.5	0.68	2.12	1.14	29.7	74.6
	1980	4	3098	317.0	37.7	59.4	10.5	1.17	2.18	1.08	16.0	61.8
		6	3122	408.6	54.7	81.6	13.5	0.96	2.16	1.09	20.6	64.7
		8	3139	481.1	70.2	98.9	16.0	0.83	2.19	1.06	24.3	66.8
		10	3152	525.6	84.2	113.4	18.0	0.74	2.18	1.07	26.5	67.9
		12	3163	545.9	196.9	125.9	19.5	0.68	2.10	1.16	27.6	68.2
440	1620	4	2701	296.7	24.0	66.0	9.0	1.22	2.22	1.15	18.3	79.4
		6	2722	381.0	53.5	90.6	21.0	1.00	2.24	1.15	23.5	81.1
		8	2736	428.6	93.7	109.9	39.0	0.87	2.26	1.15	26.4	80.6
		10	2748	452.1	146.6	126.0	66.5	0.78	2.27	1.15	27.9	78.7
		12	2757	457.2	219.8	139.9	115.5	0.71	2.29	1.15	28.2	75.0
	1800	4	2835	328.2	16.1	66.0	5.0	1.22	2.26	1.11	18.2	74.8
		6	2857	420.6	32.2	90.6	10.0	1.00	2.26	1.12	23.4	77.4
		8	2872	476.3	54.8	109.9	17.0	0.87	2.24	1.14	26.5	78.1
		10	2884	512.4	82.8	126.0	26.0	0.78	2.23	1.15	28.5	78.1
		12	2894	540.5	116.6	139.9	38.0	0.71	2.25	1.15	30.0	77.5
	1980	4	2959	342.3	22.4	66.0	6.0	1.23	2.27	1.10	17.3	69.0
		6	2981	443.3	34.2	90.6	8.5	1.00	2.26	1.11	22.4	72.1
		8	2997	502.6	46.1	109.9	11.0	0.87	2.22	1.15	25.4	73.7
		10	3010	551.2	60.6	126.0	14.5	0.78	2.22	1.16	27.9	74.7
		12	3020	589.6	78.1	139.9	19.0	0.71	2.22	1.16	29.8	75.3
484	1620	4	2582	304.8	41.2	72.6	18.5	1.29	2.36	1.14	18.8	83.7
		6	2602	381.8	95.2	99.7	47.5	1.05	2.38	1.15	23.5	83.4
		8	2616	409.7	182.4	120.9	109.0	0.91	2.41	1.15	25.3	79.3
		10	2627	360.3	298.5	138.6	200.0	0.82	2.20	1.40	22.2	69.3
		12	2636	275.8	360.1	153.9	200.0	0.75	1.79	2.14	17.0	58.3
	1800	4	2714	331.3	24.1	72.6	8.5	1.28	2.34	1.14	18.4	79.2
		6	2734	425.1	53.4	99.7	19.5	1.05	2.35	1.14	23.7	81.1
		8	2749	478.3	92.8	120.9	35.5	0.91	2.36	1.15	26.6	80.9
		10	2761	509.0	144.4	138.6	59.5	0.82	2.38	1.15	28.3	79.5
		12	2770	521.3	212.6	153.9	98.5	0.75	2.40	1.15	29.0	76.7
	1980	4	2835	362.0	16.9	72.6	5.0	1.28	2.37	1.10	18.3	75.0
		6	2857	464.1	33.8	99.7	10.0	1.05	2.37	1.12	23.4	77.6
		8	2872	526.3	57.5	120.9	17.0	0.91	2.35	1.14	26.6	78.4
		10	2884	567.5	86.8	138.6	26.0	0.82	2.35	1.15	28.7	78.5
		12	2894	599.1	122.4	153.9	38.0	0.75	2.36	1.14	30.3	78.0

Table 5.12 Summary of most significant results for the open cycle linear MHD generator. Mach number is constant (M = 0.9), B_{max} = 6 T, $|E_{x,max}|$ = 3 kV/m, $|E_{y,max}|$ = 4 kV/m, β_{max} = 4, Voltage drop = 150 V and Faraday load factor k_f = 0.8.

$\dot{m}$ kg/s	P_{in} MW	p_{st} bar	T_{in} K	P_{MHD} MW	P_{wall} MW	P_{comp} MW	l m	d_{in} m	d_{out} m	p_{dif} bar	η_{ent} (-)	η_{is} (-)
396	1620	4	2835	303.8	19.1	59.4	6.5	1.16	2.11	1.15	18.7	78.7
		6	2857	390.9	41.8	81.6	14.5	0.95	2.12	1.14	24.1	80.7
		8	2872	442.6	71.6	98.9	25.5	0.82	2.12	1.15	27.3	80.9
		10	2884	473.4	108.7	113.4	40.5	0.74	2.13	1.15	29.3	80.1
		12	2894	491.0	153.7	125.9	61.0	0.67	2.14	1.15	30.3	78.3
	1800	4	2972	342.4	19.1	59.4	5.5	1.16	2.20	1.05	19.0	73.8
		6	2995	428.8	30.7	81.6	18.5	0.95	2.15	1.11	23.8	76.4
		8	3011	488.1	46.8	98.9	13.0	0.83	2.13	1.12	27.1	77.7
		10	3023	527.8	68.2	113.4	19.0	0.74	2.12	1.14	29.3	78.0
		12	3034	554.4	94.4	125.9	26.5	0.68	2.11	1.15	30.8	77.7
	1980	4	3098	340.0	30.0	59.4	18.0	1.17	2.16	1.10	17.2	67.2
		6	3122	433.6	44.0	81.6	10.5	0.96	2.11	1.14	21.9	69.9
		8	3139	512.1	57.7	98.9	13.0	0.83	2.15	1.10	25.9	72.1
		10	3152	561.6	71.1	113.4	15.5	0.74	2.14	1.11	28.3	73.3
		12	3163	598.9	185.6	125.9	18.5	0.68	2.14	1.11	30.2	74.0
440	1620	4	2701	313.7	32.4	66.0	13.0	1.22	2.23	1.15	19.3	83.7
		6	2722	396.0	72.2	90.6	31.0	1.00	2.24	1.15	24.4	84.4
		8	2736	438.6	128.3	109.9	60.5	0.87	2.26	1.15	27.1	82.6
		10	2748	451.1	208.0	126.0	114.0	0.78	2.29	1.15	27.9	78.5
		12	2757	419.2	313.7	139.9	200.0	0.71	2.21	1.26	25.9	70.8
	1800	4	2835	337.2	20.1	66.0	6.5	1.22	2.22	1.15	18.8	78.9
		6	2857	435.6	44.1	90.6	14.5	1.00	2.23	1.15	24.2	81.0
		8	2872	493.3	75.6	109.9	25.5	0.87	2.23	1.15	27.4	81.4
		10	2884	530.4	114.9	126.0	40.5	0.78	2.25	1.15	29.5	80.7
		12	2894	550.5	162.1	139.9	60.5	0.71	2.25	1.15	30.6	79.1
	1980	4	2959	357.3	18.7	66.0	5.0	1.23	2.22	1.14	18.0	73.9
		6	2981	469.3	31.9	90.6	8.5	1.00	2.24	1.13	23.7	77.0
		8	2997	536.6	50.4	109.9	13.5	0.87	2.23	1.14	27.1	78.3
		10	3010	586.2	75.4	126.0	20.5	0.78	2.25	1.13	29.6	78.7
		12	3020	614.6	104.2	139.9	28.5	0.71	2.23	1.15	31.0	78.4
484	1620	4	2582	317.8	54.8	72.6	26.5	1.29	2.35	1.15	19.6	87.5
		6	2602	388.8	131.0	99.7	74.0	1.05	2.39	1.15	24.0	85.2
		8	2616	384.7	270.4	120.9	200.0	0.91	2.39	1.19	23.7	75.6
		10	2627	298.3	336.0	138.6	200.0	0.82	1.92	1.84	18.4	64.1
		12	2636	218.8	393.9	153.9	200.0	0.75	1.59	2.69	13.5	51.7
	1800	4	2714	346.3	32.2	72.6	12.0	1.28	2.33	1.16	19.3	83.5
		6	2734	441.1	71.9	99.7	28.5	1.05	2.35	1.15	24.5	84.6
		8	2749	493.3	127.4	120.9	55.0	0.91	2.37	1.15	27.4	83.3
		10	2761	513.0	202.7	138.6	99.0	0.82	2.39	1.15	28.5	80.1
		12	2770	500.3	321.8	153.9	200.0	0.75	2.43	1.15	27.8	73.7
	1980	4	2835	371.0	21.1	72.6	6.5	1.28	2.33	1.15	18.8	79.1
		6	2857	480.1	46.4	99.7	14.5	1.05	2.34	1.15	24.3	81.3
		8	2872	545.3	79.4	120.9	25.5	0.91	2.34	1.15	27.6	81.7
		10	2884	588.5	120.7	138.6	40.5	0.82	2.36	1.14	29.7	81.2
		12	2894	611.1	170.4	153.9	60.5	0.75	2.37	1.15	30.9	79.8

higher electrical fields and higher Hall parameters. To fulfil the constraints on electrical fields and Hall parameter, the magnetic induction has to be decreased. The overall effect on enthalpy extraction is therefore small.

Calculations have been carried out also for an inlet stagnation pressure p_{st} = 8.0 bar, a total thermal input P_{in} = 1635 MW and a mass flow $\dot{m}$ = 412 kg/s for various load factors k_f from 0.74 to 0.94. The main results are collected in table 5.13 and in figure 5.11. From these calculations the following conclusions can be drawn:

- for a given pressure there are optimum load factors k_f with respect to enthalpy extraction and isentropic efficiency which are nearly the same, and
- an increase of load factor has a large impact on the length of the MHD channel and thus on the investment costs of the superconducting magnet system.

Table 5.13 Summary of most significant results for the open cycle linear MHD generator. Mach number is constant (M = 0.9), B_{max} = 6 T, $|E_{x,max}|$ = 3 kV/m, $|E_{y,max}|$ = 4 kV/m, β_{max} = 4, Voltage drop = 150 V and inlet stagnation pressure p_{st} = 8.0 bar.

$\dot{m}$ kg/s	p_{st} bar	k_f (-)	T_{in} K	P_{MHD} MW	P_{wall} MW	P_{comp} MW	l m	d_{in} m	d_{out} m	p_{dif} bar	η_{ent} (-)	η_{is} (-)
412	8	0.74	2832	403.0	46.4	103.0	14.5	0.84	2.15	1.16	24.6	73.9
		0.76	2832	415.5	50.8	103.0	16.5	0.84	2.17	1.14	25.4	75.7
		0.78	2832	422.1	55.5	103.0	18.5	0.84	2.16	1.15	25.8	77.2
		0.80	2832	433.7	61.8	103.0	21.5	0.84	2.18	1.13	26.5	78.9
		0.82	2832	437.9	68.5	103.0	24.5	0.84	2.16	1.15	26.8	80.2
		0.84	2832	443.7	78.1	103.0	29.0	0.84	2.16	1.16	27.1	81.3
		0.86	2832	448.5	91.3	103.0	35.5	0.84	2.17	1.15	27.4	82.1
		0.88	2832	451.3	109.3	103.0	45.0	0.84	2.18	1.15	27.6	82.5
		0.90	2832	448.1	133.5	103.0	58.5	0.84	2.17	1.15	27.4	82.0
		0.92	2832	439.7	169.3	103.0	80.5	0.84	2.18	1.15	26.9	80.4

As previously mentioned these calculations only consider the nozzle, MHD generator and subsonic diffuser. The highest enthalpy extraction does not necessarily lead to the highest coal to busbar efficiency. The coal to busbar efficiency is further determined by the isentropic efficiency, compressor power, friction losses and wall heat losses.

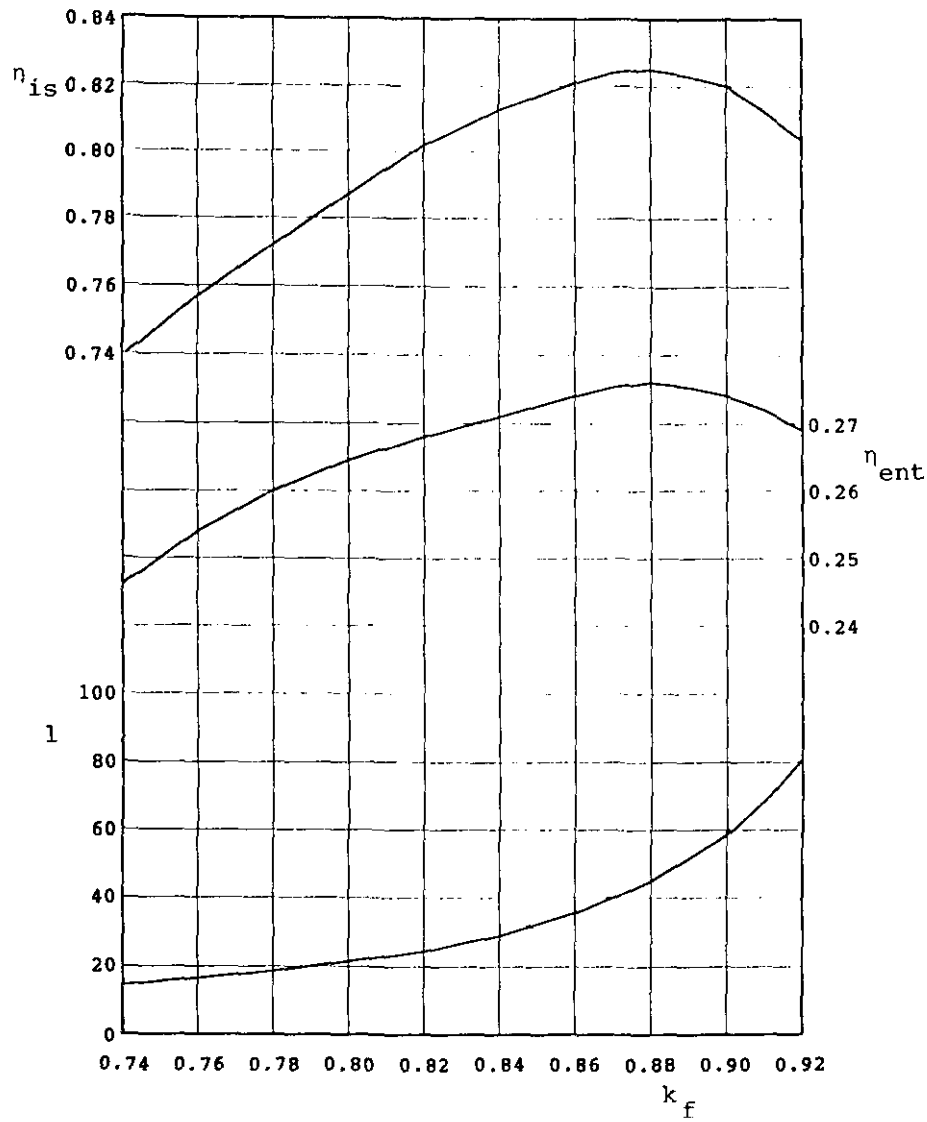

Figure 5.11 Effect of enthalpy extraction, isentropic efficiency and generator length with variation of the load factor k_f for a stagnation pressure p_{st} = 8.0 bar.

5.2 Discussion of results

When this project was initiated it was anticipated that the system studies which have been presented in chapter 5.1, would lead to the conclusion that the open cycle disk MHD generator would need further research and development. The calculations have shown, however that the system based on the open cycle disk MHD generator leads to the lowest value of the coal to busbar efficiency (η_{cb}). The two most

attractive systems are based on the closed cycle disk generator and the open cycle linear generator. The first question that arises now is what phenomena have led to the limitations in the operation of the open cycle disk MHD generator. Because of the time and manpower available for this study, the variation of parameters was limited so, the authors can not guarantee completely that no better performance data can be obtained. This point requires further investigations. The second question which pertains to all four systems studied, is the accuracy of the calculated values of η_{cb}. Assuming the validity of the models that were used the accuracy of the results should be determined. On the other hand it is legitimate to ask to what extent the theoretical models that were used have been verified by experiments in smaller scale systems. These questions can not be answered very accurately at the moment either and would require further research effort.

5.3 Summary

In this chapter a series of calculated results have been discussed for the different types of MHD generators as well as some aspects of superconducting magnet systems for commercial systems. The results can be summarized in the following points:

- comparison of the four systems gives the following coal to busbar efficiencies η_{cb} for the MHD/steam systems under common constraints and ground rules:
  - closed cycle disk generator 50.0 %
  - closed cycle linear generator 47.6 %
  - open cycle disk generator 42.8 %
  - open cycle linear generator 49.4 %,
- comparison of the best closed cycle system with the best open cycle system shows an advantage of less than 1 percentage point in η_{cb} for the closed cycle disk MHD/steam cycle in comparison with the open cycle linear MHD/steam cycle (both at B = 5 T),
- for the closed cycle system the disk MHD generator leads to an advantage of 2.4 percentage points in the coal to busbar efficiency η_{cb} in comparison with the linear MHD generator (both at B = 5 T).
- for the open cycle system the linear MHD generator leads to an advantage of 6.4 percentage points in η_{cb} in comparison with the

disk MHD generator (both at B = 5 T),

- for the open cycle disk MHD channel an increase of magnetic induction from 5 to 9 T results in an increase of η_{cb} from 42.8 % to 45.5 %,
- the highest coal to busbar efficiency will in general not lead to the lowest cost of electricity because longer channels need more expensive superconducting magnet systems.

6 CONCLUSIONS

- In this report an experimental disk MHD facility has been designed.
- After designing the superconducting magnet for the open cycle disk MHD generator, the warm bore of the magnet has been used as a constraint in designing the closed cycle disk MHD generator.
- In the experimental MHD facility an enthalpy extraction of 8.7 % could be obtained with a 10 MWt open cycle MHD generator and 37.0 % by means of a 5 MWt closed cycle MHD generator.
- System studies of four commercial scale (≈ 1000 MWt) MHD/steam systems have also been performed.
- The 1000 MWt open cycle disk generator leads to the smallest coal to busbar efficiency of 42.8 %.
- The highest coal to busbar efficiency of 50.0 % is obtained in a commercial system with a closed cycle disk generator.
- The open cycle linear MHD/steam system leads to a coal to busbar efficiency of 49.4 %. When the details of the heat source and the required heat exchangers are considered, it can be anticipated that the system with an open cycle linear MHD generator will have the lowest cost of electricity (fl/kWh) of the four systems.
- The design of the superconducting magnet system for the experimental disk facility has used principles that are valid also for large commercial systems. However, verification of these principles in an actual 1000 MWt superconducting magnet design needs further investigation.

7 ACKNOWLEDGEMENTS

The authors are grateful to prof. dr. L.J.M van de Klundert of the University of Twente and prof. dr. L.H.Th. Rietjens of the Eindhoven University of Technology for encouragement and the stimulating discussions. They also would like to thank the Foundation for Fundamental Research on Matter FOM and the Netherlands Technology Foundation STW for the financial support of this study.

8 BIBLIOGRAPHY

The interested reader is referred to the following text books for further reading:

1. Sutton, G.W. and Sherman, A., Engineering magnetohydrodynamics, Mc.Graw Hill (1965).
2. Mitchner, M. and Kruger, C.H., Partially ionized gases, John Wiley and Sons, New York (1973).
3. Rosa, R.J., Magnetohydrodynamic energy conversion, Mc Graw Hill (1968).
4. Kirillin, V.A. and Sheyndlin, A.E.(editors), MHD energy conversion, physiotechnical problems, American Institute of Aeronautics and Astronautics (1986).
5. Petrick, M. and Shumyatsky, B.Ya. (editors),Open-cycle magneto-hydrodynamic electrical power generation, A joint USA/USSR publication, Argonne National Laboratory, Argonne (1978).
6. Wilson, M.N., Superconducting magnets, Oxford University Press, Oxford, (1983).
7. Collings, E.W., Applied superconductivity, metallurgy and physics of titanium alloys, Volume 1: Fundamentals, Volume 2: Applications, Plenum Press, New York (1986).
8. Van Sciver, S.W., Helium cryogenics, Plenum Press, New York (1986).

9 REFERENCES

[1.1] Kirillin, V.A. and Sheyndlin, A.E. (editors), MHD energy conversion, physiotechnical problems, American Institute of Aeronautics and Astronautics (1986).

[1.2] Yamasaki, H. et al., High enthalpy extraction in the Fuji-I disk generator experiment, Proc. 10th Intern. Conf. on MHD Electrical Power Generation, Tiruchirapalli, Vol. III, p XII.30 (1989).

[1.3] Nakamura, T., Lear, W.E. and Fang, Y., Results of combustion driven inflow disk generator experiments, Proc. 8th Intern. Conf. on MHD Electrical Power Generation, Moscow, Vol. 4, p 185 (1983).

[2.1] Klepeis, J.E. and Louis, J.F., The disk generator applied to open cycle power generation, Proc. 5th Intern. Conf. on MHD Electrical Power Generation, Munich, Vol. 1, p 649 (1971).

[2.2] Solbes, A., Instabilities in nonequilibrium MHD plasmas, a review, AIAA paper no. 70-40, New York (1970).

[2.3] Nakamura, T. and Riedmüller, W., Stability of nonequilibrium MHD plasma in the regime of fully ionized seed, AIAA Journal, Vol. 12, p 661 (1974).

[2.4] Massee, P., Stabilization of nonequilibrium MHD plasmas by means of metastable nitrogen, Proc. 5th Intern. Conf. on MHD Electrical Power Generation, Munich, Vol. 2, p 275 (1971).

[2.5] Massee, P., Gasdynamic performance in relation to the power extraction of an MHD generator, Ph.D. thesis, Eindhoven Univ. of Techn., Eindhoven (1983).

[2.6] Massee, P., Performance of closed cycle disk generators operating with stable or unstable plasma, Proc. 19th Symp. on Engineering Aspects on MHD, Tullahoma, Tenn., p 7.1.1 (1981).

[2.7] Mc Bride, B.J. and Gordon, S., Computer program for calculation of complex chemical equilibrium compositions, rocket performance, incident and reflected shocks and Chapman-Jouguet detonations, NASA SP-273, Rev. (1976).

[2.8] Retallick, F.D., Disk MHD generator study, NASA report CR-759872, Cleveland, Ohio (1980).

[2.9] Marston, P.G., Superconducting magnet system for a space-based 100 MW MHD disk generator. IEEE MAG-24 (1988) p 885.

[2.10] Okamura, T., Kabashima, S. and Shioda, S., Superconducting magnet for a full scale helium-driven disk MHD generator. 9th

Intern. Conf. on MHD Electr. Power Generation, Tsukuba, (1986) p 125.

[2.11] Nakamura, T., Lear, W.E. and Eustis, R.H., Feasibility study of the inflow disk generator for open-cycle MHD power generation. 19th Symp. on Eng. Aspects of MHD, Tullahoma, (1981) p 3.1.1.

[2.12] Okamura, T., Kabashima, S., Shioda, S and Sanada, Y., Superconducting magnet for a disc generator of the FUJI-1 MHD facility. Cryogenics 25 (1985) p 483.

[2.13] Louis,J.F., Disk generators. AIAA Journal vol 6, no 9 (1968) p 1674.

[3.1] Alff, J.J., Strain problems associated with the winding of reacted Nb_3Sn superconductors. Proc. MT-9 Zurich (1985) p 669.

[3.2] Roeterdink, J.A., Klok, J., Elen, J.D. and Franken, W.M.P., Application of A-15 conductors in NET TF-coils. Proc. MT-9 Zurich (1985) p 622.

[3.3] Chernoplekov, N.A. and Monoszon, N.A., T-15 facility and tests. IEEE MAG-23 (1987) p 826.

[3.4] Elen, J.D., Development of niobium-tin conductors at SLE. Cryogenics 27 (1987) p 106.

[3.5] Agatsuma, K., Kaiho, K. and Komuro, K., A forced cooled Nb_3Sn superconducting magnet. Proc. MT-9 Zurich (1985) p 379.

[3.6] Veringa, H., van Wees, A.C.A. and Hoogendam, P., Development of high current Nb_3Sn multifilament superconducting material following the ECN powder method. IEEE Mag 19 (1983) p 773.

[3.7] Ekin, J.W., Mechanical properties and strain effects in superconductors. In Superconducting Materials Science: Metallurgy Fabrication and Application, Editors Foner, S. and Schwartz, B.B, Plenum Press, New York, (1981) p 455.

[3.8] Liedl, J., Gauster, W.F., Haslacher, H. and Grossinger, R., Calculation of the mechanical stresses in a high field magnet by means of a layer model. IEEE MAG-17 (1981) p 3256.

[3.9] Volterra, E. and Gaines, J.H., Advanced strength of materials. Englewood Cliffs, N.J. :Prentice Hall (1971).

[3.10] Ekin, J.W., Transverse stress effect on multifilamentary Nb_3Sn superconductors, Adv. Cryo. Eng. 34 (1988) p 547.

[3.11] Boschman, H. and van de Klundert, L.J.M., Degradation of the critical current of multifilamentary Nb_3Sn wires under transverse mechanical load, Presented at MT-11 Tsukuba (1989) Japan.

[3.12] Boschman, H., Fornerod, P.P.E. and van de Klundert, L.J.M., The

influence of transverse, compressive stress on the critical current of multifilamentary Nb_3Sn and NbTi wires. MAG-25 (1989) p 1976.

[3.13] Van Sciver, S.W., Helium Cryogenics, Plenum Press, New York (1986).

[4.1] Petrick, M. and Shumyatsky, B.Ya. (editors), Open-cycle magnetohydrodynamic electrical power generation, A joint USA/USSR publication, Argonne National Laboratory, Argonne (1978).

[5.1] Mc. Bride, B.J. and Gordon, S., Computer program for calculation of complex chemical equilibrium compositions, rocket performance, incident and reflected shocks and Chapman-Jouguet detonations, NASA SP-273, Rev. (1976).

[5.2] Cervenka, S. et al., Conceptual design study of a 600 MWe coal fired open cycle MHD plant, Proc. 20th Symp. on Engineering Aspects of MHD, Irvine, p 13.4.1 (1982).

[5.3] Geutjes, A.J. and Kleyn, D.J., A parametric study of 1000 MWe combined closed cycle MHD/steam electrical power generation plants, report Eindhoven University of Technology, nr. 78-E-91, Eindhoven, (1978).

[5.4] Retallick, F.D., Disk MHD generator study, NASA report CR-759872, Cleveland, Ohio (1980).

[5.5] Massee, P., Performance of closed cycle disk generators operating with stable or unstable plasma, Proc. 19th Symp. on Engineering Aspects on MHD, Tullahoma, Tenn., p 7.1.1 (1981).

[5.6] Simpson, S.W., Marty, S.M. and Messerle, H.K., Open-cycle disk MHD generators: laboratory experiments and predictions for base-load operation, Magnetohydrodynamics: an International Journal, Vol. 2, No. 1, p 57 (1989).

[5.7] Lewis Research Center, Comparative evaluation of phase I results from energy conversion alternatives study (ECAS), Report no. NASA TM-X-71855 (1976).

[5.8] Netherlands MHD Association, Final Report Netherlands MHD Project Phase 1, Report nr. FDO-MHD-82-001, Amsterdam (1982) (in Dutch).

Eindhoven University of Technology Research Reports
Faculty of Electrical Engineering

ISSN 0167-9708
Coden: TEUEDE

(222) Jóźwiak, L.
THE FULL-DECOMPOSITION OF SEQUENTIAL MACHINES WITH THE SEPARATE REALIZATION OF THE NEXT-STATE AND OUTPUT FUNCTIONS.
EUT Report 89-E-222. 1989. ISBN 90-6144-222-2

(223) Jóźwiak, L.
THE BIT FULL-DECOMPOSITION OF SEQUENTIAL MACHINES.
EUT Report 89-E-223. 1989. ISBN 90-6144-223-0

(224) Book of abstracts of the first Benelux-Japan Workshop on Information and Communication Theory, Eindhoven, The Netherlands, 3-5 September 1989.
Ed. by Han Vinck.
EUT Report 89-E-224. 1989. ISBN 90-6144-224-9

(225) Hoeijmakers, M.J.
A POSSIBILITY TO INCORPORATE SATURATION IN THE SIMPLE, GLOBAL MODEL OF A SYNCHRONOUS MACHINE WITH RECTIFIER.
EUT Report 89-E-225. 1989. ISBN 90-6144-225-7

(226) Dahiya, R.P. and E.M. van Veldhuizen, W.R. Rutgers, L.H.Th. Rietjens
EXPERIMENTS ON INITIAL BEHAVIOUR OF CORONA GENERATED WITH ELECTRICAL PULSES SUPERIMPOSED ON DC BIAS.
EUT Report 89-E-226. 1989. ISBN 90-6144-226-5

(227) Bastings, R.H.A.
TOWARD THE DEVELOPMENT OF AN INTELLIGENT ALARM SYSTEM IN ANESTHESIA.
EUT Report 89-E-227. 1989. ISBN 90-6144-227-3

(228) Hekker, J.J.
COMPUTER ANIMATED GRAPHICS AS A TEACHING TOOL FOR THE ANESTHESIA MACHINE SIMULATOR.
EUT Report 89-E-228. 1989. ISBN 90-6144-228-1

(229) Oostrom, J.H.M. van
INTELLIGENT ALARMS IN ANESTHESIA: An implementation.
EUT Report 89-E-229. 1989. ISBN 90-6144-229-X

(230) Winter, M.R.M.
DESIGN OF A UNIVERSAL PROTOCOL SUBSYSTEM ARCHITECTURE: Specification of functions and services.
EUT Report 89-E-230. 1989. ISBN 90-6144-230-3

(231) Schemmann, M.F.C. and H.C. Heyker, J.J.M. Kwaspen, Th.G. van de Roer
MOUNTING AND DC TO 18 GHz CHARACTERISATION OF DOUBLE BARRIER RESONANT TUNNELING DEVICES.
EUT Report 89-E-231. 1989. ISBN 90-6144-231-1

(232) Sarma, A.D. and M.H.A.J. Herben
DATA ACQUISITION AND SIGNAL PROCESSING/ANALYSIS OF SCINTILLATION EVENTS FOR THE OLYMPUS PROPAGATION EXPERIMENT.
EUT Report 89-E-232. 1989. ISBN 90-6144-232-X

(233) Nederstigt, J.A.
DESIGN AND IMPLEMENTATION OF A SECOND PROTOTYPE OF THE INTELLIGENT ALARM SYSTEM IN ANESTHESIA.
EUT Report 90-E-233. 1990. ISBN 90-6144-233-8

(234) Philippens, E.H.J.
DESIGNING DEBUGGING TOOLS FOR SIMPLEXYS EXPERT SYSTEMS.
EUT Report 90-E-234. 1990. ISBN 90-6144-234-6

(235) Heffels, J.J.M.
A PATIENT SIMULATOR FOR ANESTHESIA TRAINING: A mechanical lung model and a physiological software model.
EUT Report 90-E-235. 1990. ISBN 90-6144-235-4

(236) Lammers, J.O.
KNOWLEDGE BASED ADAPTIVE BLOOD PRESSURE CONTROL: A Simplexys expert system application.
EUT Report 90-E-236. 1990. ISBN 90-6144-236-2

(237) Ren Qingchang
PREDICTION ERROR METHOD FOR IDENTIFICATION OF A HEAT EXCHANGER.
EUT Report 90-E-237. 1990. ISBN 90-6144-237-0

Eindhoven University of Technology Research Reports
Faculty of Electrical Engineering

ISSN 0167-9708
Coden: TEUEDE

(238) Lammers, J.O.
THE USE OF PETRI NET THEORY FOR SIMPLEXYS EXPERT SYSTEMS PROTOCOL CHECKING.
EUT Report 90-E-238. 1990. ISBN 90-6144-238-9

(239) Wang, X.
PRELIMINARY INVESTIGATIONS ON TACTILE PERCEPTION OF GRAPHICAL PATTERNS.
EUT Report 90-E-239. 1990. ISBN 90-6144-239-7

(240) Lutgens, J.M.A.
KNOWLEDGE BASE CORRECTNESS CHECKING FOR SIMPLEXYS EXPERT SYSTEMS.
EUT Eeport 90-E-240. 1990. ISBN 90-6144-240-0

(241) Brinker, A.C. den
A MEMBRANE MODEL FOR SPATIOTEMPORAL COUPLING.
EUT Report 90-E-241. 1990. ISBN 90-6144-241-9